TG–912
MAY 1967
Copy No. 66

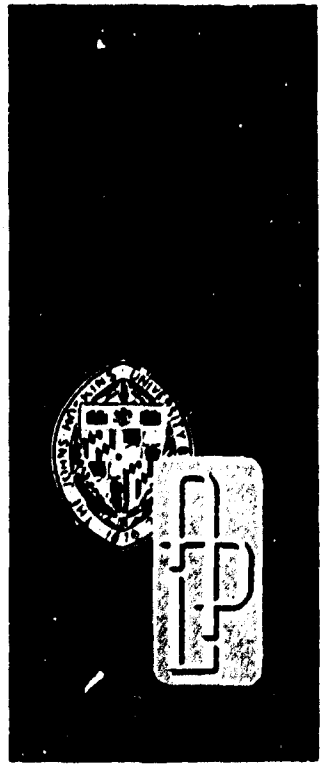

Technical Memorandum

EXTERNAL BURNING IN SUPERSONIC STREAMS

by F. S. BILLIG

TG–912
MAY 1967

Technical Memorandum

EXTERNAL BURNING IN SUPERSONIC STREAMS

by F. S. BILLIG

THE JOHNS HOPKINS UNIVERSITY • APPLIED PHYSICS LABORATORY
8621 Georgia Avenue, Silver Spring, Maryland 20910
Operating under Contract NOw 69-0604-c with the Department of the Navy

TABLE OF CONTENTS

LIST OF ILLUSTRATIONS

LIST OF TABLES

LIST OF SYMBOLS

a	Acoustic velocity, ft/sec
A	Area, ft^2
A_F	Frontal area, ft^2
A_R	Reference area, ft^2
c_p	Specific heat at constant pressure, $ft^2/sec^2 - {}^oR$
C	Chord length, ft
C_D	Drag coefficient
C_{Df}	Friction drag coefficient = friction drag/$q_0 A_F$
C_F	Gross thrust coefficient
C_L	Lift coefficient
C_N	Normal force coefficient
C_P	Pressure coefficient = $p - p_0/q_0$
d	Width, ft
d_j	Injector diameter, cm (Eq. (49))
d_C	Volume mean droplet diameter, cm (Eq. (49))
D	Drag, lb_f or diameter, ft
ER	Equivalence ratio = f/f_S
f	Fuel/air weight ratio
f_S	Stoichiometric fuel/air ratio
F	Force, lb_f
F_N	Normal force, lb_f
g	Gravitational constant = 32.16 ft/sec^2
h	Height, ft or heating value of fuel Btu/lb fuel
I_f	Thrust minus drag specific impulse, sec

I_{fN}	Normal force specific impulse, sec
J	Mechanical equivalent of heat 778 ft lb/Btu
ℓ	Length, ft
L	Lift lb_f or length, ft
M	Mach number
$\mathfrak{M}$	Molecular weight
p	Pressure, lb/ft^2 (or psia if specified)
q	Dynamic pressure = $\rho u^2/2$ lb/ft^2
$\dot{q}$	Heating rate, Btu/ft^2 sec or $ft\text{-}lb/ft^2$ sec
Q	Heating rate/lb or air, Btu/lb
R	Gas constant $ft^2/sec^2 - {}^oR$
R^o	Universal gas constant = 49,700 $ft^2/sec^2\ {}^oR\mathfrak{M}$
R	Cruise range parameter, $\frac{L}{\dot{w}_f}\frac{u_0}{6076}\left[\frac{1}{1-(u_0/u_s)^2}\right]$, naut. mi.
T	Temperature, ${}^oR$ (or ${}^oF$ if specified)
u	Velocity, ft/sec
u_s	Mean earth satellite velocity, low circular orbit = 25,900 ft/sec
$\dot{w}$	Weight flow, lb/sec
$\dot{w}_a$	Weight flow of air, lb/sec
$\dot{w}_f$	Weight flow of fuel, lb/sec
W	Weight, lb
x	Longitudinal dimension in flow direction, ft
X_f	Flame length, ft

y	Lateral dimension, ft
Y	Stream tube height, ft
Z	Altitude, ft
α	Angle-of-attack, degrees or radians
β	Mach angle, degrees
γ	Ratio of specific heats
δ	Wedge angle, degrees
δ_H	Heater or deflection angle, degrees
δ_S	Surface inclination angle, degrees
ϵ	Wedge angle, degrees
η_c	Combustion efficiency
η_d	Diffuser kinetic energy efficiency
η_n	Nozzle efficiency
θ	Shock angle, degrees
μ	Mach angle, degrees or viscosity, poise
ρ	Density, slug/ft^3
σ	Average flow turning angle, (Eq. (37)), degrees
σ_L	Liquid surface tension, dyne/cm, (Eq. (49))
τ	Thickness dimension, ft

Subscripts

a	Air
C	Cold
f	Fuel

H	Hot
N	Normal
t	Tangential
T	Total
0	Freestream condition

ACKNOWLEDGMENT

This report was prepared for the United States Naval Ordnance Systems Command under Contract NOw 62-0604-C. It is an abridgment of a more comprehensive study which was supported by the United States Air Force, Headquarters Air Force Systems Command, Andrews Air Force Base, Washington, D. C. under Contract USAF MIPR SC-5-11. The experimental and theoretical studies performed at the Johns Hopkins University, Applied Physics Laboratory and the General Dynamics, Ordnance Aerophysics Laboratory were supported by previous contracts with the Bureau of Naval Weapons, Department of the Navy.

The author gratefully acknowledges the guidance and the advice of Dr. Gordon L. Dugger both for his technical contributions and for editing the manuscript. Thanks are due to Mr. Richard Bonney and Mrs. C. S. Davis for assistance in preparing the illustrations and to Mrs. Janice W. VanNoy for typing the manuscript.

ABSTRACT

Theoretical and experimental studies of heat addition to external supersonic streams are reviewed following a brief explanation of the basic fluid mechanical model and possible applications of external burning. The theoretical section begins with a terse review of the extension of the method of characteristics to diabatic flows and then discusses the linearized heat addition models including a new simplified method for obtaining the linearized equations. The numerous analyses of combustion via a stationary detonation wave are categorized into four models for planar heat addition and the equations are developed for the most interesting case of the oblique Chapman-Jouget detonation. Performance estimates are presented for constant area and constant pressure heat addition processes with and without a consideration of the expansion zone following heat addition. The governing equations for the constant pressure analysis are developed for heat addition adjacent to both a double wedge and a flat plate surface.

In the experimental section all of the available results from external burning tests are discussed beginning with the pioneering tests at NACA and Texaco, Experiment, Inc., and including tests of two-dimensional and axisymmetric bodies at the Applied Physics Laboratory and the Boeing Co. Pertinent conclusions are drawn from each of the tests and a final compilation and summarization of all the data are given. It is concluded that the maximum expected pressure coefficient will be near that associated with a separated boundary layer and that to obtain the theoretical maximum specific impulse, highly reactive fuels with a combustion length of a few feet will be required.

The Johns Hopkins University
APPLIED PHYSICS LABORATORY
Silver Spring, Maryland

EXTERNAL BURNING IN SUPERSONIC STREAMS

Frederick S. Billig

1. INTRODUCTION

The term "external burning ramjet" (and the abbreviation, ERJ) refers herein to any system in which a combustible liquid or gas is injected from a vehicle into the external flow field of the body and burns, thereby altering the flow field and producing forces on the body due to the combined effects of flow interactions and heat addition. Although subsonic applications of external burning may be feasible, only supersonic flight velocities are considered. Systems of this type have been rather extensively studied during the past several years and experiments have been made which have demonstrated the feasibility of the external burning concept, but in general they have shown only part of the performance potential of the system. The available unclassified literature in this area is reviewed and conclusions are drawn regarding the limitations of external burning systems based principally on the phenomena observed in the tests reported.

The generation of useful forces on the external surfaces of an aerodynamic body requires deflection of the streamlines in the flow field about the body in such a manner that increased pressures are produced on chosen surface areas. Consider the external flow fields above the flat plates sketched in Fig. 1. Undisturbed streamlines are shown in (a), and the other sketches show the disturbed streamlines pattern caused by an aerodynamic flap (b), mass addition, (c), and mass addition plus heat addition (external burning) (d). The corresponding surface pressure profiles also are

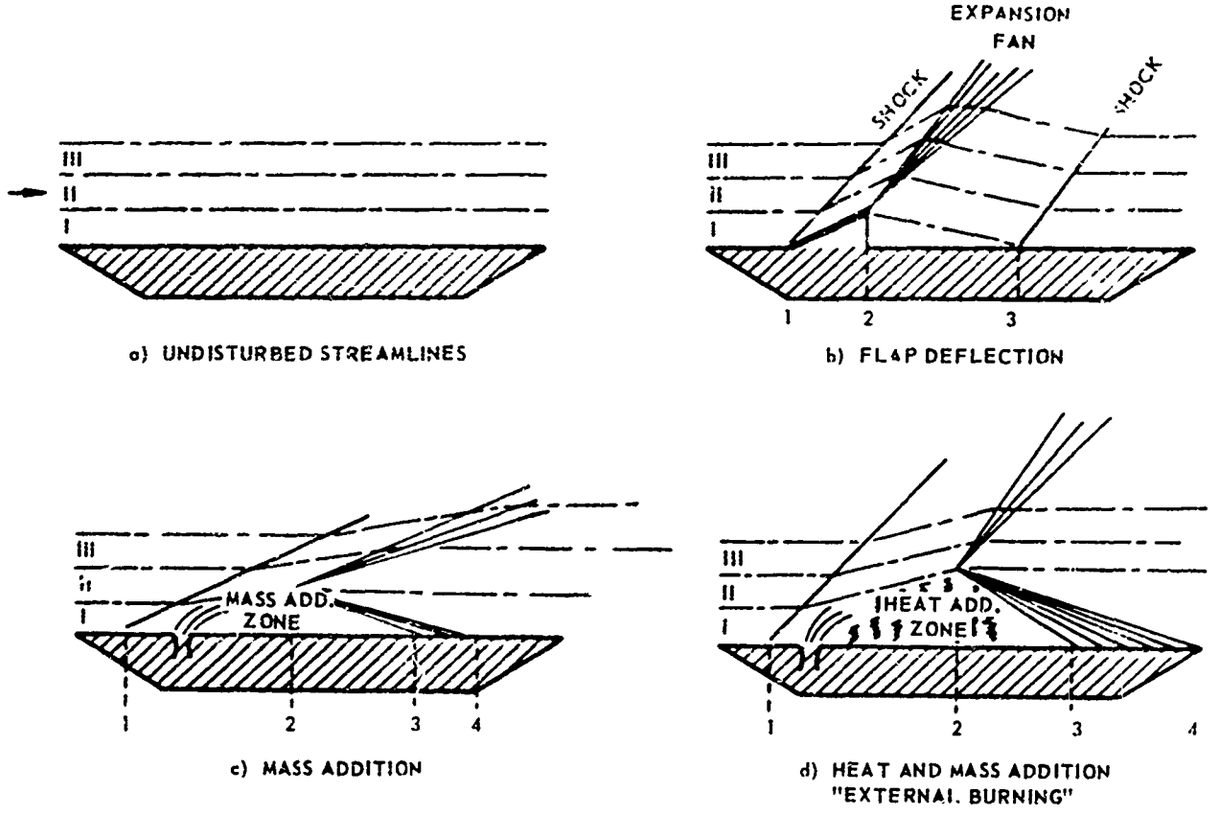

a) UNDISTURBED STREAMLINES

b) FLAP DEFLECTION

c) MASS ADDITION

d) HEAT AND MASS ADDITION
"EXTERNAL BURNING"

A) STREAMLINE PATTERNS

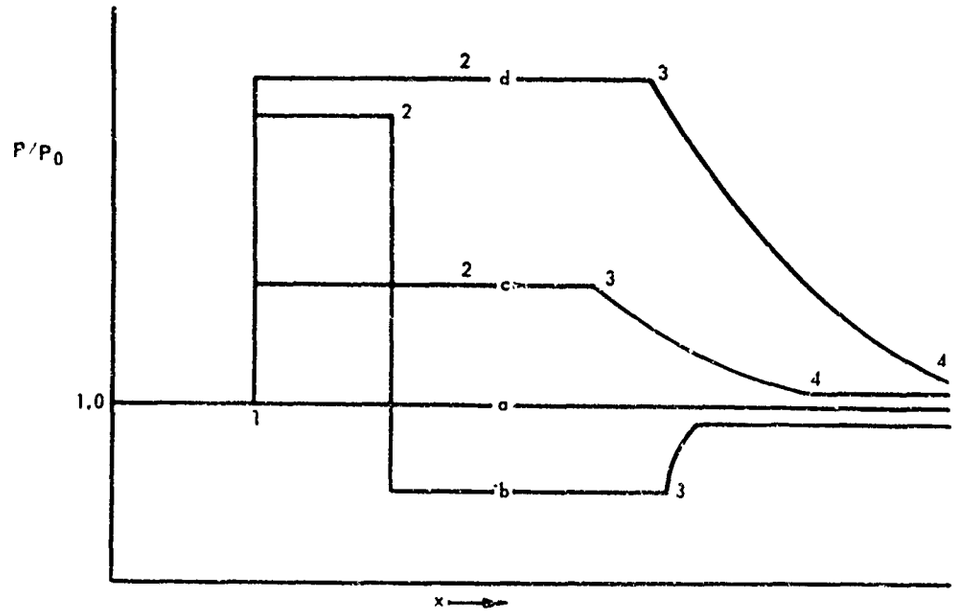

B) SURFACE PRESSURE PROFILES

Fig. 1 STREAMLINE PATTERNS FOR VARIOUS FLAT PLATE SYSTEMS IN A SUPERSONIC FLOW, AND THE CORRESPONDING SURFACE PRESSURE PROFILES

shown in Fig. 1 by the correspondingly lettered curves. For case (b), the pressure rise due to streamline deflection at station 1 must be followed by expansion to below ambient pressure at 2 and then recompression to about p_0 at 3. Thus, to obtain the greatest net positive force, the flap should be positioned sufficiently far aft so that station 2 corresponds to the trailing edge of the plate. Furthermore, there is an attendant drag force penalty on the flap. For simplicity, in cases c and d the heat and/or mass addition is confined to streamtube I in a zone of finite length 1-2 and is assumed to occur at constant pressure. The surface pressure is sustained, however, until the first expansion wave strikes the surface at 3, then the pressure declines to a value near p_0 at 4. In effect, the heat addition (and the mass addition to a lesser degree) represents a volume source in streamtube I which turns adjacent streamtubes (II, III, etc.) giving a pressure rise, similar to the case of the flap but with a significantly lesser expansion effect and no drag penalty. In addition to the pressure force there is a reaction force caused by injection, which has components in the thrust and/or lateral directions, depending on the angle of injection.

The foregoing crude description of the effects of the heat and mass addition zones is oversimplified, because they need not be zones of constant pressure, and the details of boundary layers and possible attendant separated zones have been omitted. However, from sketch d it is apparent that to obtain the greatest total normal force from the positive pressure field developed by the external burning case, it is necessary to extend the surface to the end of the expansion zone (point 4). On the other hand, a higher force coefficient [force/(dynamic pressure x area)] would be obtained if the plate were cut off

at point 3. This point and the effect of initial pressure level are discussed further in a later section.

The possible applications of the external burning principle fall into three classes: (A) side-force generating devices for attitude control, (B) thrust-generating (or drag-reducing) devices, and (C) devices which produce both thrust and attitude control (or lift). Sketches of possible configurations are shown in Fig. 2. The attitude controller for an axisymmetric vehicle [Fig. 2(A)] has injection aft of the center-of-gravity in any one of four quadrants. Longitudinal "fences" separate the quadrants to reduce the dissipation of the positive pressure field through circumferential spillover. Note that the downward force due to external burning leads to positive pitch and therefore puts the external burning region in the leeward zone, which could, at large pitch angles, produce adverse conditions for combustion. However, if the external burning is being used solely to trim the body, then it is conceivable to design an aerodynamically unsteady vehicle, in which case the external burning will always occur in the windward zone. Attitude control systems based on external burning ahead of the c.g. are conceivable but appear to be less attractive due to the difficulty of confining the positive pressure field to produce an effective pitching moment. The thrust generating device, Fig. 2(B), could conceivably be either the total vehicle or a podded or airfoil engine. At the "knee" fuel is added to the air compressed by oblique shock and/or isentropic turning on the forebody, and combustion maintains a positive pressure field on the aft body which is greater than that or the compression

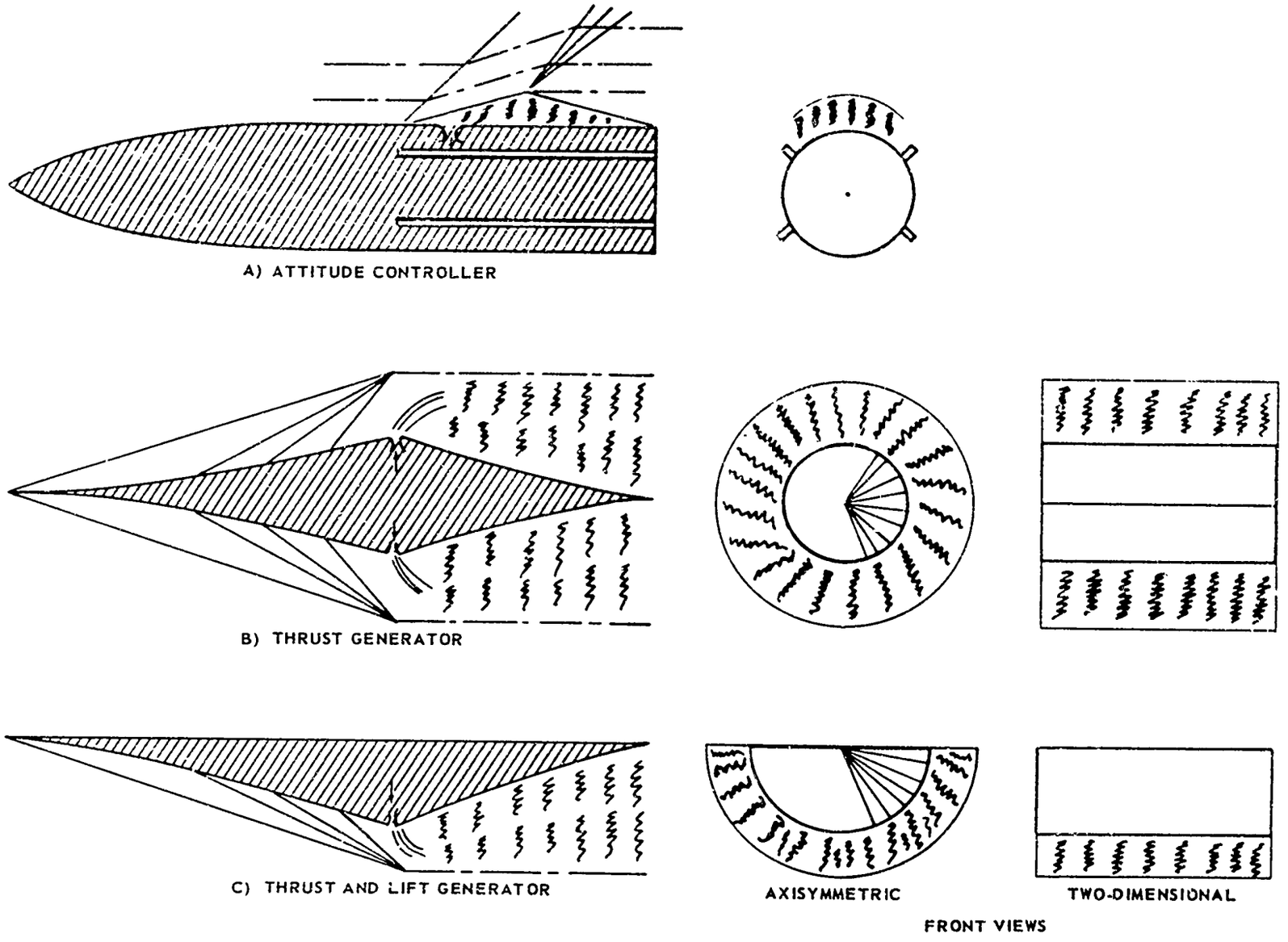

Fig. 2 EXTERNAL BURNING CONFIGURATIONS

surface, thus producing net thrust. Both axisymmetric and two-dimensional configurations are possible for this case and the combined thrust and lift case, 2(C). The combined device, which has a flat top (hence no positive pressure on top) but a positive pressure field over its entire lower surface develops considerable lift. It could be used as a "propulsive wing" or "external burning ramjet (ERJ)". Analysis of configurations (B) or (C) has shown them to have efficient thermodynamic cycles only at very low thrust levels, i.e., in cruising flight, as shown later. For accelerating missions, ducted conventional ramjets or supersonic combustion ramjets (scramjets) are considerably more efficient.

2. LITERATURE REVIEW OF THEORETICAL ANALYSES OF EXTERNAL BURNING

Theoretical analyses of the effect of heat addition to external supersonic flow fields began to appear in the literature about fifteen years ago, and the first (then) classified experimental results followed one to two years later. Following the very fundamental work in one-dimensional diabatic flow, [1-9] Pinkel and Serafini[10] extended the method of characteristics to include the effects of heat addition in an irrotational supersonic flow and developed a graphical method of solution for shock-free flow with heat addition. Using this technique it is possible to find an exact solution (with the above constraints to the flow field and pressure distribution) for flows having continuous total temperature variation in the streamwise direction. In Reference 11 this method was used to determine the pressure distribution and aerodynamic coefficients of a symmetrical circular arc/wing (Fig. 3) for flight Mach numbers (M_0) of 3 and 5. For moderate total temperature ratios over

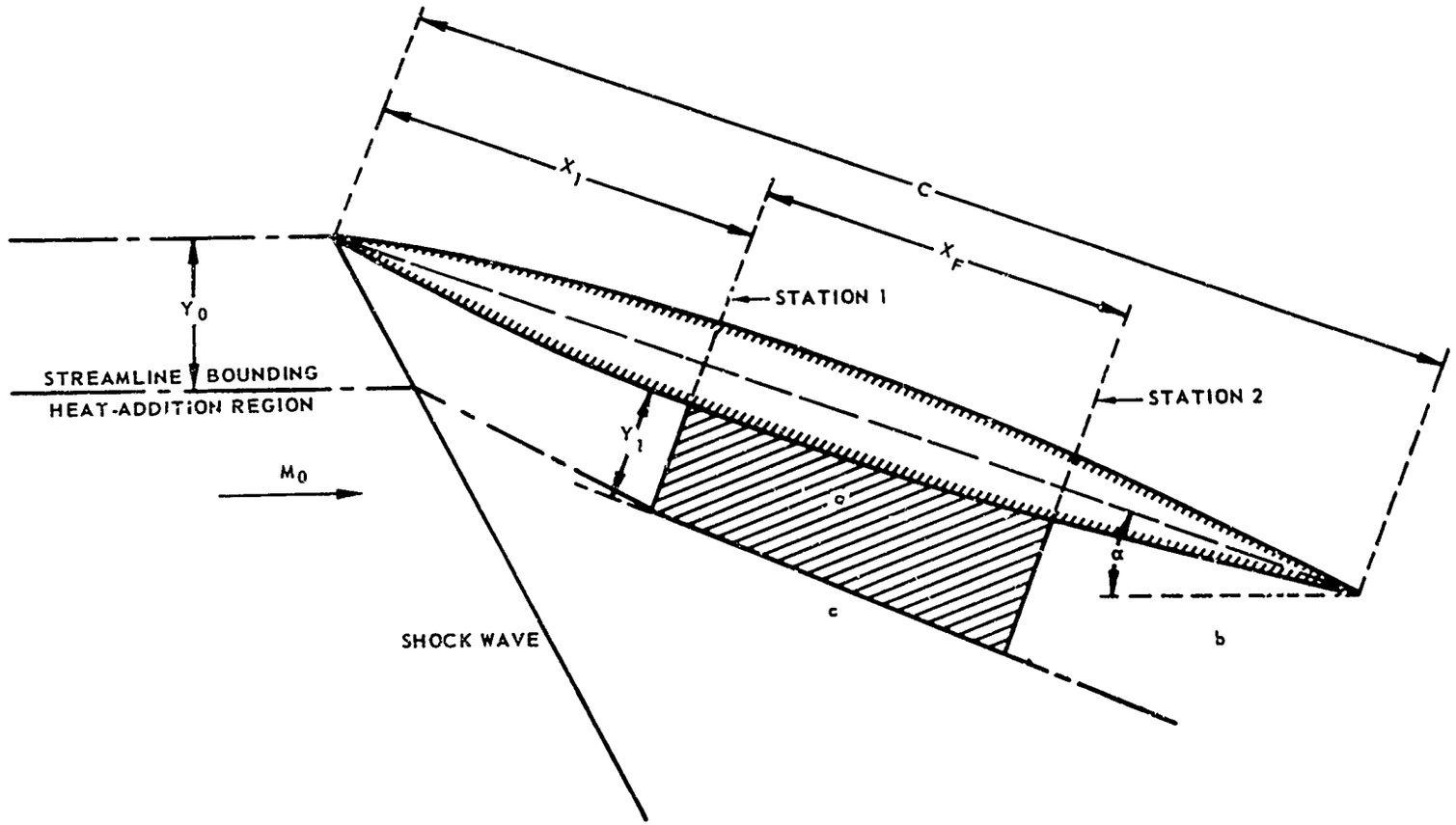

a REGION WHERE THE HEAT ADDITION IS OCCURRING
b REGION OF HEATED FLOW, BUT WITHOUT FURTHER ADDITION OF HEAT CONTENT
c REGION OF UNHEATED FLOW

Fig. 3 EXTERNAL BURNING MODEL FOR CIRCULAR ARC AIRFOIL (Ref. 11)

the heat addition zone (T_{t_2}/T_{t_1} = 1.243 and 1.126), the heat release beneath the middle portion of the airfoil produces a significant pressure rise, markedly increasing the lift and slightly decreasing net drag (5-10%) so that the lift/drag ratio (L/D) and quarter-chord moment coefficient are increased by factors of 1.7 to 2.2, and 2.5 to 4.2, respectively, compared to no-heat-addition values.

One of two motivations has inspired succeeding authors to find other methods of analyzing external burning:

1) Greater simplicity.--The method of Ref. 10 is tedious and does not lend itself to simple evaluation of the important variables which affect performance. The approaches used to simplify the problem involve either linearization of the equations of motion or postulation of a one-dimensional heat addition process (e.g., constant area or constant pressure).

2) Greater realism.--As experimental data from external burning tests have accumulated it has become possible to postulate new analytical models which include effects that have been observed and lead to closer correlation of theory with experiment.

2.1 Linearized Solutions

An approximate formula for a linearized solution for the pressure field generated by a moderate rate of heat release was developed from first principles by Chu.[12] Gazley[13] arrived at the identical result by employing a "piston" concept to translate the effect of heat addition into an effective deflection of the flow. The result given by these authors can also be obtained by considering the streamline deflection caused by heat addition in the simple

model shown in Fig. 4(A). Heat is added to streamtube I in the region from 1 to 2, increasing the streamtube height from Y_1 to Y_2 and causing a deflection, δ_H, to adjacent streamlines. If $\dot{q}$ is the rate of heat addition per unit area and Q is the heat addition per pound of air, then from continuity and the equation of state

$$\rho_1 u_1 Y_1 = \rho_2 u_2 Y_2, \qquad \text{or } p_1 u_i Y_1/T_1 = p_2 u_2 Y_2/T_2 \tag{1}$$

and from the geometry,

$$\frac{[Y_2/\cos(\delta_H/2)] - Y_1}{X_f} = \tan \delta_H \tag{2}$$

From linear theory (small deflections)

$$u_2 \approx u_1, \qquad \cos(\delta_H/2) \approx 1, \qquad \text{and } \tan \delta_H \approx \delta_H \tag{3}$$

Therefore

$$\therefore (Y_2 - Y_1)/X_f \approx \delta_H \tag{4}$$

From conservation of energy,

$$T_2 = T_1 + QgJ/c_p \tag{5}$$

From conservation of momentum, $p_2 \approx p_i$, since $u_2 \approx u_i$; Eq. (1) becomes

$$Y_1/T_1 = Y_2/T_2 \tag{6}$$

therefore, substituting (5) and (6) into (4),

$$\delta_H = \frac{\frac{Y_1}{T_1}\left(T_1 + \frac{QgJ}{c_p}\right) - Y_1}{c_p T_1 X_f} = \frac{QgJ\, Y_1}{c_p T_1 X_f} \tag{7}$$

but

$$\dot{q} = QgJ\, Y_1\, \rho_1\, u_1/X_f \tag{8}$$

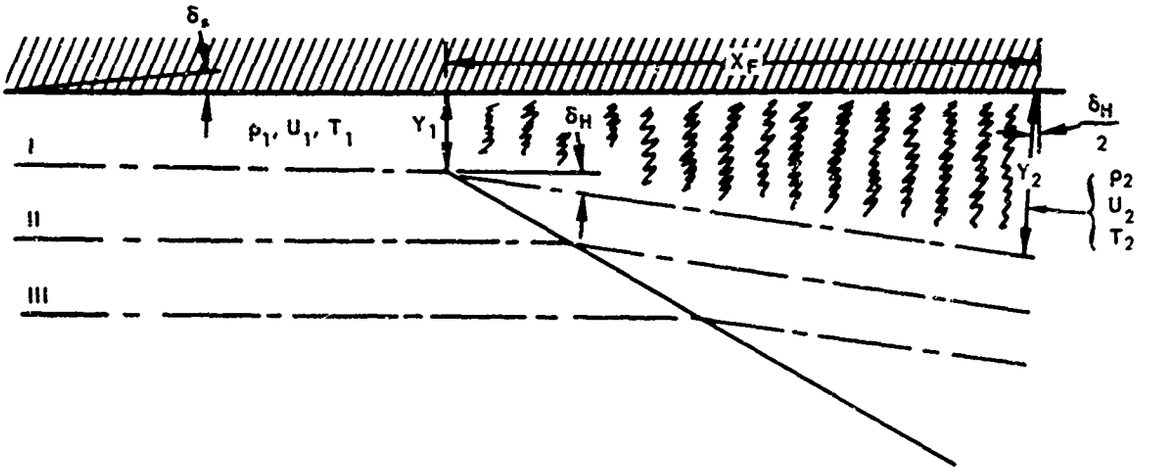

A) GENERAL THEORETICAL MODEL

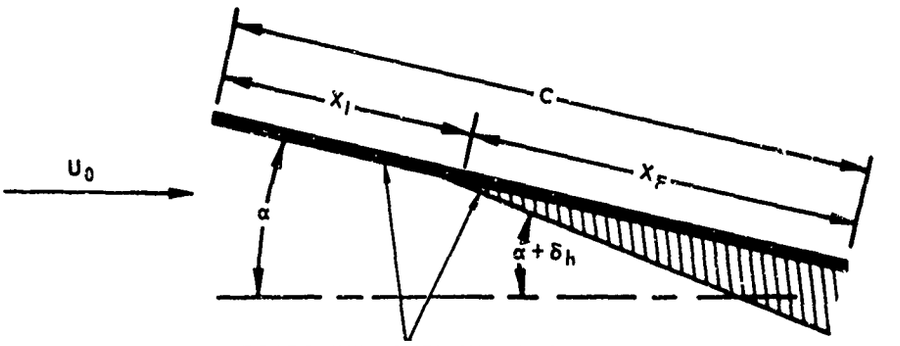

EFFECTIVE LOWER SURFACE

B) FLAT-PLATE AIRFOIL WITH LINEARIZED HEAT ADDITION ON LOWER SURFACE

Fig. 4 LINEARIZED HEAT ADDITION MODEL

so

$$\delta_H = \frac{\dot{q}}{c_p \rho_1 u_1 T_1} = \frac{\dot{q}}{c_p p_1 u_1 / R} = \left(\frac{\gamma - 1}{\gamma}\right) \frac{\dot{q}}{p_1 u_1} \tag{9}$$

resulting in the same expression for the turning angle, δ_H, as a function of the ratio of heat addition per unit area as was developed in Refs. 12 and 13. Pressure coefficients for various heat additions can then be obtained by using the familiar linearized supersonic flow result,

$$C_p = 2\,\delta/(M_0^2 - 1)^{\frac{1}{2}} \tag{10}$$

Since linear solutions may be superimposed, a general equation for the pressure coefficient of a body with heat addition deflection δ_H and surface inclination δ_S, can be obtained, viz:

$$C_p = 2\,(\delta_S + \delta_H)/(M_0^2 - 1)^{\frac{1}{2}} \tag{11}$$

Using this approach Gazley showed that the lift and drag coefficients for a flat plate airfoil at angle-of-attack, α, with heat addition over a fraction, $f = X_f/C$, of the plate (Fig. 4B) are:

$$C_L = 4\,(\alpha + \tfrac{1}{2}\,\alpha\, f\, \delta_H)/(M_0^2 - 1)^{\frac{1}{2}} \tag{12}$$

and

$$C_D = 4\,(\alpha^2 + \tfrac{1}{2}\,\alpha\, f\, \delta_H)/(M_0^2 - 1)^{\frac{1}{2}} \tag{13}$$

For a biconvex airfoil of thickness-chord ratio of τ/C the same expression Eq. (11) holds for C_L and

$$C_D = \frac{4\left[\frac{4}{3}\left(\frac{\tau}{C}\right)^2 + \alpha^2 + \frac{1}{2}\alpha f \delta_H - \frac{\tau}{C} f (1 - f) \delta_H\right]}{\left(M_0^2 - 1\right)^{\frac{1}{2}}} \tag{14}$$

He then shows (Fig. 5) for the 5-percent-thick biconvex airfoil that the linear and exact solutions of Pinkel,[11] et al agree well at low heat addition rates and start to deviate at higher heating rates where both methods become inaccurate. The calculations show that for small negative angles-of-attack and heating deflections of greater than 5 or 6 degrees, net thrust can be produced. Moreover, by defining a specific impulse based on (drag cold - drag hot)/(fuel flow rate) for a given lift force, where the angle-of-attack for the hot flow,

$$\alpha_H = \alpha_C - \tfrac{1}{2} f \delta_H, \tag{15}$$

is smaller than the cold value, specific impulses of 300 to 1800 sec are computed for a fuel with a heating value of 20,000 Btu/lb.

Mager[14] arrived at essentially the same results as Gazley and showed good agreement with the more exact solution of Ref. 10 for the circular arc-airfoil. He started with the general definition of the pressure, velocity and density disturbances caused by a heat source in supersonic flow as suggested by Tsien[15] and used a slightly different method of linearization. In addition, he developed a set of performance indices to compare external burning (ERJ) configurations with a winged vehicle using conventional ducted subsonic combustion ramjets (CRJ). He concluded that the energy requirements during cruise were comparable for the two engine systems. He included the estimated skin friction drag and concluded that it is more profitable to take advantage of the additional force generated by heat addition by decreasing

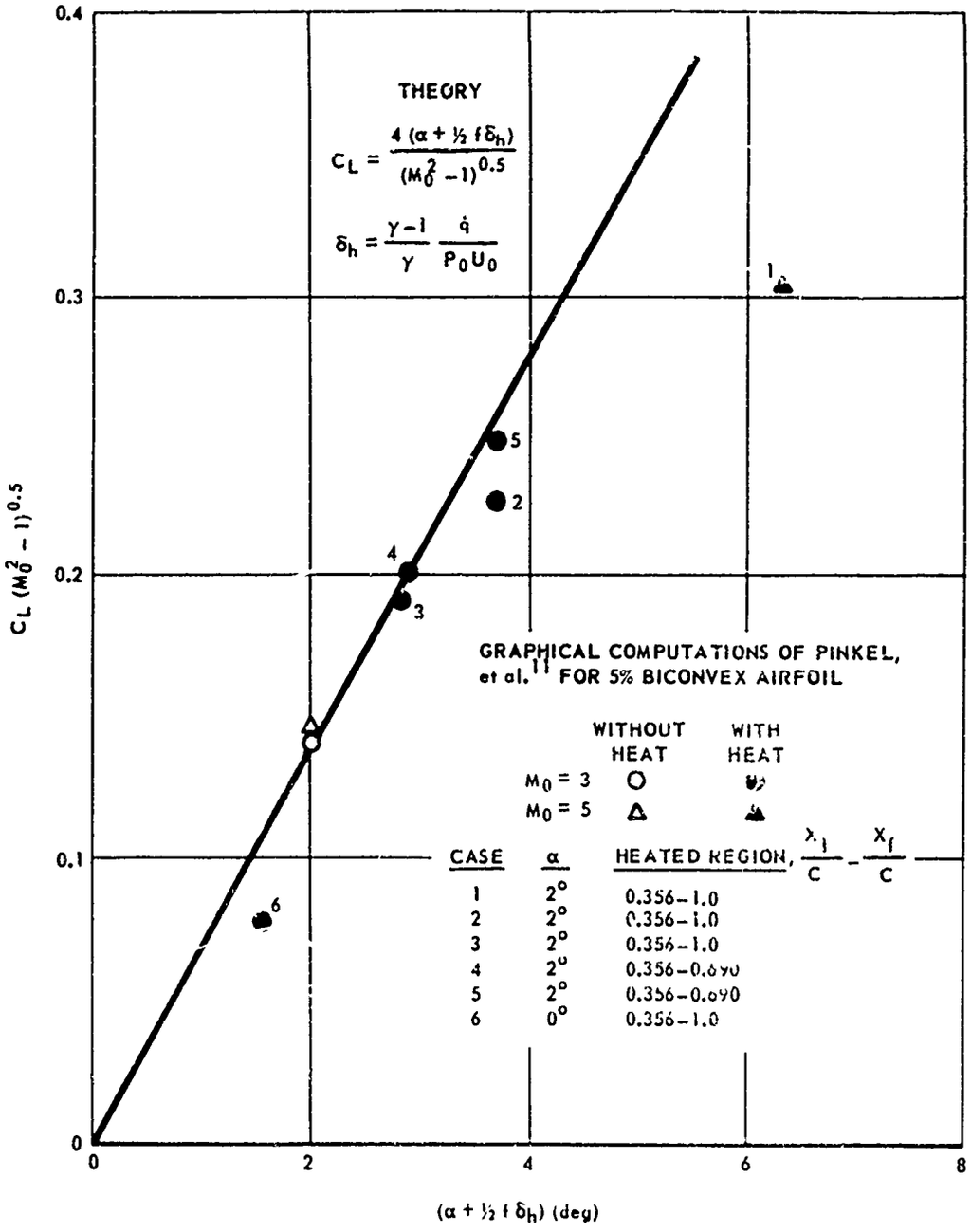

Fig. 5 LIFT OF SUPERSONIC AIRFOIL WITH HEAT ADDITION ON LOWER SURFACE. (Ref. 13)

wing area (and friction drag) and operating at the same angle-of-attack rather than maintaining the same wing area and reducing α (and wave drag).

2.2 Planar Heat Addition

Another simplified method of approach to the theoretical solution of the external heat addition problem is to postulate planar heat addition at some angle to the air flow, i.e., from a physical standpoint, an infinitely fast heat release. The theoretical models which have been postulated include both normal and oblique planar heat additions, with or without accompanying shock waves, as shown in Fig. 6. Figure 6(A) shows a simple, normal, planar heater, which in effect is a one-dimensional, constant-area heat addition. All of the changes in properties across the heater can be obtained from the well-known one-dimensional equations.[16] For incoming supersonic flow ($M_0 > 1$) of streamtube I there is a pressure rise due to head addition and a corresponding downstream Mach number, $M_2 \geq 1$. Adjacent streamtubes (II, III, etc.) must compensate for this pressure rise by turning through an oblique shock wave. The incompatability in flow direction and pressure downstream is then resolved by a series of expansion waves downstream. In Fig. 6(B) the normal heater is preceded by a normal shock wave, so that the flow upstream of the heater (1) is subsonic. Subsonic constant-area combustion must then be postulated, with $M_2 \leq 1$. This process is generally referred to as a strong detonation, and its limiting case for $M_2 = 1$, when the distance between the shock wave and the heating wave becomes vanishingly small, is called a Chapman Jouguet detonation. Although solutions of the equations of motion permit both the reverse order of the processes and supersonic Mach numbers at 2, the very unrealistic kinetic situation of combustion occurring

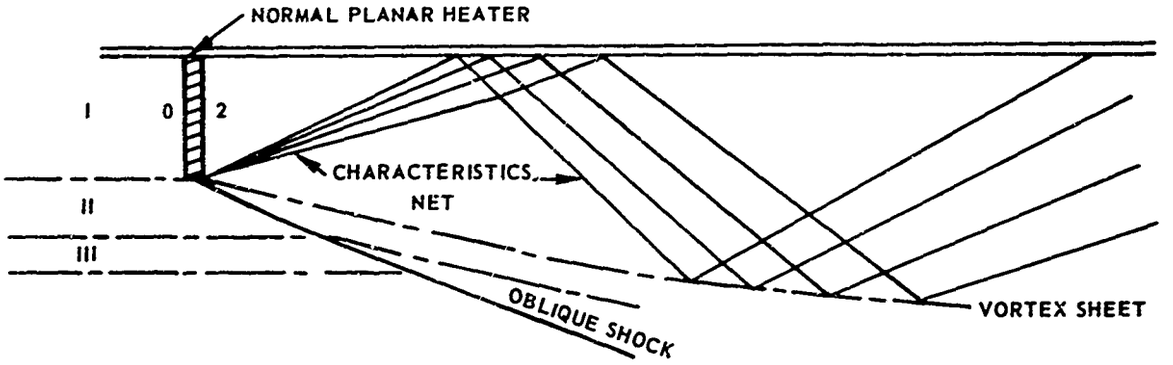

A) NORMAL WEAK DETONATION

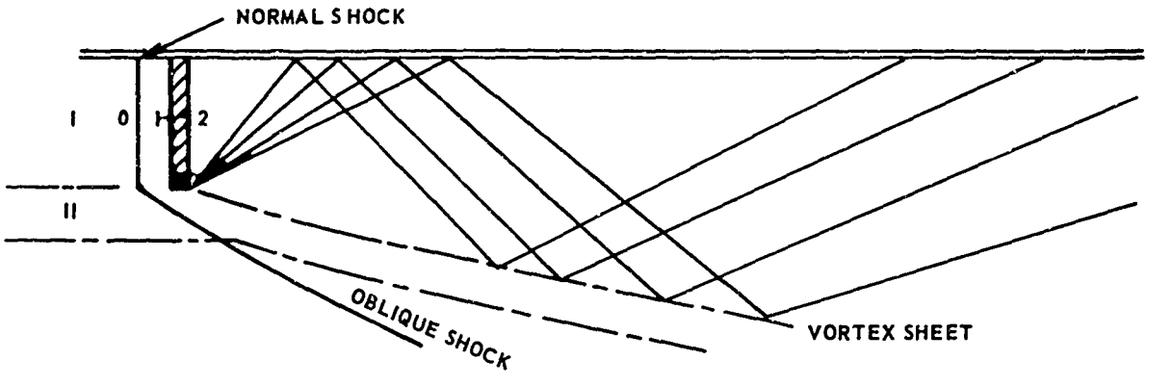

B) NORMAL STRONG OR CHAPMAN-JOUGET DETONATION

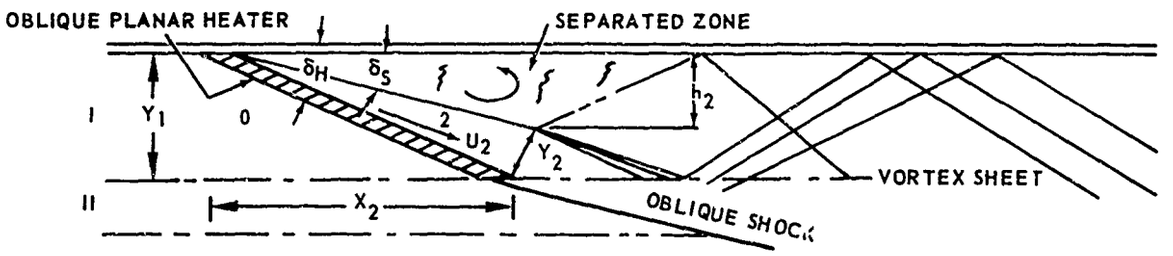

C) OBLIQUE WEAK DETONATION

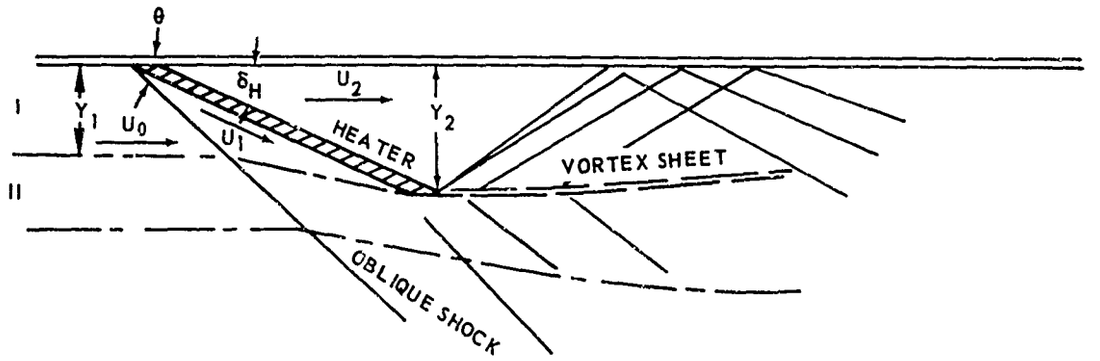

D) OBLIQUE STRONG OR CHAPMAN-JOUGET DETONATION

Fig. 6 THEORETICAL MODELS FOR PLANAR HEAT ADDITION

at lower rather than higher pressure and temperature forbids the former, and entropy considerations rule out the latter. Again, pressure compensation in the external stream can be accomplished by an oblique wave, because although the pressure at 1 is the normal-shock value, the pressure at 2 is lower (subsonic, constant-area heat addition), so that a shock weaker than a normal shock will balance the pressure. Rather than considering the difficult expansion case of $M_2 < 1.0$, most authors have chosen to study the Chapman Jouguet case of $M_2 = 1.0$, which for the model shown, will only occur at a specified temperature ratio, T_2/T_1, for each free stream condition. To avoid this limitation, a subsonic compression (streamtube enlargement) of the flow is postulated in region 1' in such a manner that the condition of $M_2 = 1.0$ is always met.

Figure 6(C) shows an oblique heater of normal height Y_1. This is analytically handled by applying the one-dimensional, constant-area heat addition equations to the normal component of the upstream velocity. Note, however, that the downstream velocity vector, u_2, must be directed away from the surface, which means that some type of separated zone would have to exist downstream of the heat addition plane and would have to extend to a height, h_2:

$$h_2 = 1 - (\rho_1 u_1/\rho_2 u_2) \cos \delta_S \tag{16}$$

and the tangent of the separation angle is $\tan \delta_S = \dfrac{h_2 \sin (\delta_H - \delta_S)}{Y_1 - h_2}$ (17)

Downstream of X_2 the flow would have to expand and turn to adjust pressure and flow direction. The flow in streamtube II which does not undergo a rise in stagnation temperature needs to be turned through a lesser angle (by an

oblique shock) to reach p_2 than does the flow in streamtube I, so that a vortex sheet must exist downstream of X_2. Note that in these simplified models the heat addition is limited to streamtube I and there is no mixing with adjacent streamtubes. Therefore, even though the pressure is matched along the boundary between I and II, the entropy is greater in I, and a vortex sheet must divide these two regions of the flow.

The last case, shown in Fig. 6(D) and detailed in Fig. 7, is the strong oblique detonation, i.e., the oblique planar heat addition is preceded by an oblique shock wave, and the component of velocity u_{2N}, normal to the heater plane angle, δ_H, is subsonic. Again, the special case of $M_{2N} = 1.0$ would be called an oblique Chapman Jouquet detonation. Presumably all combinations of oblique shock angles, θ, and heater angles, δ_H, are possible as long as; a) the flow behind the oblique shock is supersonic, b) θ is below the shock detachment angle for the local Mach number, and c) the required heat release is not excessive. However, as noted by Willmarth,[17] for each θ there is one value of δ_H which results in a velocity vector u_2 after heat addition which is aligned to the surface. The model based on this particular situation has the virtue of not requiring a separated zone as in Fig. 6(C). The vector diagram shown in Fig. 7 for this special case shows that for a given θ and δ_H the tangential components of velocity are related

$$u_{0T} = u_{1T} = u_0 \cos \theta \quad . \tag{18}$$

$$u'_{1T} = u_{2T} = u_2 \cos \delta_H \tag{19}$$

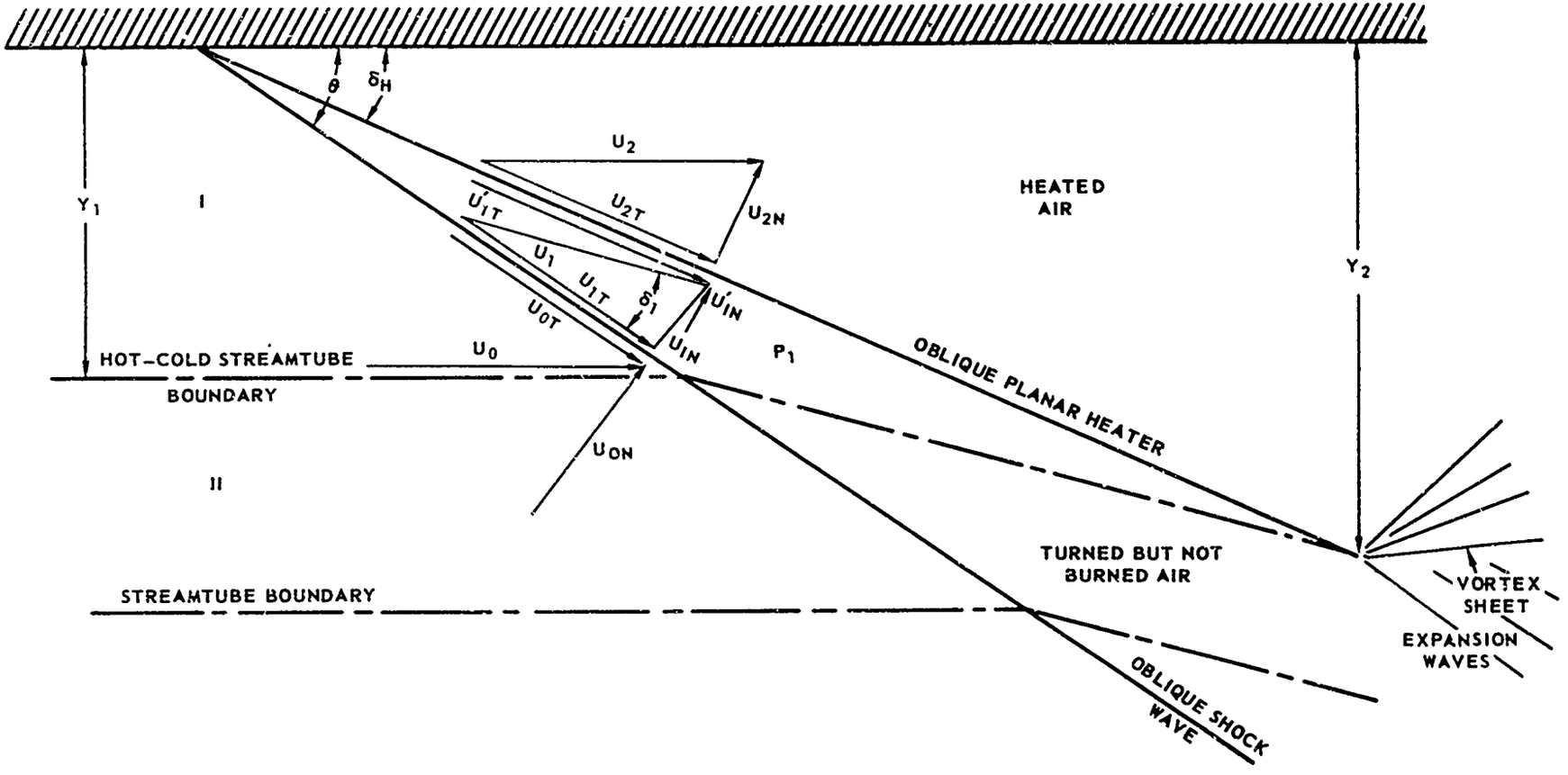

Fig. 7 SCHEMATIC DIAGRAM FOR STRONG OBLIQUE DETONATION

From the oblique shock relationships[16]

$$u_{1N} = u_0 \left[\frac{(\gamma - 1) M_0^2 \sin^2 \theta + 2}{(\gamma + 1) M_0^2 \sin \theta} \right] \tag{20}$$

$$p_1 = p_0 \left[\frac{2 \gamma M_0^2 \sin^2 \theta - (\gamma - 1)}{\gamma + 1} \right] \tag{21}$$

$$T_1 = T_0 \left[\frac{[2 \gamma M_0^2 \sin^2 \theta - (\gamma - 1)][(\gamma - 1) M_0^2 \sin^2 \theta + 2]}{(\gamma + 1)^2 M_0^2 \sin^2 \theta} \right] \tag{22}$$

From the geometry

$$u'_{1N} = \frac{u_{IN} \sin (\delta_1 + \delta_H - \theta)}{\sin \delta_1} \tag{23}$$

and

$$u_{2N} = \frac{u'_{IN} \tan \delta_H}{\tan (\delta_1 + \delta_H - \theta)} \tag{24}$$

where

$$\delta_1 = \tan^{-1} u_{IN}/u_0 \cos \theta \tag{25}$$

The required amount of heat is found by using the conservation equations for one-dimensional constant area heat addition[16]

$$gJ Q = \frac{u_{2N}^2}{2} - \frac{u_{1N}^2}{2} + c_p T_1 \left(\frac{p_2}{p_1} \frac{u_{2N}}{u'_{1N}} - 1 \right) = \dot{q}/\rho_1 u'_{1N} \tag{26}$$

where

$$\frac{p_2}{p_1} = 1 + \frac{\rho_0 u_0 (u'_{IN} - u_{2N}) \sin \theta \sin (\delta_1 + \delta_H - \theta)}{p_1 \sin \delta_1} \tag{27}$$

Using the example chosen in Ref. 17 of $M_0 = 2.0$ at 30,000 ft altitude but extending the planar heat addition analysis to large heater angles gives the results shown in Figs. 8 and 9. In Fig. 8, $\dot{q}$, the heating rate per unit area is shown as a function of the surface pressure rise, $p_2 - p_1$, for various heater angles, δ_H. Lines of constant turning, $\theta - \delta_1$, which imply constant shock angles, θ, are also shown. The curves are bound on the left by the Chapman Jouguet limit ($M_{2N} = 1.0$) at low pressure rise and by the maximum attached-shock strength at higher pressure. On the right, the curves are bounded by a maximum heating rate, because the temperature rise across the heater becomes infinite as $\delta_H \rightarrow (\theta - \delta_1)$. For a given pressure rise the oblique detonation processes require more heat release than that predicted by linear theory because of the inclusion of the turning losses. In Fig. 9 this effect is shown in curves of pressure rise per unit energy release, or "lifting efficiency" for various turning angles. As the heater and turning angles approach zero, the linear theory value of $\Delta p/\dot{q}$ obtained by combining Eq.s (9) and (10),

$$\frac{\Delta p}{\dot{q}} = \frac{(\gamma - 1)M_0^2}{u_0 (M_0^2 - 1)^{\frac{1}{2}}} \tag{28}$$

or 4.65×10^{-4} sec/ft in the example, is approached.

Woolard[18,19] studied the same case of strong oblique detonations and lists tables of properties for a range of conditions in Ref. 18. Similar tables have been generated by Chinitz, et al.[20] In Ref. 19, Woolard develops a set of equations similar to Eqs. (18-27) for conical rather than two-dimensional flows. Parametric curves are presented for Chapman Jouguet detonative flows about cones.

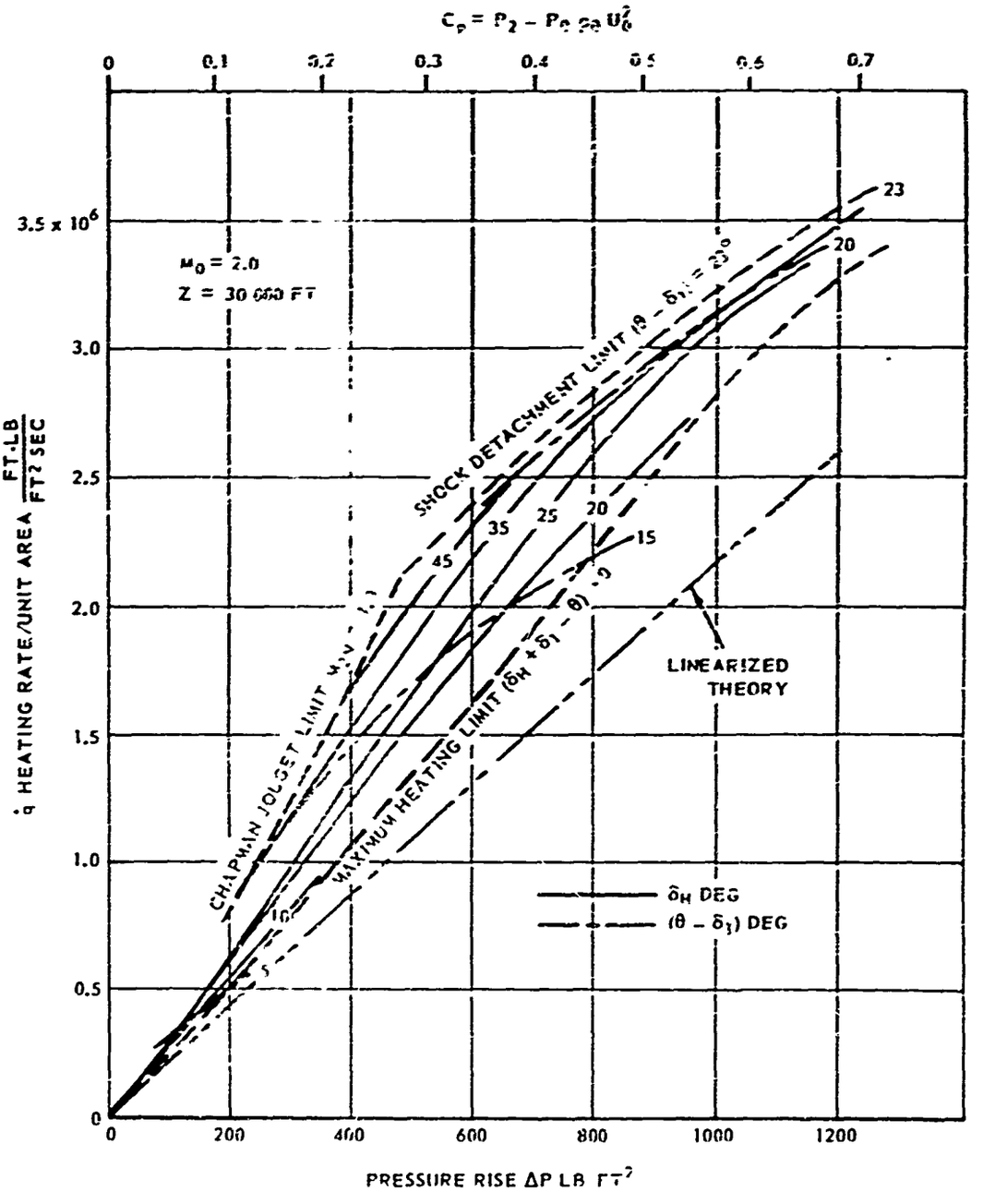

Fig. 8 PRESSURE RISE DUE TO OBLIQUE DETONATION FOR VARIOUS HEATER ANGLES.

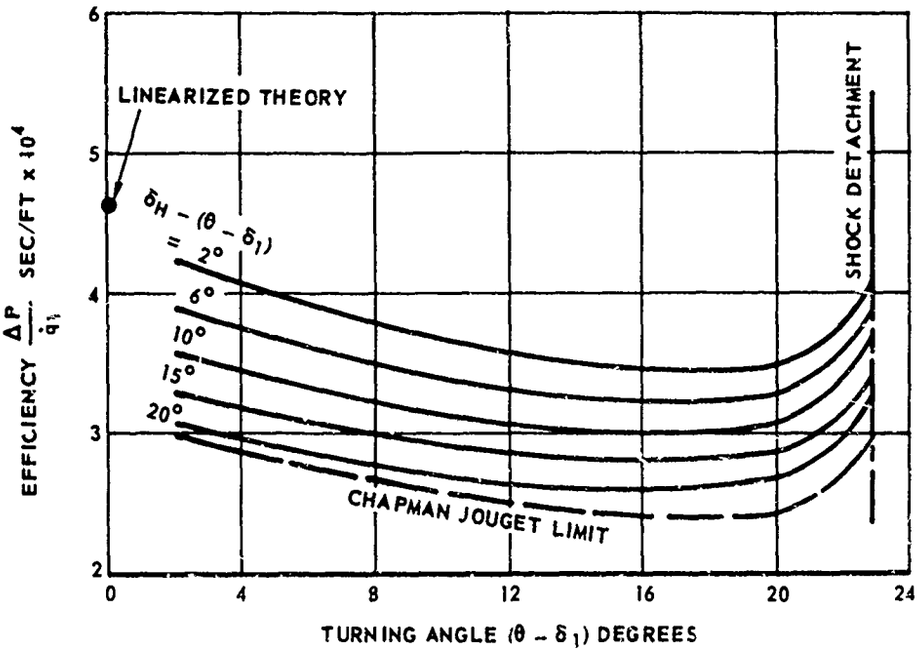

Fig. 9 PRESSURE RISE PER UNIT ENERGY RELEASE FOR OBLIQUE DETONATIONS

Refinements to the oblique planar heater model of Wilmarth can be made. One of these is to consider multiple oblique heater planes having a common origin rather than a single planar heater. For example, in the case of two oblique heater planes, the analysis for the first heater plane is the same as before except that the flow velocity vector behind this heater is directed away from the plate. Turning through the second heater, which can be described by Eqs. (18-27), changing subscripts, then aligns the flow with the plate. Typical calculations made at $M_0 = 6.0$ and $Z = 20{,}000$ ft showed that for a given heater flux the two heater plane case predicts a 3-3.5 per cent lower pressure rise than the single heater. In effect, in the limit, an infinite number of weak centered planar heaters becomes a wedge-shaped continuous heat addition process. From a physical point of view, this implies the rather untenable situation of a reaction requiring a rate of temperature rise in the streamwise direction that is proportional to the distance from the surface.

A second extension is to consider the expansion region downstream of the constant pressure zone for a finite heater height (Y_2, Fig. 7). The pressure decays in the region behind the first Mach line emanating from the terminal point of the planar heater, thus, the surface pressure drops when the Mach line reaches the surface. This decaying (but still positive) pressure field which occurs without an additional expenditure of energy therefore results in a higher specific impulse than that shown by Wilmarth. Several methods of calculation of this decaying pressure field have been suggested by other authors and are described in the subsequent discussion.

Luidens and Flaherty applied the normal weak detonation[21] model of Fig. 6(A) to the ERJ model of Fig. 10(A). Calculations were made for various combinations of wedge angles ϵ_1 and ϵ_2 at different angles-of-attack in order to determine the optimum wing geometry and angle-of-attack. The ERJ performance was based on a specific lift parameter L/h $\dot{w}_f$, where h is the heating value of the fuel, which can be related to range through the conventional Breguet range equation for the case when thrust equals drag and lift equals weight:

$$R = \frac{L}{\dot{w}_f} \frac{u_0}{\left[1 - \left(\frac{u_0}{u_s}\right)^2\right]} \ell n \frac{W_0}{W_B} \tag{29}$$

Most of the calculations were made using the linearized theory and showed that "... a wing designed for maximum L/h $\dot{w}_f$ will have the following characteristics: a moderate thickness ratio, a flat top surface, and the maximum-thickness point of the wing well downstream (i.e., $\epsilon_2 > \epsilon_1$). It should be operated at maximum angle-of-attack (i.e., 1° to 3°)....." More rigorous calculations, using the method of characteristics for the downstream expansion [Fig. 6(A)] were made and showed efficiencies of about half those estimated by linear theory. A few calculations were made to show that performance could be improved by distributing heat sources in Region II of Fig. 10(A). Finally, they compared ERJ's with conventional ramjet (CRJ) cruise vehicles with wings and obtained Fig. 10(B). Curves A and B are for CRJ's, A being quite optimistic and B more conservative. Curve C represents optimistic performance of an ERJ

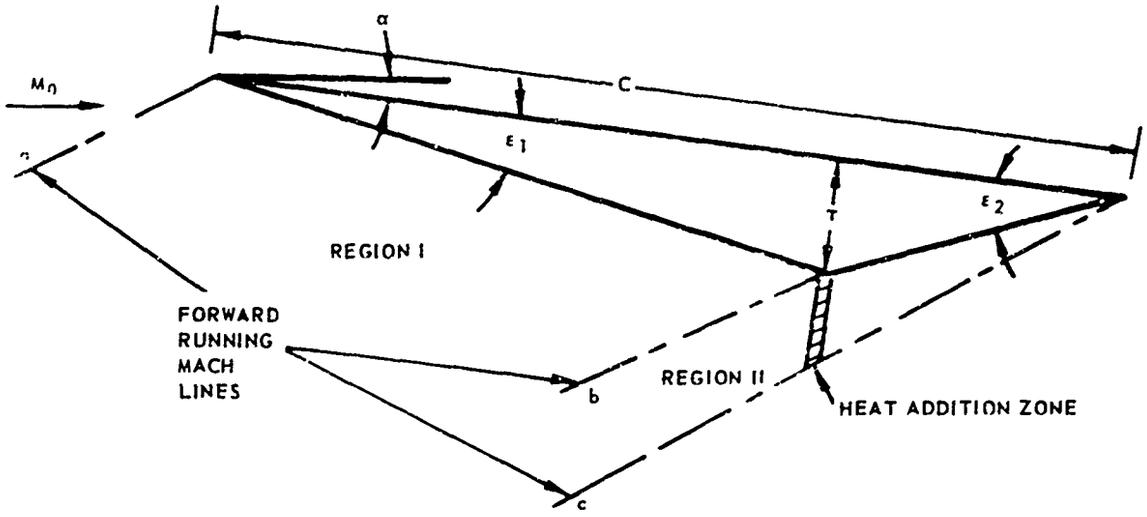

A) MATHEMATICAL MODEL.

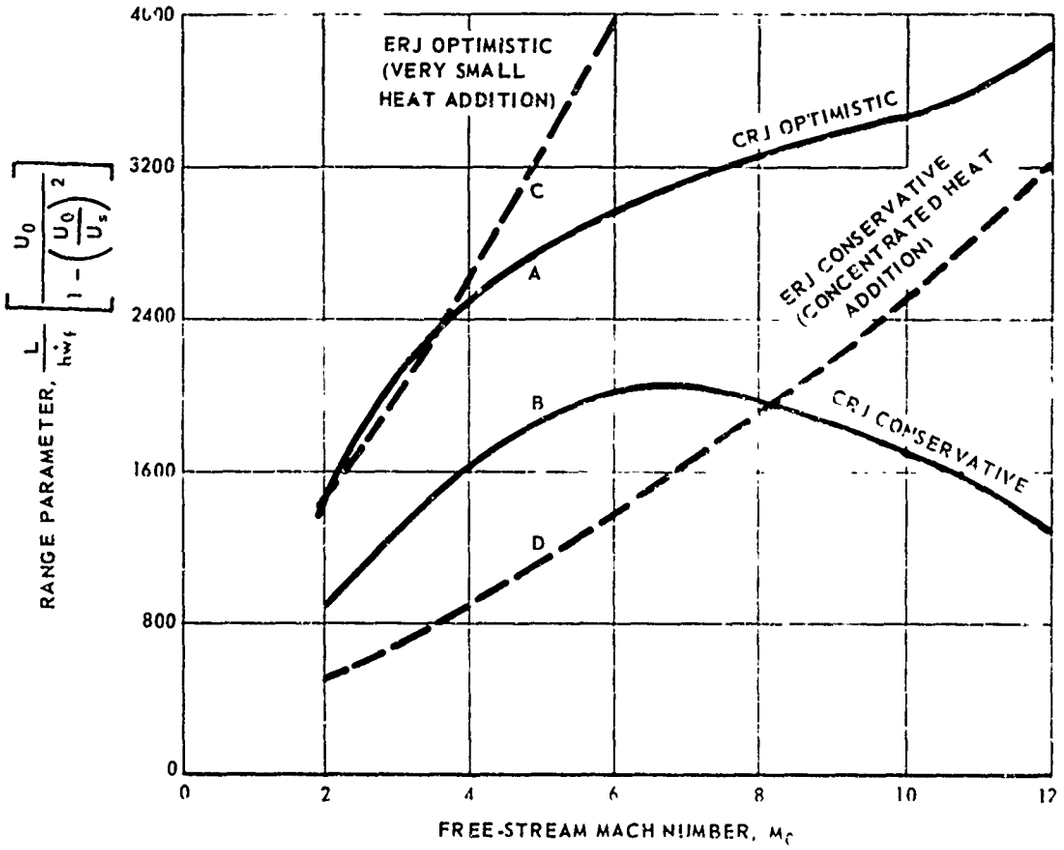

B) COMPARION OF CRUISE EFFICIENCY OF UNDERWING HEAT ADDITION AND CONVENTIONAL WING PLUS RAMJET.

Fig. 10 PLANAR FLAME MODEL (NORMAL WEAK DETONATION) AND RANGE PERFORMANCE FROM LUIDENS AND FLAHERTY. (Ref. 21)

with a distributed heat source, and curve D is for an ERJ with a single planar flame. They conclude that at Mach numbers greater than 8, the ERJ has greater cruise efficiency than the (subsonic combustion) CRJ vehicle. Lomax[22] also considered distributed heat sources throughout region II of Fig. 10(A) and found sizeable gains (> 200%) above linear theory, however, it is indeed difficult to imagine how such a fuel distribution could be obtained in practice.

Smith and Davis at Experiment Inc. were the first to consider the normal strong detonation case of Fig. 6(B). They had reasoned that the stabilization of a supersonic flame would be difficult and, therefore, postulated a subsonic heat addition preceded by a normal shock. The particular case of $M_2 = 1.0$ was chosen for study and the pressure distribution behind the planar heater was found by balancing the pressure in streamtube I with that in external streamtubes by taking successive oblique turns. In region 1, between the shock and the heater, the pressure coefficient was based on the linear theory value [Eq. (10)] which now introduces a geometric factor, the ratio of flame height to shock-flame separation distance, $Y_2/X_s \approx \delta$. For stoichiometric burning of hydrogen adjacent to a flat plate they obtained side force specific impulses of 2140, 3560 and 4860 secs at Mach numbers of 2, 3 and 4. For lean limit operation, (no separation between shock and heater) the corresponding impulses were 7200, 8800 and 9600 sec. They also applied the planar flame concept to a double wedge (equal fore and aft wedge angles) model similar to Fig. 2(B) and obtained a specific impulse defined as (thrust with burning) - (cold flow drag) ÷ (fuel flow rate). . Table I, their M is the local Mach number on the aft wedge ahead of the normal shock. This

author calculated the corresponding flight Mach numbers, M_0, shown in Table I, based on a leading-edge oblique shock and Prandtl-Meyer turning at the "knee".

Monchick and Dugger [23] considered the case of strong detonation on the aft surface of the two-dimensional airfoil shown in Fig. 11, which in effect is the Smith and Davis model split on the centerline. For the particular case of wedge angles (α) of 10° and stoichiometric hydrogen combustion with sonic burned gas, the flame height to surface length ratio, h/ℓ, was found for the condition of zero net thrust.

TABLE I

Smith and Davis Results for Specific Impulse on Double-Wedge Model

Wedge Half-Angle	M	M_0	$I_f = \frac{\text{(Thrust Hot-Drag Cold)}}{\dot{w}_f}$, sec	
			Lean Limit	Stoichiometric
5°	2.0	1.87	630	185
	3.0	2.76	770	310
	4.0	3.65	840	425
10°	2.0	1.67	1250	370
	3.0	2.56	1530	620
	4.0	3.38	1670	850

Figure 11(B) shows that h/ℓ would exceed 0.75 even for flight Mach numbers in the range of 3 to 5. This result was rather discouraging from a practical design standpoint, and an endeavor was made to make a more refined analysis of the expansion process to see if the result was due only to the simplifying assumptions. Since the expansion process in region 5 begins at the hot-cold

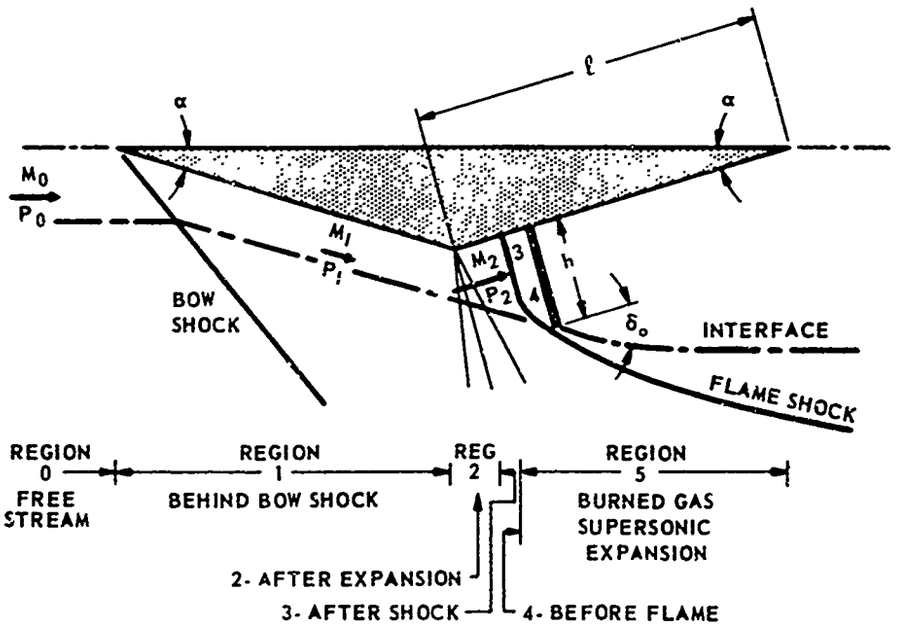

A) MATHEMATICAL MODEL

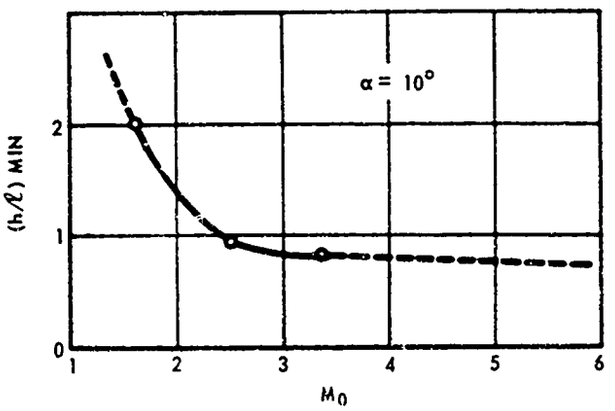

B) MINIMUM RATIO OF PLANE FLAME HEIGHT TO EXPANSION RAMP LENGTH REQUIRED FOR NET THRUST

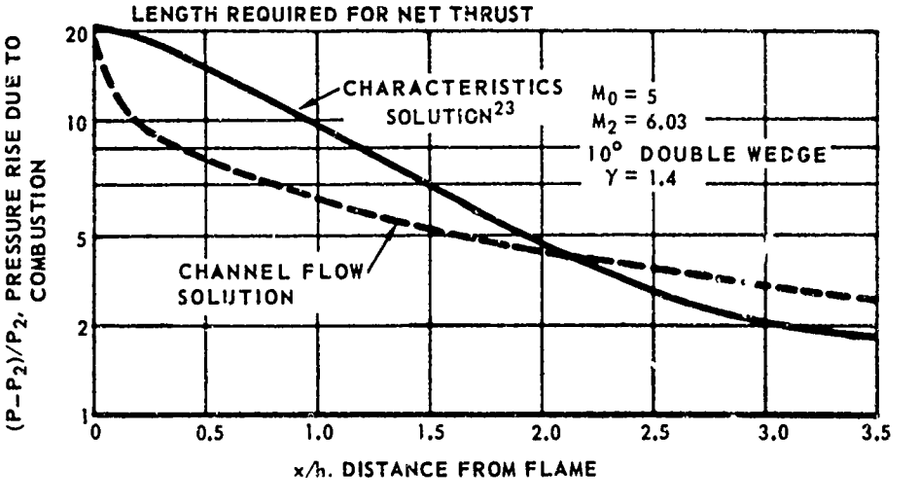

C) COMPARISON OF CHARACTERISTICS WITH CHANNEL FLOW SOLUTION FOR PRESSURE DISTRIBUTION ON SURFACE BEHIND FLAME

Fig. 11 TWO DIMENSIONAL AIRFOIL WITH NORMAL PLANAR HEAT ADDITION. (Ref. 23)

interface (see Fig. 6) the wedge surface pressure decay in the actual expansion process would first lag and then lead the interface pressure decay used in the first study. Thus, the integrated net force on the aft wedge could result in a larger thrust in the actual expansion case. For the same $\alpha = 10^{\circ}$ model, a method-of-characteristics solution for $M_0 = 5$, with $M_3 = M_4$ (i.e., no subsonic compression and below stoichiometric fuel-air ratios) and $M_5 = 1.0$ gave the surface pressure decays shown in Fig. 11(C) (solid curve). Integration of the pressure force showed that the minimum h/ℓ for the characteristics solution was 0.42 compared to 1.4 for the "channel flow" solution. From Fig. 11(B), $(h/\ell)_{min}$ is 0.75 at $M_0 = 5$, thus the $M_3 = M_4$ case requires a larger flame height than the stoichiometric (ER = 1.0) case. Presumably, if the characteristics solution were applied to the stoichiometric case, lower, and therefore more physically realizable, flame heights would occur.

A further refinement in the planar flame model was suggested by Woolard [24] to handle the subsonic compression region between the normal shock and the planar heater. Instead of assuming the linearized flow solution in region 1 of Fig. 12, an approximate but more realistic description of the flow was made. The shape of the detached shock wave from A to B was assumed to be a hyperbola becoming assympotic to the free stream Mach line C-D at point B. The shape of the hyperbola, attachment distance and the average pressure coefficient for region 1 were based on the method of Moeckel.[25] As before, the second shock wave emanating from the top of the heater balances the pressure between the burned and unheated stream tubes. The flow in

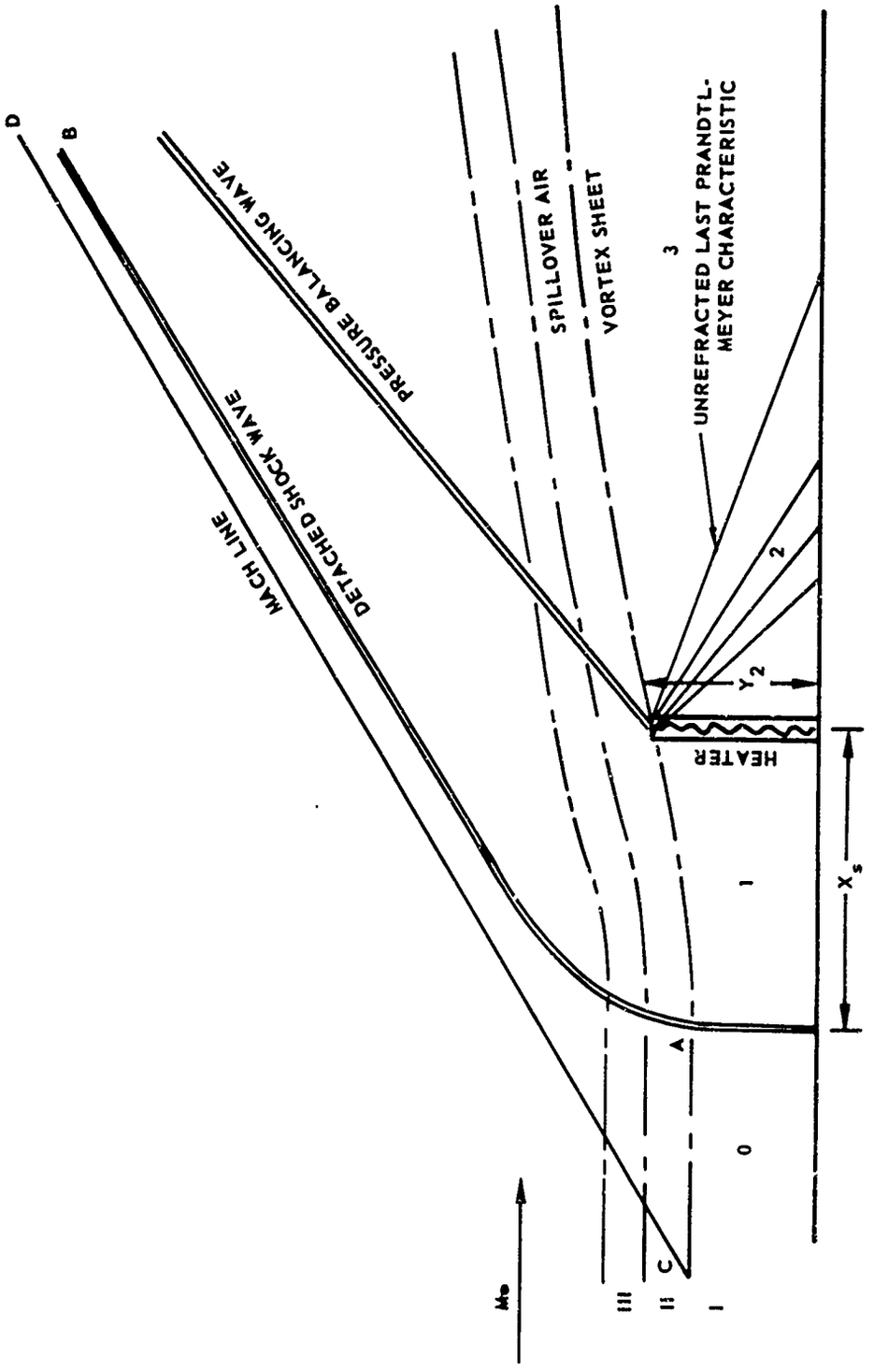

Fig. 12 NORMAL STRONG DETONATION MODEL AFTER WOOLARD. (Ref. 24)

streamtube II is analogous to the spillover flow in a ramjet inlet operating supercritically. As the mass flow in this streamtube approaches zero, X_s goes to zero and the flow situation is again that of Fig. 6(B) (critical). Woolard also developed an approximate method for obtaining the pressure decay downstream of the heater based on an exponential pressure decay beyond the last simply reflected Prandtl-Meyer characteristic. Charts for determining all of the pertinent flow field parameters and the normal force coefficients as a function of the rate of heat addition are presented for free-stream Mach numbers ranging from 2.0 to 7.0 in Ref. 24. The principal difference in this model from that of the linear theory is the elongation of X_s, hence a greater side force.

Dugger, et al,[23] at APL reexamined the same general model shown in Fig. 11 using Woolard's[24] results for the forces due to the shock-flame system. The model and a typical pressure profile are shown in Fig. 13. Air is compressed by the bow shock and expanded by Prandtl-Meyer turning around the knee before approaching the normal shock. The length X_2 required for the bounding streamline to complete the turn is equal to $y_2 \cot \beta_2$, where y_2 is the height of the streamtube which will be compressed by the normal shock and captured by the normal plane flame of height y_4. If heat addition is "supercritical", the normal shock is detached from the flame (Woolard's model), and the flow will expand between the shock and the flame, so that the flame height y_4 is greater than y_2. In the special case of critical (Chapman-Jouguet, "lean limit") heat addition, the distance x_3 vanishes and $y_4 = y_2$.

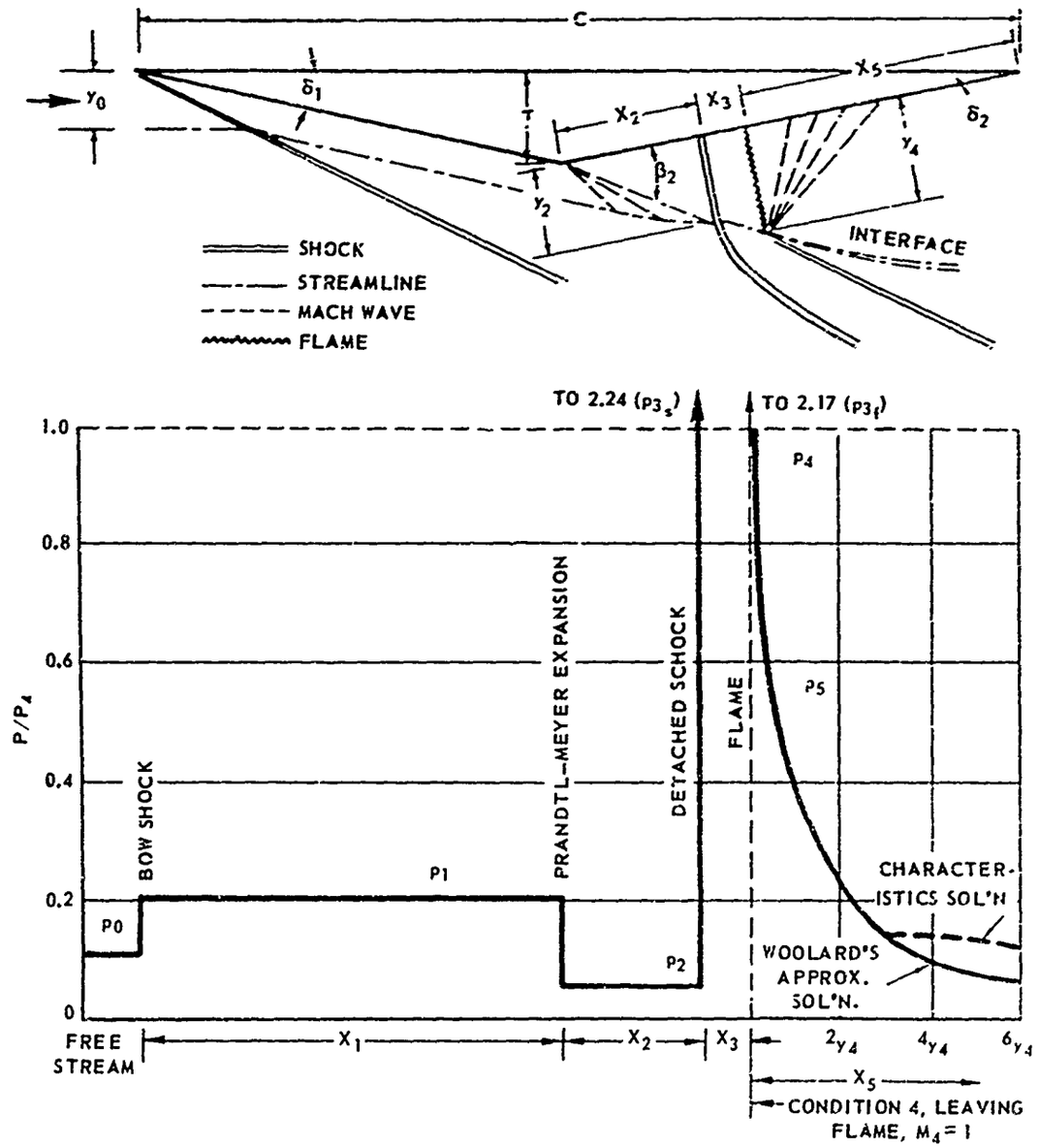

Fig. 13 SKETCH OF WEDGE-TYPE EXTERNAL RAMJET WITH PLANAR HEAT ADDITION BEHIND NORMAL SHOCK, AND TYPICAL SURFACE PRESSURE PROFILE FOR $\delta_1 = \delta_2 = 5^\circ$, $M_0 = 5.4$, $M_2 = 6$, $\gamma_0 = \gamma_2 = \gamma_4 = 1.4$.

Results for flame height to body thickness y_4/τ and range parameter R are shown in Fig. 14. The triangular points are based on the model of Fig. 13 using Woolard's approximate solution in the expansion region. The solid triangles show that supercritical heat addition was required for $\delta_1 = \delta_2 \geq 6^\circ$ at $M_0 = 5$ and for $M_0 \geq 8$ with $\delta_1 = \delta_2 = 5^\circ$. These curves show that at a flight Mach number of 5, the required flame height increases and the range capability of the vehicle decreases as wedge angles are increased. The range falls drastically for wedge angles greater than 6°. For engines with $\delta_1 = \delta_2 = 5^\circ$, flame height decreases and range increases as flight Mach number is increased to 5 or 6, but reverse trends are in evidence by Mach 8.

The circular points in this figure are from the analysis of Fig. 11. Both methods predict about the same flame height for zero net thrust but the latter study predicts lower cruise range efficiency at higher Mach numbers. This is due to the fact as M_0 increases, β_2 decreases and the flame is shifted aft toward the trailing edge and part of the pressure field due to combustion is lost in the wake. Likewise, as the wedge angles increase the model becomes stubbier resulting in the same effect. Clearly this would be a poor method of adding heat at high Mach number; however, the problem could be relieved simply by making $\delta_2 < \delta_1$ within practical limits, thus shifting the flame forward. Also shown as dashed lines on the figure are results from the constant-pressure combustion analysis from the same reference, which is discussed next.

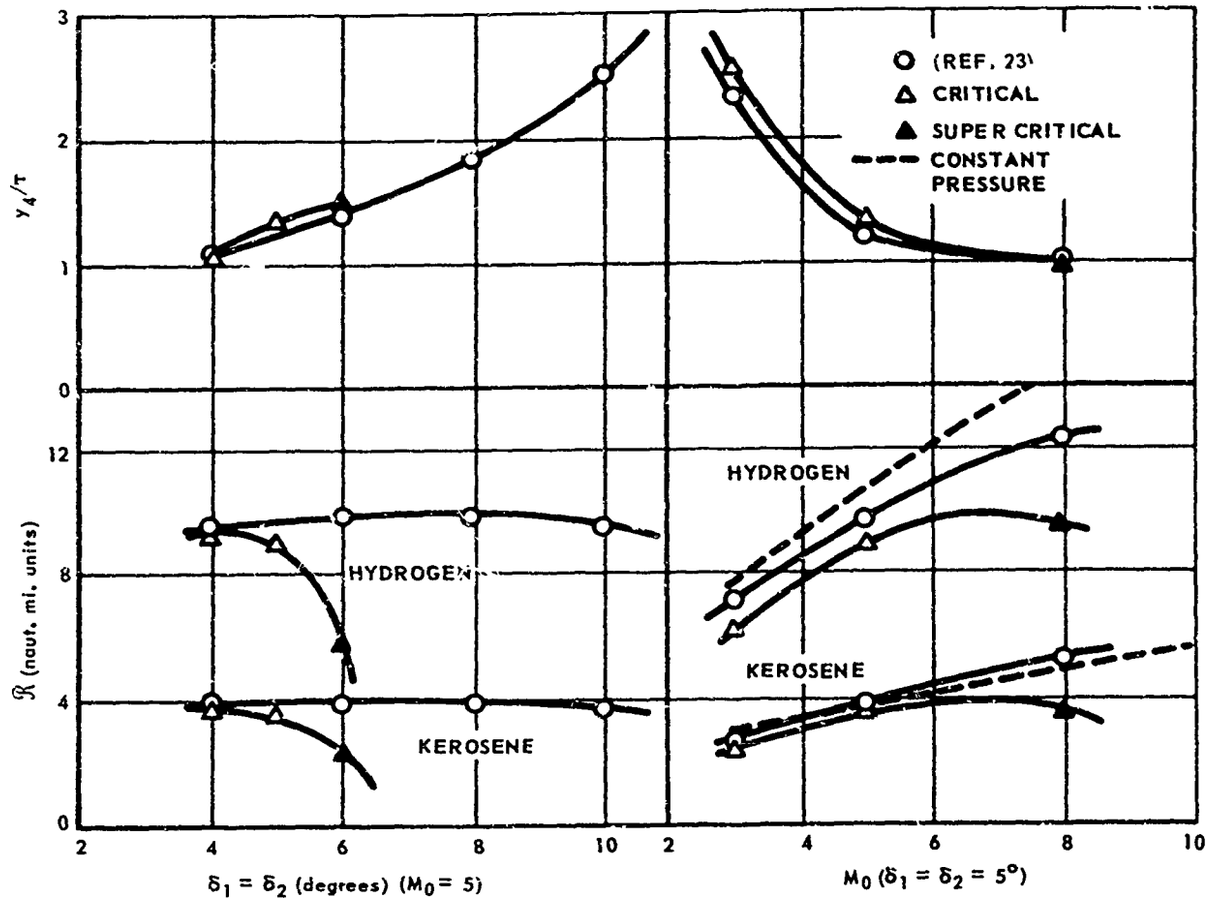

Fig. 14 PERFORMANCE OF WEDGE-TYPE ERJ WITH MINIMUM PLANAR HEAT ADDITION BEHIND NORMAL SHOCK. EFFECTS OF WEDGE ANGLE AND FLIGHT MACH NUMBER ON REQUIRED RATIO OF FLAME HEIGHT TO ENGINE THICKNESS AND ON RANGE PARAMETER

$$\mathcal{R} = \frac{L}{6076\,\dot{w}_f}\,u_0\left[\frac{1}{1-\left(\frac{u_0}{u_s}\right)^2}\right] \text{ IN NAUT. MI.}$$

2.3 Constant-Pressure Heat Addition

Although the planar flame models lead to significant simplification in the analysis of external burning and give what appears to be reasonable estimates of the integrated pressure forces, they do not, in general, predict the experimental pressure distributions obtained in most tests. This is especially true for the strong detonation models because the stationary normal shock produced by heat addition alone has as yet to be demonstrated experimentally.* Moreover, as M_0 increases, the losses across a normal shock become excessive and contribute to a decrement in performance. For these reasons, and because considerable data had shown continuous heat release at near constant pressure, the following analysis was generated.

Figure 15 shows the general representation of the analytical treatment for continuous constant-pressure heat release. In Fig. 15(A) the heat addition is large enough to support an oblique shock (called the flame shock) and in Fig. 15(B) the heat addition is only of sufficient strength to reduce the Prandtl-Meyer expansion in the flow around the knee. The particular case

---

* The stabilized detonation experiments conducted by Nicolls[26] used an under-expanded supersonic nozzle with premixed fuel to produce the normal shock and Gross[27] and Rhodes and Chriss[28] generated a Mach-reflected shock using wedges in the side of a two-dimensional supersonic tunnel.

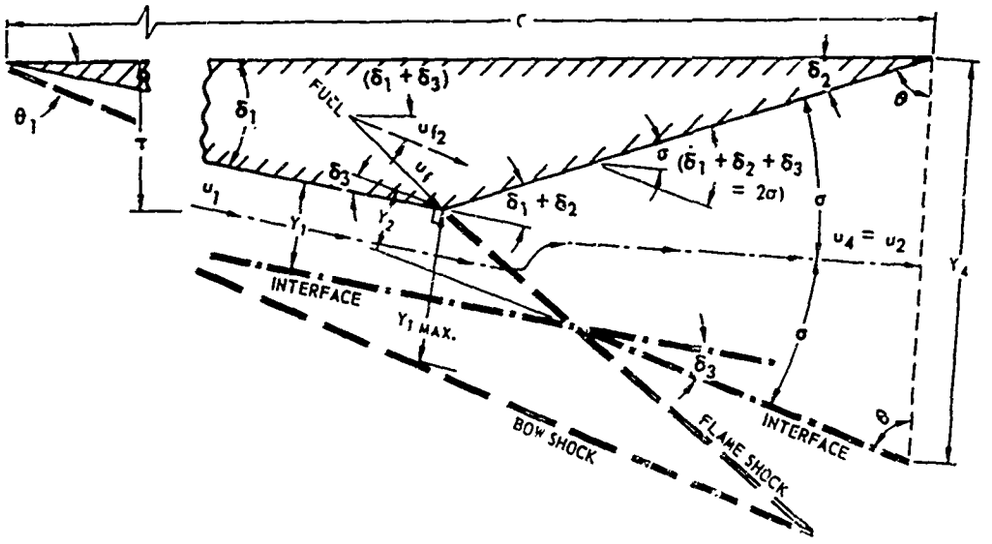

A) THEORETICAL MODEL FOR HEAT ADDITION LARGE ENOUGH TO SUPPORT AN OBLIQUE SHOCK.

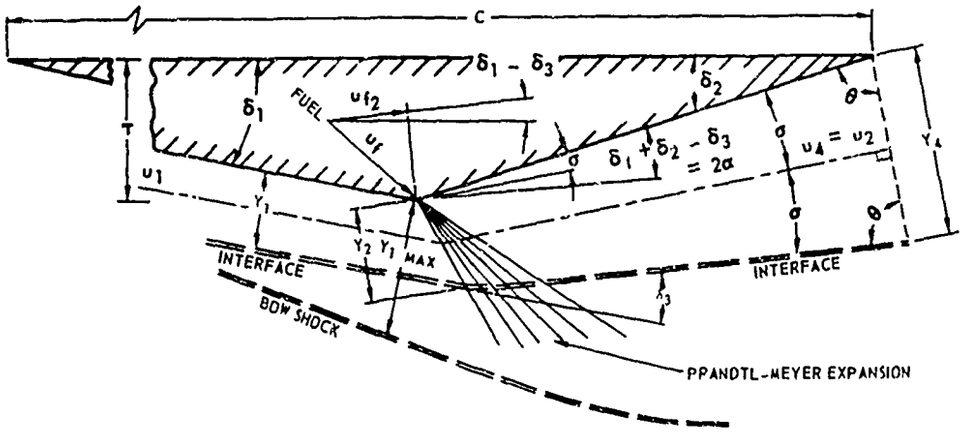

B) THEORETICAL MODEL FOR SMALL HEAT ADDITION

Fig. 15 ANALYSIS OF WEDGE-TYPE ERJ WITH CONSTANT PRESSURE HEAT ADDITION

of neither shock nor expansion corresponds to a constant pressure field on the entire underneath surface of the model.

The analysis is based on the following assumptions:

(1) The air flowing around the model outside the heated zone has properties defined in Refs. 29 and 30; the flow is two-dimensional and inviscid. The analysis is handled by stations in the flow so that analysis is actually one-dimensional.

(2) No heat or mass is transferred across the interface between the heated zone and the adjacent air flow.

(3) A given streamtube of air adjacent to the model and within the bow shock at the model knee receives all the fuel. The fuel is injected just behind the flame shock in the large heat addition case or just behind the rear-running Mach line for the Prandtl-Meyer turn case at condition u_2, T_2, p_2 (with Mach angle β_2). In either case, the static pressure and velocity component u_{f_2} in the emergent fuel jet are matched to the air static pressure p_2 and air velocity u_2. Hence, per the one-dimensional treatment the following relations apply:

$$p_4 \equiv p_2 \tag{30}$$

Mass: $$\dot{w}_4 = \dot{w}_2 + \dot{w}_f \tag{31}$$

where $$\dot{w}_2 = \dot{w}_a = g p_2 u_2 A_2 / R_2 T_2 \tag{32}$$

Momentum: $$\dot{w}_4 u_4 = \dot{w}_2 u_2 + \dot{w}_f u_{f_2} = (\dot{w}_2 + \dot{w}_f)\, u_2 \tag{33}$$

Hence $$u_4 = u_2 \tag{34}$$

and $$\dot{w}_4 = g p_4 u_4 A_4 / R_4 T_4 = \dot{w}_f + g p_2 u_2 A_2 / R_2 T_2 \tag{35}$$

It is assumed that for this analysis the maximum amount of air which can be used in the combustion is represented by the full amount captured by

by the bow shock at the model knee. This will be referred to as the "bow-shock limit", for which

$$y_1 = y_{1max} = x_1 \tan (\theta_1 - \delta_1) = (\dot{w}_f/d)/f\ \rho_i u_1 \qquad (36)$$

where d is the width of the two-dimensional engine, and θ_1 is the bow shock angle, and $x_1 = \tau/\sin \delta_1$.

(4) The side boundaries of the heated zone are the model and the hot-cold interface. The exit area A_4 (represented by y_4) is in a plane which forms equal angles θ with the model surface and the interface. The upstream boundary of the heated zone is either the flame shock or the last Mach wave in the Prandtl-Meyer expansion. The effective cross sectional area normal to the velocity vector u_2, at the start of the heat addition is found for either case by extrapolating the interface plane back to the model knee and is represented by y_2. In either case, constant pressure heat release is assumed to supply the expansion (by temperature increase) to bring the flow to the area represented by y_4. The relationship between y_4 and y_2 is:

$$y_4 = y_2/\cos \sigma + 2\ x_2 \sin \sigma \qquad (37)$$

(5) Heat release is completed at station 4 with 100% combustion efficiency. Properties of combustion products of kerosene-air and hydrogen-air systems are taken from Refs. 31 and 32 respectively.

With the above assumptions (since velocity is constant) the energy equation may be based simply on static enthalpies:

$$\dot{w}_{f_2}\ h_{f_2} = \dot{w}_4 h_4 - \dot{w}_2 h_2 \qquad (38)$$

Equations (32), (35), (37) and (38) can be combined to give the fuel flow rate per unit engine width:

$$\dot{w}_f/d = \frac{2g\, p_2 u_2 x_2 f\, h_4 \sin\sigma}{R^o \left[\frac{T_4 h_f f}{\mathfrak{M}_4} + \frac{h_2 T_4}{\mathfrak{M}_4} - \frac{h_4 T_2}{(\cos\sigma)\,\mathfrak{M}_2}\right]} \tag{39}$$

Solution procedure is as follows. Conditions at station 2 are determined for various δ_3's from two-dimensional oblique shock equations. Then for selected values of f, Eq. (38) is used to determine h_4 at $p_4 = p_2$. Other properties at station 4 can now be found from combustion tables. For each combination of f and δ_3 $\dot{w}_f$ is calculated from Eq. 39. Equation (36) is then tested for $y_1 \leq y_{1_{max}}$ and limits on δ_3 are established.

Lift and thrust forces per unit width are:

$$L/d = p_1 x_1 \cos(\delta_1 + \alpha) + p_2 x_2 \cos(\delta_2 - \alpha) - p_{top}\, c \cos\alpha \tag{40}$$

$$F/d = -p_1 x_1 \sin(\delta_1 + \alpha) + p_2 x_2 \sin(\delta_2 - \alpha) + p_{top}\, c \sin\alpha \tag{41}$$

For the special case $\alpha = 0$ and $\delta_1 = \delta_2$, these equations are simply:

$$L/d = \left[\left(\frac{p_1 + p_2}{2}\right) - p_0\right] c$$

$$F/d = (p_2 - p_1)\,\tau$$

List and thrust coefficients are defined:

$$C_L \equiv L/d\tau q_0 = L/A_F\, q_0 \tag{42}$$

$$C_F \equiv F/d\tau q_0 = F/A_F\, q_0 \tag{43}$$

It is assumed that to a first approximation the friction drag is the same with or without burning, so that

$$C_{D_f} \equiv (\text{friction drag without combustion})/A_f\, q_0 \tag{44}$$

and the coefficient of net thrust is

$$C_T \equiv C_F - C_{D_f} \tag{45}$$

A cruise range parameter (in nautical miles units) is defined:*

$$\mathcal{R} \equiv L\, u_0/6076\, \dot{w}_f \left[1 - (u_0/u_s)^2\right] \tag{46}$$

Results of calculations from the above theory are given in Fig. 16 for kerosene (C_nH_{2n}) fuel, and the effects of substituting hydrogen fuel are shown in Fig. 17. All curves presented are for zero angle-of-attack ($\alpha = 0$), because preliminary calculations showed that the optimum α would always be zero for zero gross thrust ($C_F = 0$) and would always be near zero ($0^\circ < \alpha < 3^\circ$) for small net thrusts ($C_T \leq 0.1$). Figures 16(A) and (B) illustrate effects of engine wedge angles at zero gross thrust and effects of required thrust level for a given configuration, respectively, for stoichiometric combustion of kerosene (ER = 1). Figures 16(C) and (D) then illustrate equivalence ratio effects, which in turn determine the optimum δ_2 for given thrust requirement and flight conditions, as shown in Fig. 16(E),

---

* The Breguet cruise range would be found by multiplying $\mathcal{R}$ by the natural logarithm of (gross weight/burnout weight). This logarithmic term is unity when the fuel load is 63.2% of gross weight, in which case $\mathcal{R}$ becomes the range in nautical miles. The $\dot{w}_f$ must provide thrust equal to vehicle drag, and L must equal vehicle weight. The $\left[1 - (u_0/u_s)^2\right]$ factor corrects for centrifugal lift.

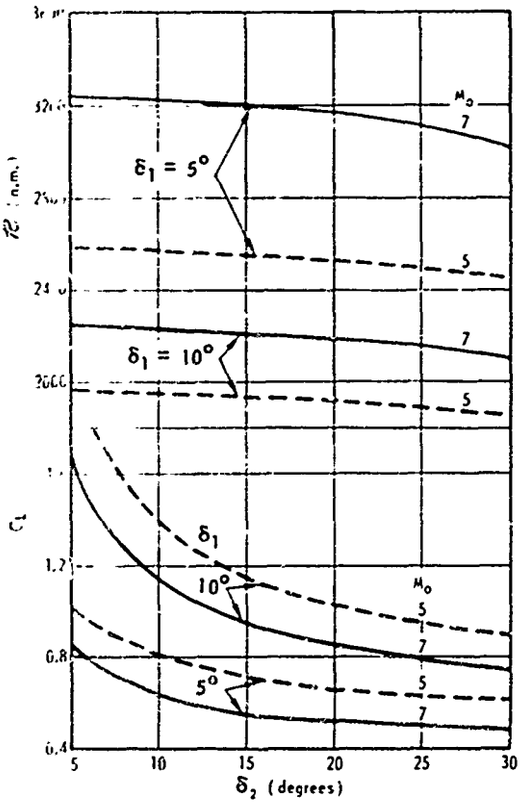

A) EFFECT OF WEDGE ANGLES ON LIFT COEFFICIENT AND RANGE PARAMETER $\alpha = 0°$, $C_F = 0$, $q_o = 350$ PSF, KEROSENE, ER = 1.

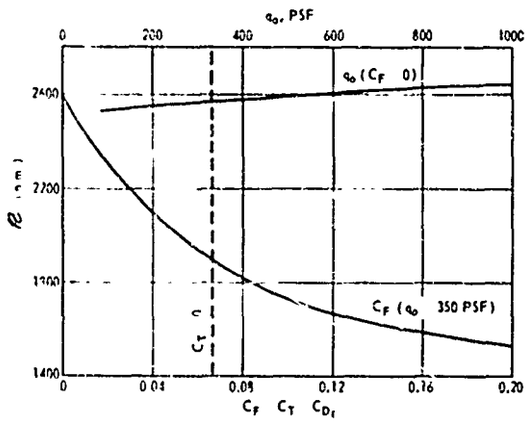

B) EFFECT OF REQUIRED THRUST COEFFICIENT AND DYNAMIC PERSSURE ON RANGE PARAMETER M = 5, $\alpha = 0°$, $\delta_1 = \delta_2 = 5°$, KEROSENE, ER = 1.

Fig. 16 ANALYSIS OF WEDGE-TYPE ERJ WITH CONSTANT PRESSURE HEAT ADDITION USING KEROSENE.

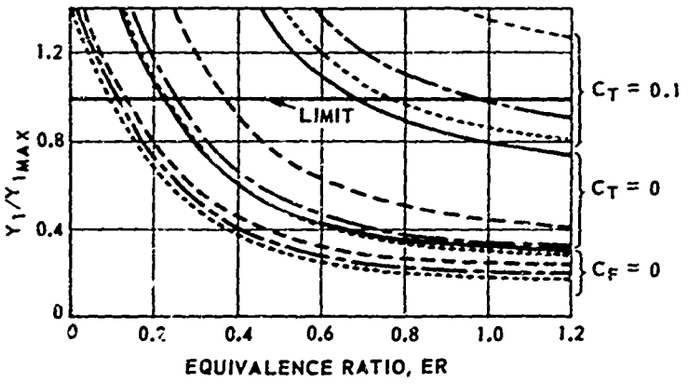

C) $Y_1/Y_{1\,max}$ AS FUNCTION OF ER AND AFT WEDGE ANGLE δ_2 FOR ERJ AT M_0 = 9.0 AND q_0 = 1000 PSF.

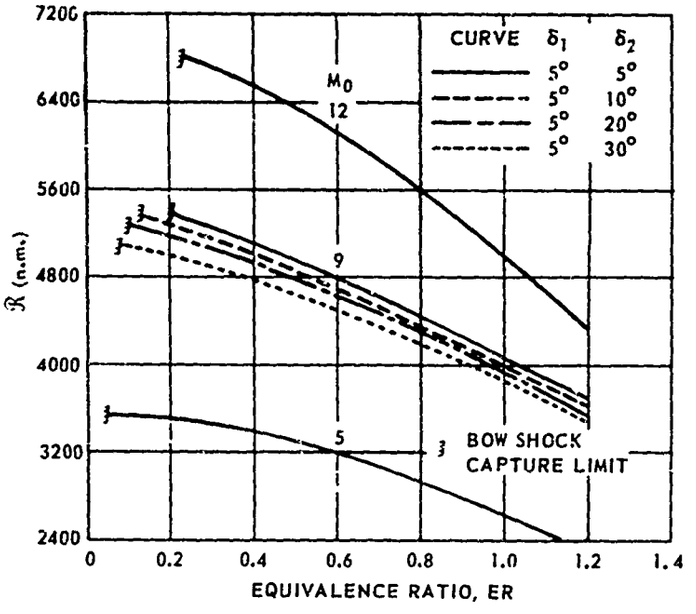

D) RANGE FACTOR AS FUNCTION OF ER AND M_0 FOR ERJ WITH C_F = 0 AND q_o = 1000 PSF.

Fig. 16 (Continued)
ANALYSIS OF WEDGE-TYPE ERJ WITH CONSTANT PRESSURE HEAT ADDITION USING KEROSENE.

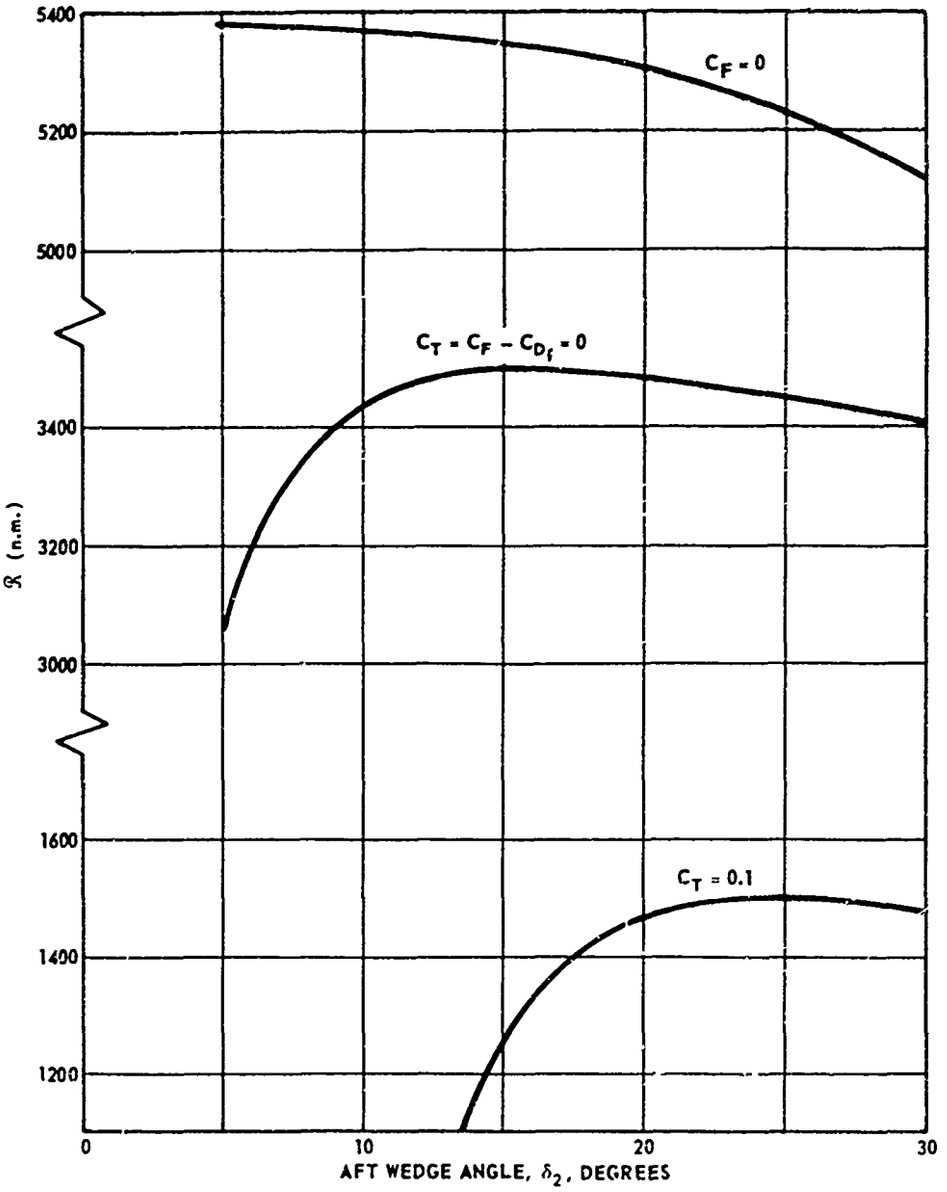

E) EFFECT OF AFT WEDGE ANGLE ON RANGE FOR ERJ AT $M_o = 9.0$, $q_o = 1000$ PSF AND $\delta_1 = 5^\circ$ AT OPTIMUM KEROSENE - AIR EQUIVALENCE RATIO.

Fig. 16 (Continued)
ANALYSIS OF WEDGE-TYPE ERJ WITH CONSTANT PRESSURE HEAT ADDITION USING KEROSENE.

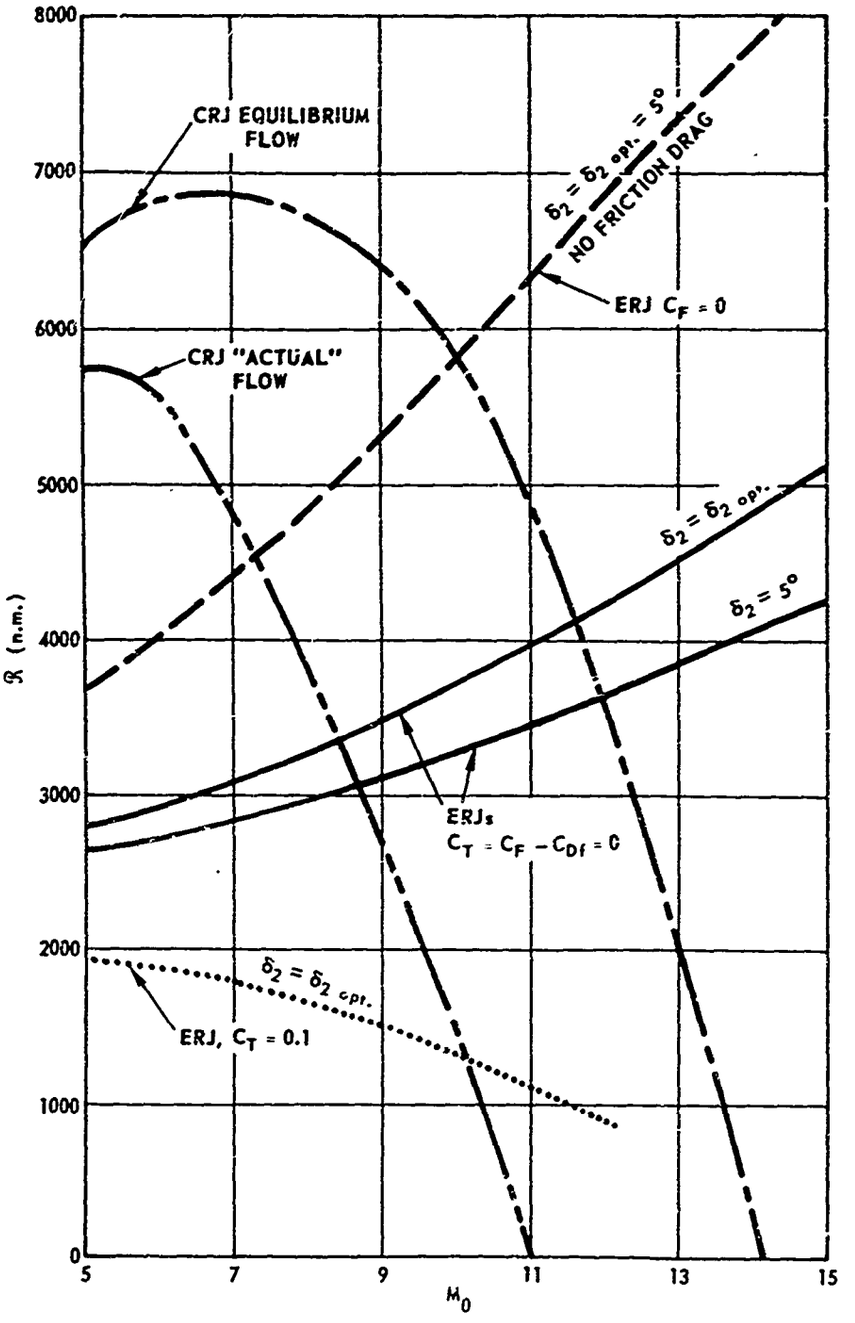

(F) COMPARISON OF ERJs WITH VARIOUS THRUST REQUIREMENTS TO CRJ VEHICLES WITH OVER-ALL L/D = 6. ALL ENGINES CRUISE WITH KEROSENE FUEL AT OPTIMUM ER.

Fig. 16 (Concluded)
ANALYSIS OF WEDGE-TYPE ERJ WITH CONSTANT PRESSURE HEAT ADDITION USING KEROSENE.

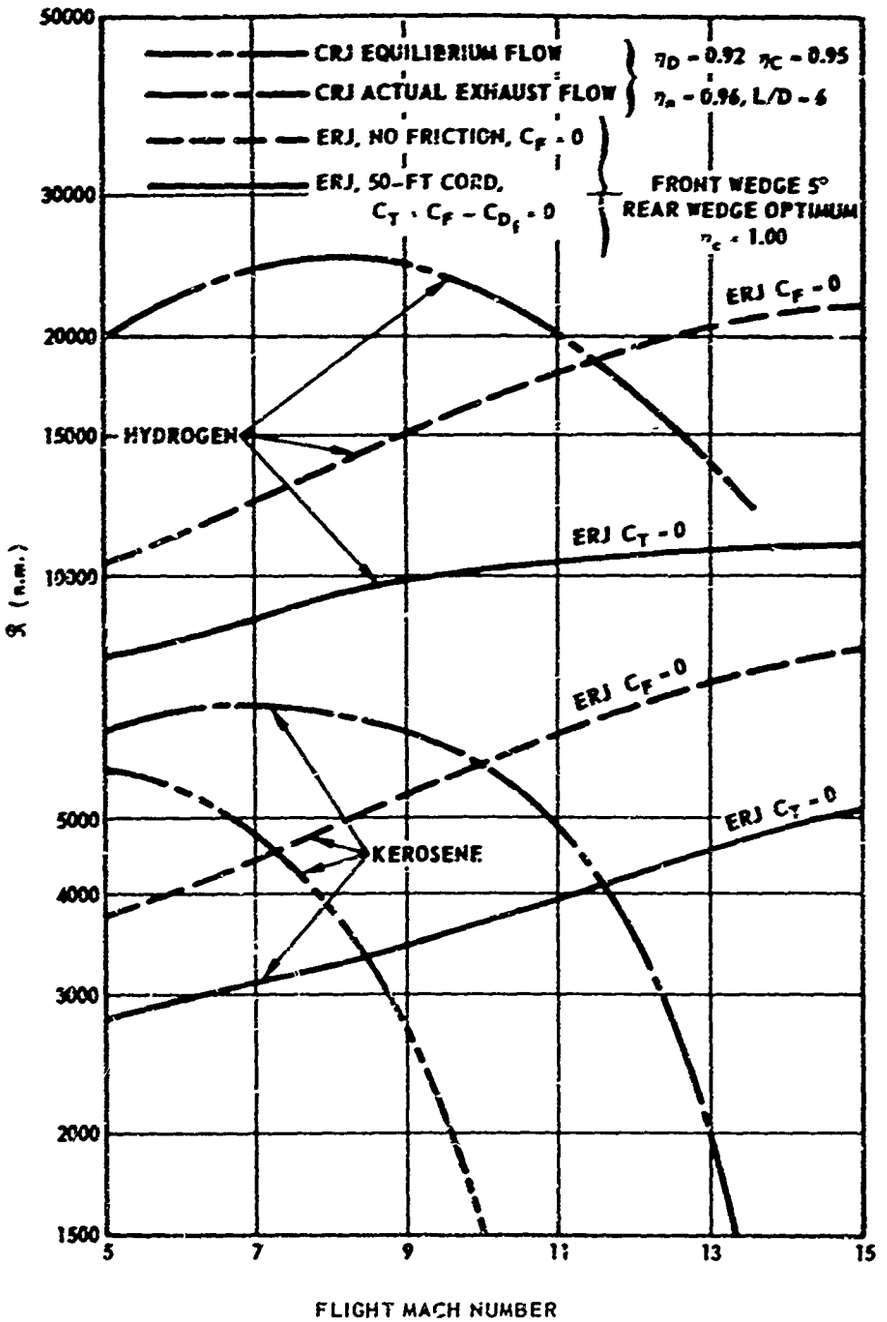

Fig. 17 COMPARISON OF THEORETICAL CRUISE RANGE PARAMETER FOR ERJs AND CONVENTIONAL RAM-JET (CRJ) VEHICLES. ALL VEHICLES CRUISE AT q_o = 1000 psf WITH OPTIMUM FUEL-AIR RATIO

and hence the optimized or on-design $\mathcal{R}$ vs M_∞ characteristics as shown in Fig. 16 (F). Notable conclusions and explanatory remarks from these figures are:

(1) From Fig. 16(A) it is seen that cruise range parameter for a frictionless cruise vehicle ($C_F = 0$) decreases slightly as aft wedge angle δ_2 is increased from 5° to 30° for a given fore wedge angle δ_1.

(2) For a given δ_2, the cruise range parameter increases as δ_1 is decreased, because the bow shock compression is decreased, the wave drag is correspondingly reduced, a small air mass flow is "captured" by the bow shock, and the net result is that less fuel is required to produce $C_F = 0$ by stoichiometric combustion. The total lift force L decreases, but the required fuel rate decreases faster, so that $L/\dot{w}_f$ and $\mathcal{R}$ increase.

(3) Lift coefficient referred to frontal area per Eq. (42) decreases as δ_2 is increased, because the pressure due to burning is felt on a smaller planform area and the total lift force for an engine of fixed frontal area is reduced. (Lift coefficient referred to planform area would be the same for all δ_2 when $C_F = 0$ and $\alpha = 0^\circ$ since in this case the lift is proportional to planform area).

(4) It is concluded from the above and from other similar calculations that maximum ranges will be obtained with slender configurations having the smallest practical δ_1 which probably will be near 5°. Remaining figures are for $\delta_1 = 5^\circ$ and $\delta_2 \geq 5^\circ$, depending upon required thrust level.

(5) The effect of required thrust level is illustrated by the plot of $\mathcal{R}$ versus C_F in part B for $\delta_1 = \delta_2 = 5^\circ$. It is seen that $\mathcal{R}$ decreases

rapidly as required thrust is increased, even to the amount required to overcome friction drag.* This is probably the most significant general result of the theory, because it suggests that ERJ's probably will not be attractive for high thrust or accelerating missions. It is discussed further in connection with Figs. 16(E), 16(F) and 17.

(6) Figure 16(B) also shows that the effect of flight dynamic pressure q_0 is small per this analysis. (As discussed elsewhere, experimental factors, such as boundary layer effects and non- ideal fuel distribution, may lead to much stronger real effects of q_0 or flight altitude).

(7) Figure 16(D) shows that for a given configuration at given flight conditions, $\mathcal{R}$ increases as ER is decreased. However, the extent to which ER can be decreased is limited in the present analysis by the criterion $y_1 \leq y_{1\ max}$ per Eq. (36). Figure 16(C) shows how these "bow shock limits" are established for various thrust levels and δ_2's at $M_0 = 9$. It is seen that ER decreases as $y_1/y_{1\ max}$ increases; the optimum or bow-shock-limited value, which represents the minimum ER and hence the maximum $\mathcal{R}$ by these rules, is that corresponding to $y_1/y_{1\ max} = 1.0$. Typical values of this optimum ER for various conditions are given in Table II.

---

* The friction drag coefficients calculated for part (D) and subsequent parts are based on a 50-ft chord; for similar geometries, longer engines would have smaller C_{D_f}'s and vice versa.

TABLE II

Bow-Shock-Limited Values of Kerosene Equivalence Ratio** for Various Flight Mach Numbers, Thrust Levels, and δ_2's for ERJ's of 50-ft Chord at q_0 = 1000 psf.

	$C_F = 0$			$C_T = 0$			$C_T = 0.1$		
M_0	$\delta_2 = 5^\circ$	10°	20°	5°	10°	20°	5°	10°	20°
5	$\leq .10$	$\leq .10$	$\leq .10$	.20	.14	.10	.44	.25	.18
9	.23	.14	.11	.68	.37	.20	≥ 1.0	≥ 1.0	.97
12	.25	.16	.11	.77	.47	.32	≥ 1.0	≥ 1.0	≥ 1.0

As one would expect, Table II shows that ER must be increased as required thrust is increased. For given thrust level and engine length, the minimum ER decreases as δ_2 is increased, because frontal area and $y_{1\ max}$ increase as the maximum thickness point is shifted toward the rear of a fixed-length engine. The latter effect is more pronounced at positive net thrust.

(8) Figure 16(E) shows that an optimum δ_2 (with its corresponding minimum ER) will exist for any thrust level at given flight conditions. For $C_F = 0$, $\delta_{2\ opt} \simeq \delta_1$. For higher thrusts, $\delta_{2\ opt} > \delta_1$. Such optimum

** ER's less than 0.1 or greater than 1.0 are considered unrealistic. In fact, ER's < 0.3 may not be realistic for kerosene, but there might be some advantage in going slightly rich, say to ER ~ 1.2.

δ_2's are used to plot maximum R versus M_0 for various thrust levels in Fig. 16(F). The drastic deterioration in R as required thrust is increased is clearly seen in these two figures. For example, from Fig. 16(F) it is seen that:

(a) R is 8300 n.m. at $M_0 = 15$ (and still rising) if $C_F = 0$, in which case $\delta_2 = \delta_1 = 5^o$ is optimum

(b) R is reduced to 5200 n.m. at $M_0 = 15$ for $C_T = 0$ for 50-ft engines with $\delta_{2\ opt}$ or to 4500 n.m. if δ_2 is held at 5^o, and

(c) if required C_T is raised to 0.1 to accommodate external drag of other vehicle components or maneuver "noise", R decreases continuously from 2000 n.m. at $M_0 = 5$ to 900 n.m. at $M_0 = 12$.

(9) ERJ's should be superior to conventional ramjets with subsonic internal combustion (CRJ's) in cruise applications at flight Mach numbers above 9 or so, depending on the assumptions made for the two engines. Two CRJ curves are given in Fig. 16(F). Both are based on engines with inlet, combustion, and nozzle efficiencies of 0.92, 0.95 and 0.96, respectively, and on vehicles with over-all L/D's of 6. The more optimistic CRJ curve is based on chemical equilibrium in the exhaust flow, whereas the poorer curve is based on estimated "actual" exhaust flow properties. The latter flow properties are intermediate between equilibrium and frozen exhaust flow properties and are estimated as in Ref. 33. The most reasonable comparison of ERJ and CRJ from this figure is probably that between the ERJ curve for $C_T = 0$ and $\delta_{2\ opt}$ and the "actual" flow CRJ curve. On this basis, the ERJ is superior for $M_0 \geq \sim 8.5$. Longer ERJ's would have lower friction drag

coefficients and slightly improved performance or vice versa.

It should be pointed out that the ERJ curves are (as done here) properly based on equilibrium flow properties, because it has been assumed that heat is added continuously to the trailing edge of the model and no credit has been taken for subsequent expansion. (A similar assumption for the CRJ would permit only a convergent nozzle, and performance would be much poorer than the "actual" flow curve presented for the CRJ.) Furthermore, the analytical model of Fig. 15(A), is based on the assumption that heat is added all the way across a one-dimensional flow to the exit plane A_4. Actually, the heat added downstream of the last forward-running Mach wave* striking the trailing edge cannot affect the pressure on the model surface, hence it is wasted. A controlled fuel distribution and heat release program might therefore decrease the specific fuel consumption and significantly improve the relative ERJ performance at all thrust levels illustrated.

(10) Both CRJ's and ERJ's have much greater cruise ranges when hydrogen fuel is used instead of kerosene, as shown in Fig. 17. For a given fuel mass fraction and cruise Mach number, the range is increased by approximately a factor of 2.8. Thus, an ERJ with an initial hydrogen load equal to 63% of its gross weight could reach 10,500 n.m. at Mach 12 on a zero net thrust cruise.

---

* This refers to the left-running characteristic of the burned gas flow as it passes the trailing edge of the model. The pressure field in the supersonic flow downstream of this Mach wave cannot be transmitted upstream.

Two additional refinements in the constant pressure heat addition model were made by Billig in Ref. 34. These changes are the inclusion of a separated zone in the region of the fuel ports and an approximation for the pressure decay downstream of the heat release zone as shown in Fig. 18, and they are more apparent when the analysis is applied to a case of heat addition adjacent to a flat plate but are applicable to the wedge model.

Fuel is injected near the leading edge, causing a separated-flow region and a corresponding oblique injection shock. The fuel penetrates to a height Y_1 and combustion begins in the plane labeled Y_2 and is completed at plane Y_3. For additional simplicity the heat release is assumed to proceed at a rate to maintain the pressure level attained by the injection separation. Thus, the injection shock is represented by a straight line until point C is reached, where expansion commences. At point D in the Y_3 plane, expansion begins in the combustion gas, as represented by the "leading Mach lines", DE. Pressure is therefore assumed to be constant throughout the region ABDE, so that the surface pressure rise over the length X_4 from A to E is $(p_2 - p_0)$. To avoid the complex characteristic solution of the flow field of the combustion gases, the surface pressure in the expansion region (EF) is assumed to be the arithmetic mean of combustion and free stream pressures, i.e., $p_{EF} = (p_2 - p_0)/2$. Equilibrium combustion of triethyl aluminum in air with 100% combustion efficiency using the procedure developed by Browne and Williams[35] was carried out on a high-speed computer. No heat or mass transfers across the hot-cold interface.

The normal force specific impulse is defined as the total force (per unit plate width) resulting from pressure above ambient divided by the fuel

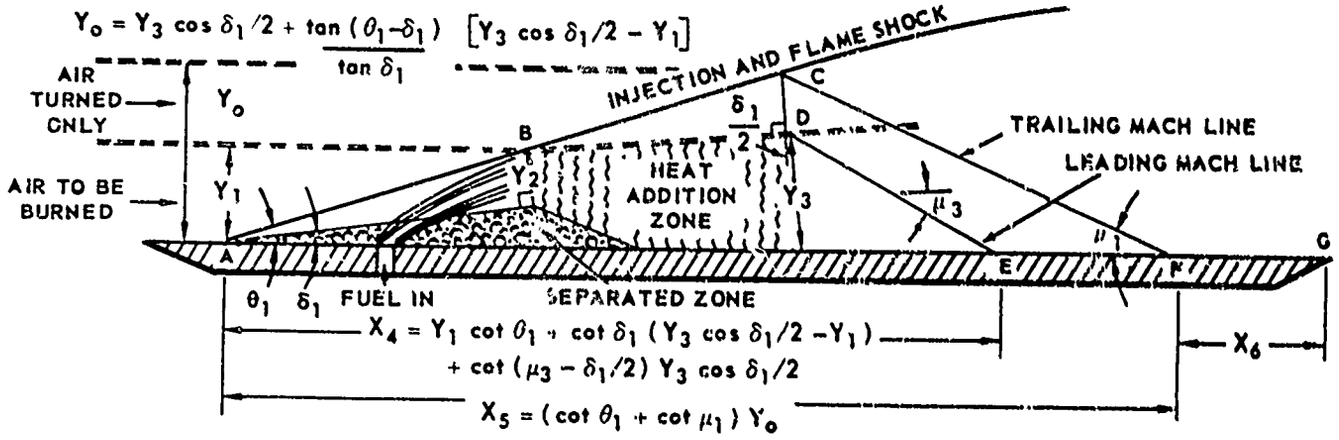

Fig. 18 THEORETICAL MODEL OF CONSTANT PRESSURE HEAT ADDITION ON A FLAT PLATE. (Ref. 34)

flow rate (per unit plate width):

$$I_{fN} = \frac{F_N}{\dot{w}_f} = \frac{(p_2 - p_0)\, X_4 + (X_5 - X_4)\,(p_2 - p_0)/2}{gf\ ER\ \rho_0 u_0 Y_1} = \frac{(p_2 - p_0)}{gf\ ER\ \rho_0 u_0} \cdot \frac{X_4 + X_5}{2\ Y_1} \qquad (47)$$

The normal force coefficient is the total side force divided by the product of the area subjected to pressure above ambient (this area per unit plate width is X_5) and free stream dynamic pressure:

$$C_N = \frac{F_N}{q_0 A} = \frac{(p_2 - p_0)\,[(X_4/X_5) + 1]}{2\ q_0} \qquad (48)$$

Table III summarizes the computer results for cases having a range of free stream Mach numbers (M_0), altitudes (Z), equivalence ratios (ER), and injection shock strengths (θ_1, as determined by δ_1, the air deflection angle due to the separation zone). Cases labeled with asterisks have injection shock strengths and pressure ratios which correspond to separation of a turbulent boundary layer as predicted by Mager.[36] Experiments with non-reactive injection[37,38] have resulted in reasonable verification of the average pressure as estimated by Mager. In the subsequent discussion of experiments of triethyl aluminum injection onto a flat plate at Mach 5 from Ref. 34, the injection shock was somewhat weaker and separation was apparent. Changes in the geometry of the fuel injector may permit control of θ_1, so that all of the cases listed can be of interest. The cases studied were limited to those in which the Mach number at the end of combustion was supersonic ($M_3 \geq 1$); however, subsonic solutions are possible and may in fact be desirable at low flight Mach numbers. (The $\bar{I}_{fN}$ and $\bar{C}_N$ columns in Table III will be discussed later.)

TABLE III Flat Plate External Burning Performance Parameters

M_0	Z K ft	δ_1 deg	θ_1 deg	ER	Y_0/Y_1	Y_2/Y_1	Y_3/Y_1	X_5/Y_1	μ_3 deg	I_{fN} sec	C_N	$\bar{I}_{fN}$	$\bar{C}_N$
3	35	5	23.16	.50	23.17	.793	5.673	119.6	68.63	7344	.0536		
"	"	"	"	.25	12.44	"	3.411	64.3	47.09	8058	.0548		
"	"	*14	31.25	.25	3.45	.572	2.105	15.4	53.85	7044	.2060		
4	35	*12.5	24.59	1.0	7.88	.503	4.534	47.7	65.84	4776	.1312	4776	.1312
5	35	5	15.09	1.0	19.83	.673	7.213	170.6	43.54	5574	.0342	5574	.0342
"	"	"	"	.75	16.69	"	6.177	143.6	39.78	6288	.0344	5294	.0290
"	"	"	"	.50	11.89	"	4.593	102.3	33.80	6798	.0348	4076	.0209
"	"	"	"	.25	6.38	"	2.776	54.9	26.02	7502	.0358	2414	.0115
5	0	*10.5	19.81	1.0	5.45	.477	3.375	41.8	39.36	3718	.0932	3718	.0932
"	35	* "	19.86	1.0	17.53	.479	4.266	54.7	45.58	4786	.0917	4786	.0917
"	"	* "	"	.75	14.25	"	3.655	45.8	41.57	5408	.0928	4526	.0777
"	"	* "	"	.50	9.32	"	2.738	32.7	35.38	5918	.0949	3534	.0567
"	"	* "	"	.25	3.68	"	1.688	17.5	27.44	6722	.1005	2158	.0323
"	83.23	* "	"	1.0	6.94	"	4.161	53.2	44.97	4662	.0919	4662	.0919
"	35	15	24.31	1.0	4.16	.393	2.988	29.6	47.94	4388	.1554	4388	.1554
"	35	20	29.75	1.0	2.67	.341	2.167	17.7	51.73	4106	.2427	4106	.2427
6	35	* 9	16.65	1.0	6.76	.328	4.127	62.5	36.08	4776	.0667	4776	.0667
8	35	5	10.86	1.0	10.49	.542	5.373	137.9	25.70	5178	.0246	5178	.0246
"	"	* 6.5	12.17	1.0	7.13	.469	7.283	89.6	25.94	4874	.0356	4874	.0356
"	"	* "	"	.75	6.01	"	3.685	75.6	24.02	5534	.0360	4666	.0304
"	"	* "	"	.50	4.30	"	2.769	54.1	20.84	6070	.0368	3666	.0222
"	"	* "	"	.25	2.31	"	1.704	29.1	16.42	6896	.0389	2234	.0126
"	"	10	15.52	1.0	3.60	.309	2.688	41.5	26.60	4374	.0690	4374	.0690
"	"	20	26.43	1.0	1.09	.252	1.083	10.8	29.75	3742	.2265	3742	.2265
10	35	* 5	9.54	1.0	7.65	.477	4.497	121.7	20.51	5008	.0216	5008	.0216
"	35	10	14.86	1.0	2.47	.309	2.029	34.2	21.26	4202	.0644	4202	.0644

*Turbulent separation deflection

In Fig. 19 the I_{fN} and C_N dependence on M_0 is shown for ER's of 1.0 and 0.25 at 35,000 ft altitude. For lean mixtures, I_{fN} is about 2000 seconds higher. For deflections equal to the defined turbulent boundary layer separation, $\delta_1 = \delta_{1\ sep}$, the impulse is essentially invariant with M_0. Even for the cases of constant $\delta_1 = 5^o$, variation of I_{fN} with M_0 is small, a monotonic decrease with increasing M_0. The normal force coefficient, C_N, is mainly dependent on deflection angle, increasing only slightly with lower ER. As for most aerodynamic surfaces, larger deflection results in a greater force coefficient.

Figures 20(A) and (B) show the ER and deflection effects on I_{fN} more clearly for cases in which all other parameters are held constant. Figure 20(C) shows the altitude effect at $M_0 = 5$, $\delta_1 = \delta_{1\ sep}$. At constant M_0 (but varying u_0), temperature rather than pressure has the dominant effect on I_{fN}, as shown by the rapid rise in I_{fN} from sea level to the tropopause (Z = 36K ft) and correspondingly slight decline in the constant-temperature, decreasing-pressure region. Of course, if a comparison were made on a constant velocity basis (say, u_0 = 5000 ft/sec), the effect of altitude would be smaller (but deflection angles would have to be adjusted for M_0 variation). ICAO Standard Day air properties were used throughout.

The results of the theoretical study are dimensionless with regard to the geometric variables. For flight models certain constraints will bound the range of practical geometries. Two principal limitations will be a minimum practical combustor length for efficient combustion and a maximum height of fuel jet penetration. The latter effect is more pronounced for low ER ratios since at the same combustion pressure low ER requires

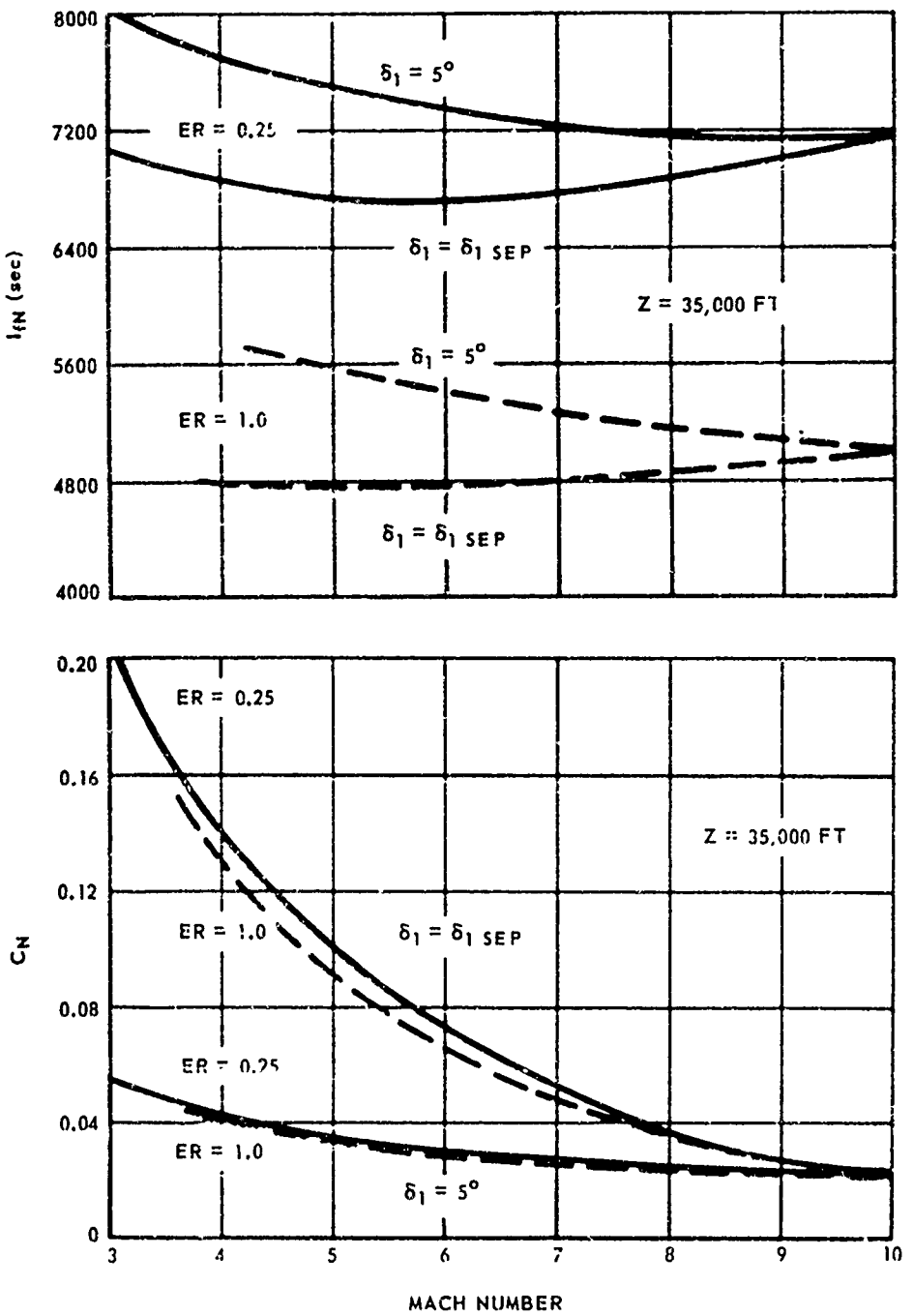

Fig. 19 NORMAL FORCE COEFFICIENTS AND SPECIFIC IMPULSES FOR A FLAT PLATE WITH CONSTANT PRESSURE COMBUSTION OF TEA FUEL

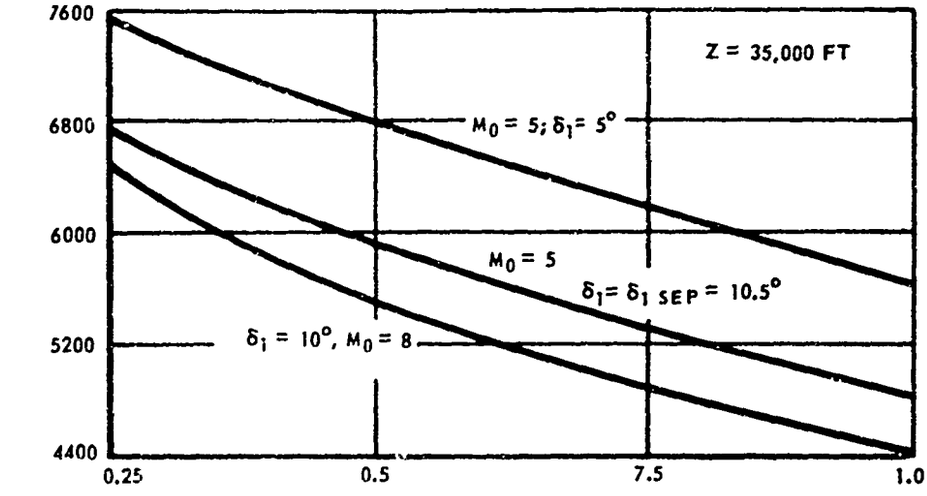

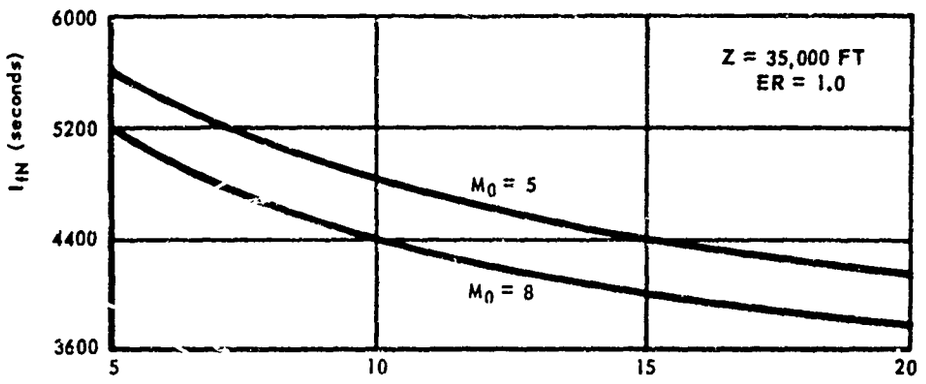

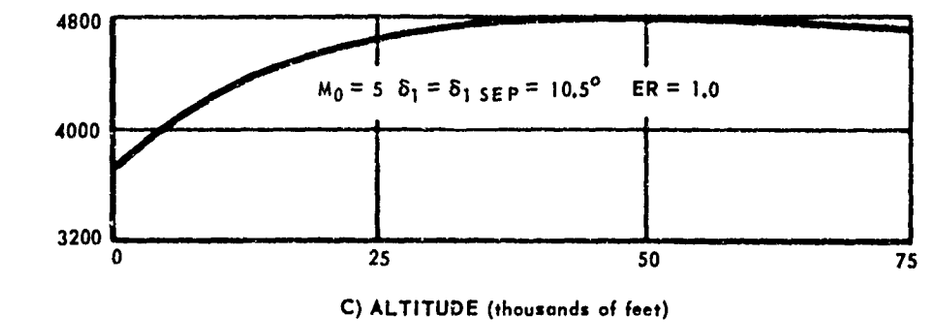

Fig. 20 NORMAL FORCE SPECIFIC IMPULSE AS FUNCTION OF EQUIVALENCE RATIO, DEFLECTION ANGLE AND ALTITUDE FOR FLAT PLATE AT MACH 5 WITH CONSTANT PRESSURE COMBUSTION OF TEA FUEL

relatively greater jet penetration to obtain the same length of the constant pressure field A-E. This effect is dramatically shown in Table III. The last two columns in Table III, $\bar{I}_{fN}$ and $\bar{C}_N$, are the impulse and force coefficients which would result if the fuel penetration depths were limited to the theoretical value for stoichiometric fuel injection, i.e., $\bar{Y}_1 = Y_{1\ @\ ER\ =\ 1}$. In effect, this constraint forces the expansion to be completed before the end of the plate is reached when ER < 1. The flow model would then include the distance X_6 (Fig.18) with zero pressure coefficient ($C_{N_6} = 0$), hence the over-all C_N would decline, and the $I_{fN} = \bar{I}_{fN}$ produced on the constrained length X_5 would decrease. The net result reverses the trend of better performance for lower ER and instead shows the desirability of rich operation if penetration rather than length is controlling.

The above theoretical treatments can be applied directly to planar surfaces at angles-of-attack (i.e., other than zero incidence to the free stream). It can also be readily modified to handle single-port rather than multiport or line-source injection by using half-conical flow surfaces and deflection surfaces rather than two-dimensional ones.

In closing this summary of theoretical studies, the work or Wald[39] of United Aircraft and Yen and McCloy[40-43] of General Dynamics should be mentioned. In particular, fundamental theoretical studies by McCloy (Department of Aeronautical and Astronautical Engineering, University of Illinois and consultant to APL in 1960-61) led to the flow model concepts used in the preceding constant pressure analysis. Noteworthy too, are the studies by Marino[44] who apparently adapted McCloy's model to the flat

plate case and studied both the simple two-dimensional (wedge heat addition) and a conical heat addition (i.e., constant pressure combustion from a point source) and concludes that the former is more efficient. He presents performance charts for M_0 = 2 to 20 and came to similar conclusions to those showed in Ref. 36.

3. LITERATURE REVIEW OF EXPERIMENTAL STUDIES OF EXTERNAL BURNING

The first experiments related to external combustion were concerned with the reduction of base drag of projectiles by combustion in the wake. Baker, et al[45] injected hydrogen into the base of a 2-1/4 inch diameter cone-cylinder placed in a Mach 1.6 free jet and obtained base drag reduction of 60-75%. Subsequent additional analysis of the data suggests that the specific impulses based on drag reduction were 1200 to 4000 secs and the combustion efficiencies were 80-90%. Similar tests were made by Scanland and Hebrank[46] who burned a solid pyrotechnic composition in the base of 40 mm projectiles. The base drag reduction at M_0 = 1.85 was 65% which corresponded to a total drag reduction of 19%. In both of these tests, the burning was external but was probably confined to the subsonic portions of the wake.

Davis, at Experiment Incorporated, made a series of tests with hydrogen injection from a flat plate at M_0 = 1.7. Typical pressure rises due to combustion are shown in Fig. 21 for hydrogen injection from the base of a rearward facing step. In nearly all tests not having a high drag flameholder immersed in the external air system the addition of oxygen was necessary to establish burning. Even with oxygen addition it is apparent (e.g., burning in Run a but not in Run b)

	P_{t_0} PSIA	T_{t_0} °R	$\dot{w}_{H2}$ lb/sec	$\dot{w}_{02}$ lb/sec	BURNING
a	85	390	0.0041	0.0115	YES
b	87	395	0.0041	0.0114	NO
c	83	400	0	0	NO

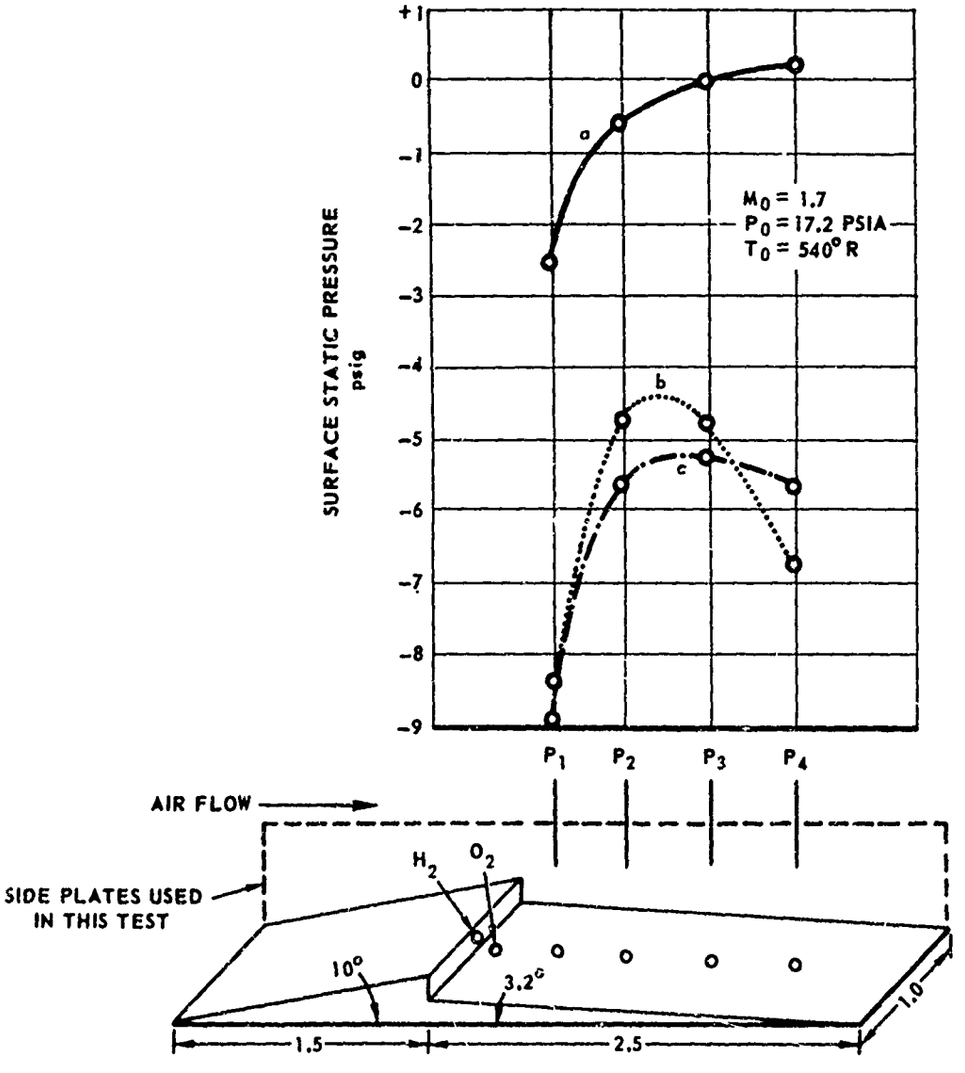

Fig. 21 EXTERNAL COMBUSTION MODEL TESTED BY DAVIS ET AL. WITH TYPICAL STATIC PRESSURE PROFILES

that the combustion is near a stability limit. The difficulties encountered in getting hydrogen to burn in these tests at 1 atm and about 530°R static are not at all surprising. In fact, on the basis of recent ignition delay experiments,[47] it is doubtful that ignition of hydrogen could have occurred unless a significant separated zone with recirculation existed downstream of the step. A large number of injector and flame-holder configurations were tried, some with supplemental oxygen and most with spark ignition source. Although most of the data are difficult to interpret due to the presence of flame-holder shock waves, a general conclusion can be drawn that when combustion occurred the "volume source" effect essentially compensated for the expansion due to the step, and thus represented a net side force increase due to combustion.

On the basis of some of the aforementioned theoretical studies, Dorsch, et al[48-53] reasoned that to obtain the desired performance from external burning it would be necessary to stabilize combustion in the supersonic portion of the flow field without the attendant drag losses of flame-holders, as were necessary in many of Smith and Davis' tests. However, since the conditions for combustion were unfavorable; i.e., near free-stream ambient pressure and temperature for the flight condition with residence times of less than 100 μs, they felt that conventional fuels were not practical. For this reason, they used very reactive fuels, principally aluminum borohydride, in their tests and it is notable that the only successful external burning experiments made since that time have been with reactive fuels. In Ref. 48, aluminum borohydride was injected from the walls of a 3.84-inch by 10 inch supersonic wind tunnel into a Mach 1.5 to 4.0 airstream. Since the maximum tunnel plenum conditions were limited to 540° to 570°R and 1-1.5 atm, the

static temperature and pressure in the test section decreased with increasing Mach number, dropping from 386°R and 0.4 atm at Mach 1.5 to 133°R and 0.01 atm at Mach 4.0. In spite of the high altitude pressure simulation (71Kft @ M_0 = 3) and unrealistically low temperatures, (~200°R low @ M_0 = 3) steady combustion was demonstrated at M_0 = 1.5, 2 and 3. Spontaneous ignition occurred in the Mach 1.5 and 2.0 tests, but at Mach 3.0, a downstream spark source was needed which, after ignition and flashback to the injector, could be terminated. In Ref.49, wall static pressures were measured in the same facility at M_0 = 2 and 3. Pressure rises of from 20 to 40 percent above the no injection values were obtained which had an increasing trend with increasing equivalence ratio and slightly higher ratios at M_0 = 3 than at M_0 = 2. These results prompted an investigation of a flat-plate model in a larger Mach 2.46, 1 ft by 1 ft tunnel.[50] In this facility, the nominal static pressure was 0.1 atm and the static temperature was 250°R in the absence of combustion. A schematic illustration of a typical flame shape, shock wave pattern and chordwise pressure distribution are shown in Fig. 22(A). The model consisted of a short basic flat plate with a 12-in span and 13-in chord plus an extension plate with an additional 12-in of chord. As suspected by the authors in their analysis of the data and later verified in a larger (10-ft x 10-ft) tunnel test of a similar model,[51] the secondary pressure rise downstream was due to tunnel effects. A comparison of static pressure distributions from the two facilities is shown in Fig. 22(B). Computed Mach numbers based on static and pitot pressures taken within the luminous flame zone showed that the Mach number was subsonic through most of the flame zone and became sonic and low supersoni as the hot-cold inter-

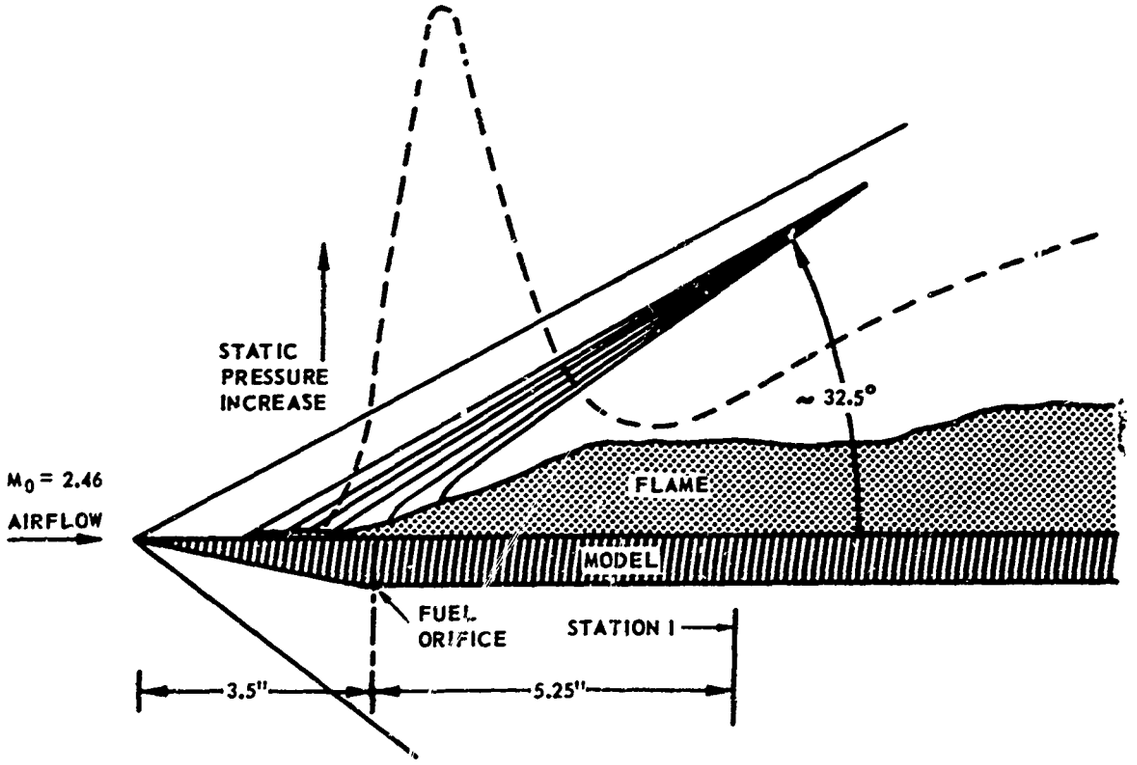

A. SCHEMATIC OF FLAME SHAPE, SHOCKWAVE PATTERN AND CHORDWISE PRESSURE DISTRIBUTION IN 1-FOOT BY 1-FOOT TUNNEL

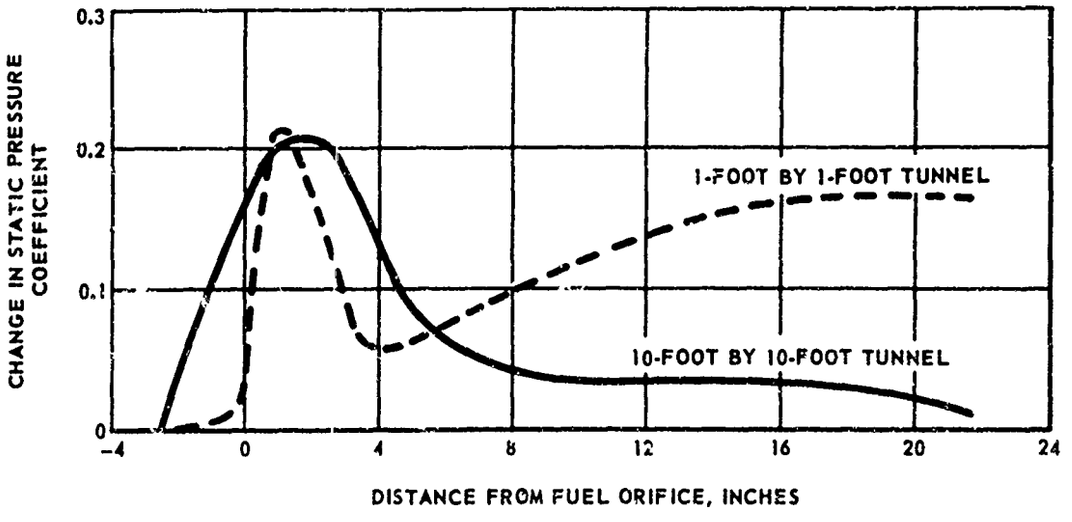

B. COMPARISON OF SURFACE PRESSURE DISTRIBUTIONS

Fig. 22 RESULTS OF FLAT-PLATE TESTS IN SMALL- AND LARGE-SCALE TUNNELS BY NASA. (Refs. 50 and 51)

face was approached. An analysis of this test will be discussed later.

A body of revolution (a 10.5-inch parabolic forebody followed by a 10.5-inch cylindrical afterbody with a 1.75-inch-diameter) was also tested in the 1-ft by 1-ft Mach 2.46 tunnel. Fuel was injected through four circumferential and equally-spaced, 0.015-inch-diameter fuel orifices which were located in the plane of the forebody-afterbody junction. As was the case in all of the tests in this series[48-53] no attempts were made to vary the fuel-flow rate or to control or measure it to a high degree of accuracy. Spark ignition was required. Combustion produced a near constant pressure field on the afterbody with a rise of about 1 psia or about 70% above the non-burning condition. A corresponding rise in base pressure from 0.68 psia to 2.5 psia also occurred but quantitatively undetermined wind tunnel effects may have influenced this result.

The remaining tests in this series were made with a two-dimensional, 6% thick, blunt-base airfoil, at 2° angle-of-attack in the 1-ft by 1-ft tunnel.[53] The model had a 13-inch chord and was tested at $M_0 = 2.47$ and 2.96. The location of the heat addition region below the wing was arbitrarily chosen to provide primarily a lift increase rather than a drag reduction, in order to facilitate comparison with the theoretical calculations of Ref. 11. Figure 23(A) is a combination open-shutter and schlieren photograph of the flame and associated shock wave system for a test at $M_0 = 2.47$. In Fig. 23(B) the typical pressure distributions with and without combustion for both surfaces at each Mach number tested are shown. Integration of the pressure-area distribution produced the forces and coefficients shown in Table IV.

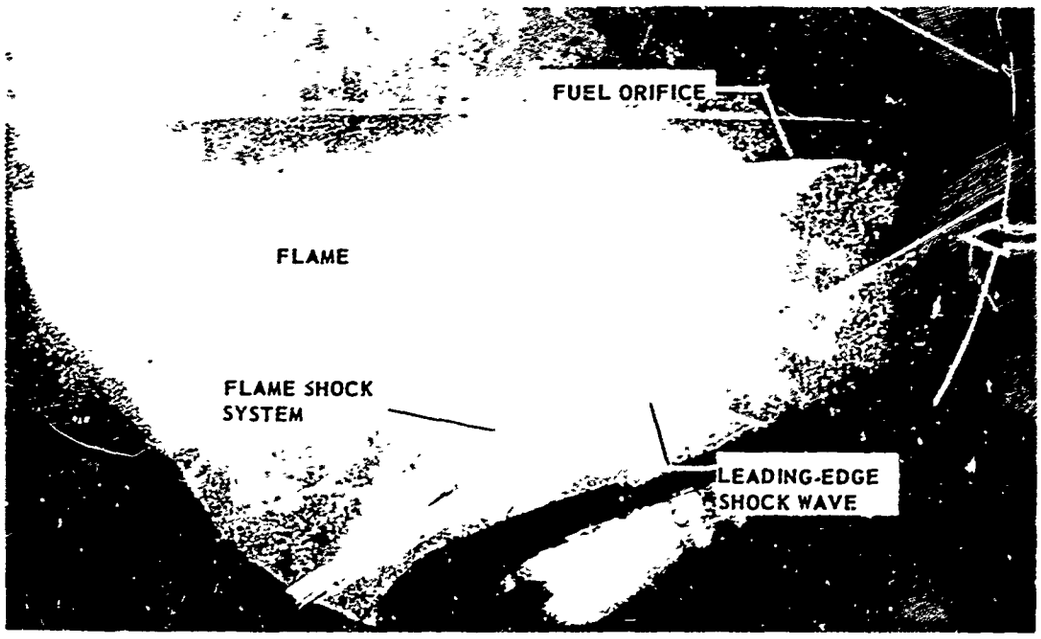

A) COMBINATION OPEN SHUTTER AND SCHLIEREN PHOTOGRAPH OF COMBUSTION AT $M_0 = 2.47$

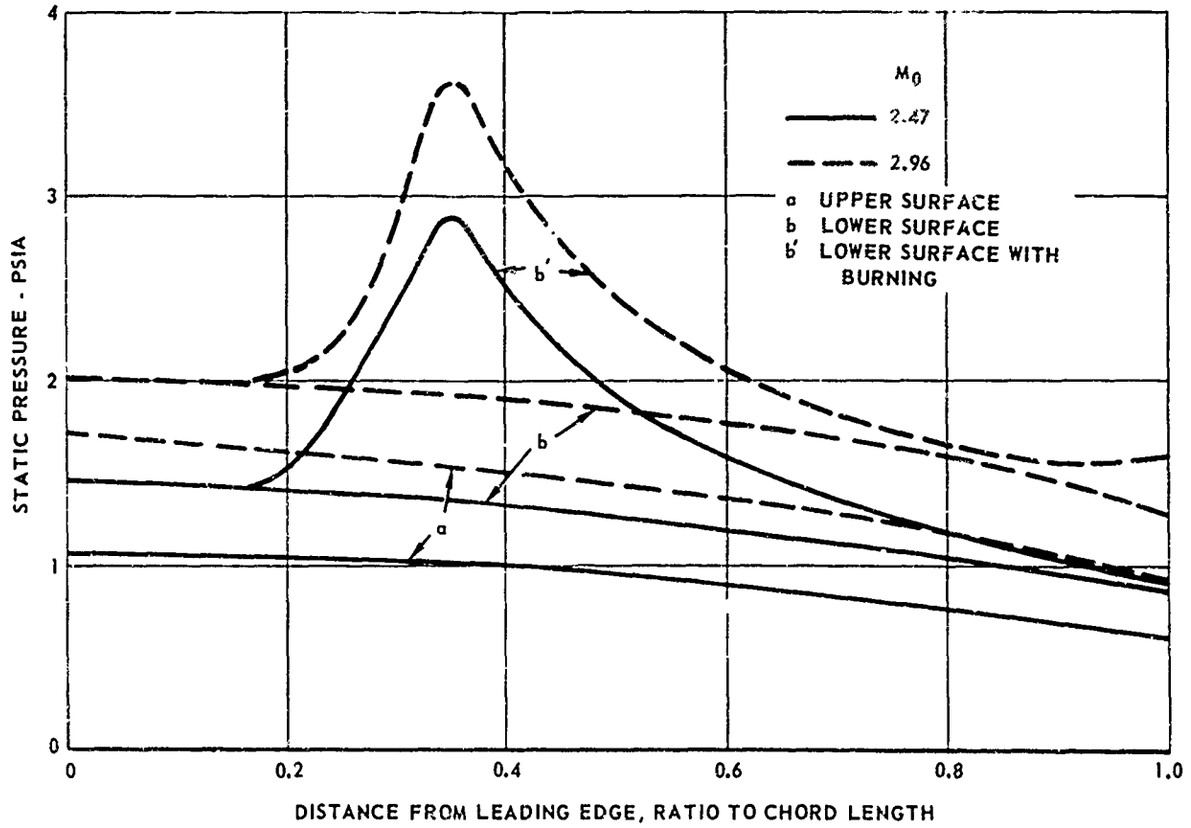

B) SURFACE STATIC PRESSURE DISTRIBUTIONS

Fig. 23 RESULTS FROM EXTERNAL BURNING TESTS OF AIRFOIL AT $M_0 = 2.47$ AND 2.96 BY NASA. (Ref. 52)

TABLE IV

Summary of Forces on Airfoil at $\alpha = 2^{\circ}$

Mach No.	Condition	Lift Force, lb/ft span	C_L	Drag Force, lb/ft span					L/D
				Upper	Lower	Base	Friction	Total	
2.47	Non-burning	60.7	0.06						
	Burning	117.7	0.12						
2.96	Non-burning	50.3	0.05	-1.4	11.5	-1.4	3.2	11.9	4.2
	Burning	113.0	0.12	-1.4	15.7	-2.8	3.2	14.7	7.7

The friction drag was based on a skin-friction coefficient (on planform area) of 0.0035 obtained from unpublished wind tunnel tests. The lift force with combustion about doubled at both Mach numbers. At $M_0 = 2.96$, which was the only Mach number that drag data were analyzed, the drag also increased with combustion. This drag increase results from an increased positive pressure coefficient of the forward facing portion of the lower surface which more than compensates for the increased pressure on the rearward facing aft surface and on the base.

With the lift coefficient defined, then the lift parameter $C_L (M_0^2 - 1)^{\frac{1}{2}}$ is known, and it is only necessary to define an effective heater deflection angle δ_H, and the fraction of chord, f, below which the heat is added, to compare the experimental results with the theoretical analysis of section 2. Within the accuracy of the measurements, δ_H was found to be about 10° at both Mach numbers and values of f = 0.6 at $M_0 = 2.47$ and f = 0.8 at 2.96 were estimated. Using these values to obtain the effective lift flow deflection parameter, $\alpha + \frac{1}{2} f \delta_H$, the experimentally determined lift parameter is compared

in Table V with the linear theory values and the graphically determined values for the 5° biconvex airfoil studied by Pinkel, et al[11] (interpolated from points shown in Fig. 5).

TABLE V

Comparison of Measured and Theoretical Lift Parameters for Airfoil

M_0	$\alpha + \frac{1}{2} f \delta_H$	$C_L (M_0^2 - 1)^{\frac{1}{2}}$		
		Measured	Linear Theory[13]	Graphical[11]
2.47	5°	0.28	0.35	0.28
2.96	6°	0.34	0.41	0.30

The significance of the rather close correlation of theory with experiment is that the selected value of δ_H is indeed reasonable, and, therefore, a reasonable evaluation of the efficiency based on the theoretical methods for the heat addition process can be made. Equation (9) can be used to find the effective $\dot{q}_A$ which can be ratioed to the maximum (complete combustion) $\dot{q}_T$ available in the fuel. In these tests, the average $\dot{w}_f$ was 0.015 lb/sec which for a heating value of 24,800 Btu/lb for aluminum borohydride gives the efficiencies listed in Table VI.

TABLE VI

Heating Rates and Efficiency for Airfoil at $\alpha = 2°$

M_0	$\dot{w}_f$ lb/sec	$\dot{q}_A$ Btu/sec ft^2 (Actual)	$\dot{q}_T$ Btu/sec ft^2 (Available)	Efficiency = $\dot{q}_A/\dot{q}_T$
2.47	0.015	311	575	0.54
2.96	0.015	226	431	0.52

Thus, about half of the effective heat release was obtained in these tests.

Even though it is evident in all of these tests that the heat addition occurs in a zone which is spread out in the streamwise direction and therefore cannot be considered as a planar flame, it is of interest to examine the results using a form of the planar heat addition models to see whether any correlations can be obtained. Woolard [54] studied the flat plate results from Refs. 50 and 51, using the pressure profiles from the 10-ft by 10-ft tests (Fig. 22(B)) and the detailed in-stream measurements from the 1-ft by 1-ft tests. Instead of the simpler single heated streamtube concept of Ref. 18, he postulated the two-layer model shown in Fig. 24. In the inner layer, the Mach number just behind the oblique planar heat addition, $\bar{M}_3$ is subsonic. The flows in regions $\bar{3}$ and 3 are assumed to be uniform, parallel and have equal static pressure. With no further constraints, there are enough free parameters to permit a favorable preferential matching of theoretical and experimental values. Those properties for which an attempt was made to obtain an approximate matching were the peak pressure rise, the downstream pressure decay, the over-all flame shape, and the total-temperature increase in the inner layer. These results are summarized in Fig. 25. The experimental flame shape was specified as the luminous-non-luminous boundary as determined from the sketch shown in Fig. 22(A) which apparently is an unrealistic description of the method of heat addition. In Fig. 25(A) the correlation between the experimental and theoretical pressure distributions and "planar flame shapes" are close, but the calculated temperature and Mach number distributions at Station I of Fig. 22(A) shown in Fig. 25 (B) and (C) are poor, although better than a linear theory approximation.

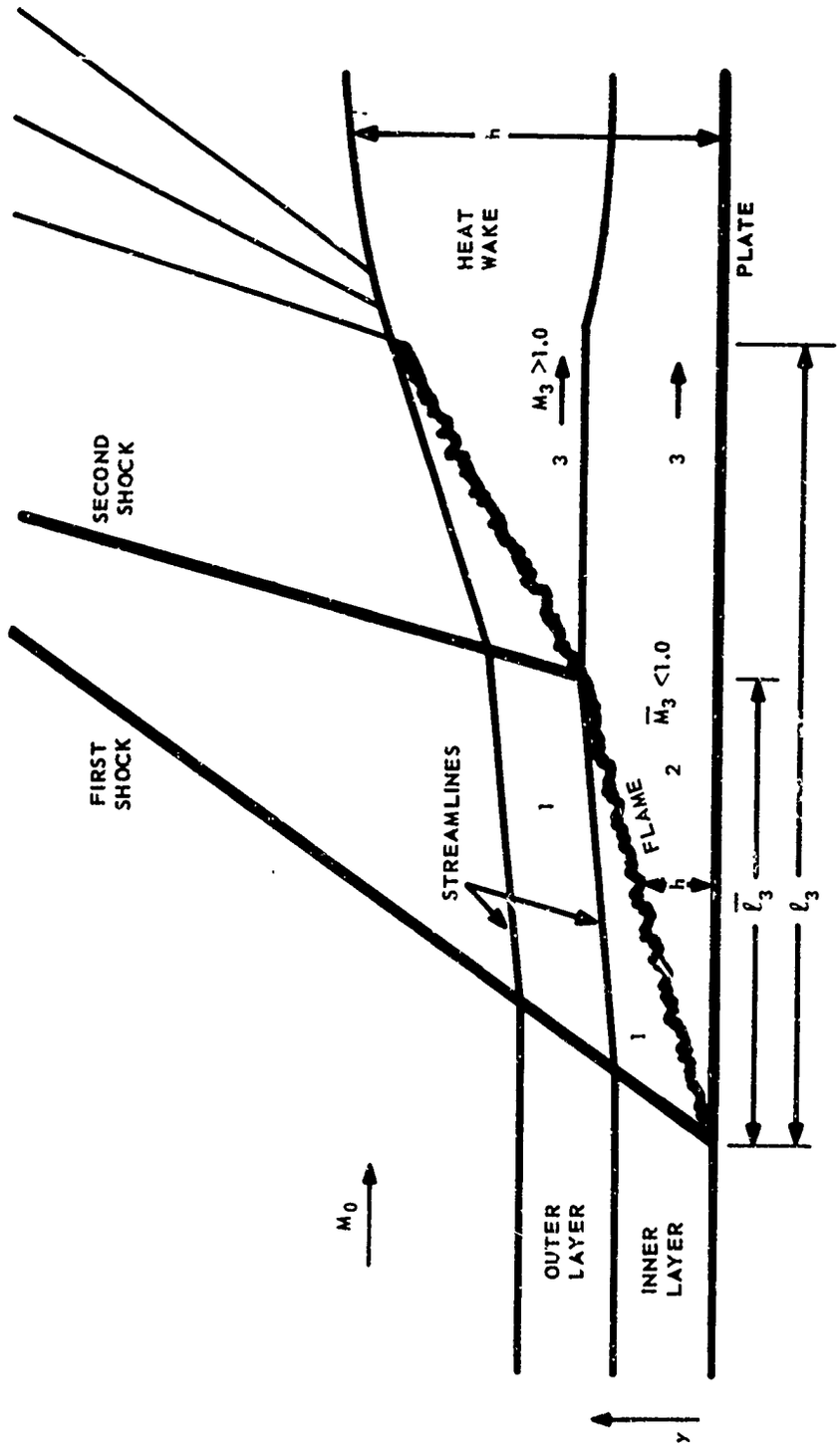

Fig. 24 ILLUSTRATION OF THE TWO STREAM OBLIQUE PLANAR HEATER AFTER WOOLARD. (Ref. 54)

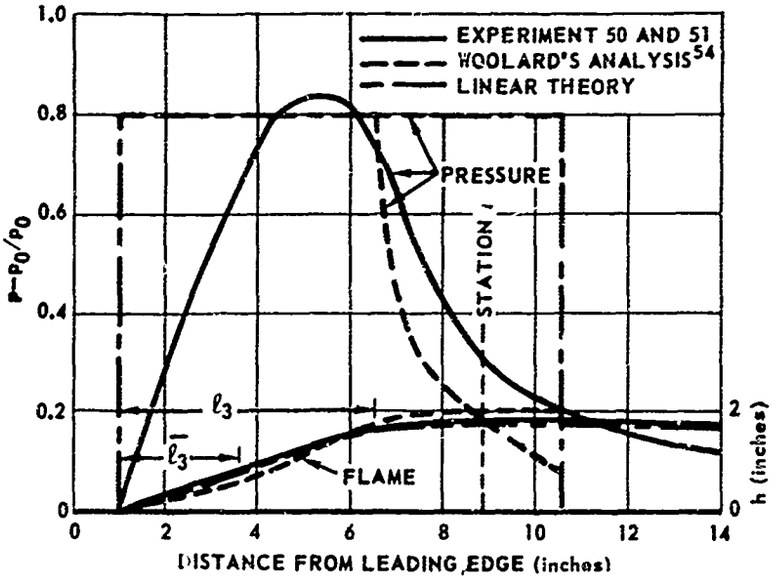

A) PRESSURE DISTRIBUTIONS AND FLAME SHAPES

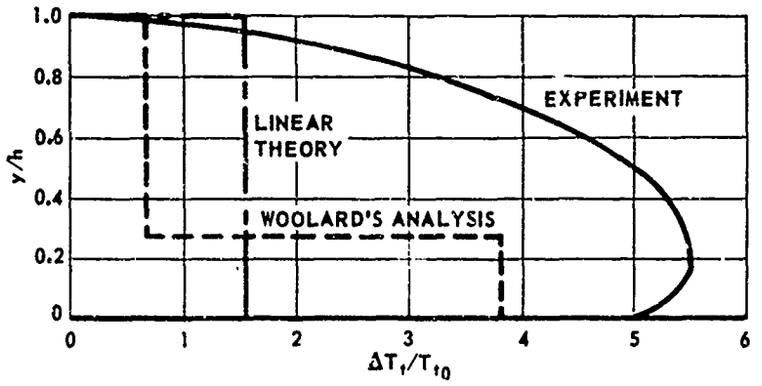

B) TOTAL TEMPERATURE DISTRIBUTIONS AT STATION I

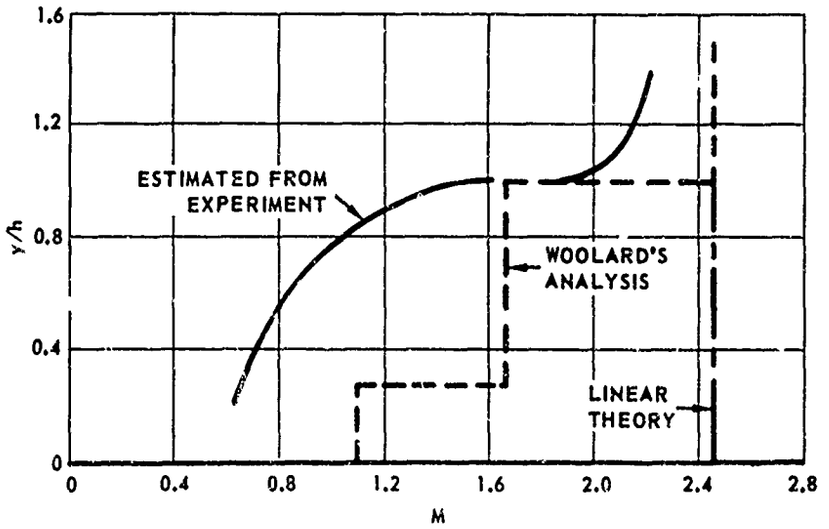

C) MACH NUMBER DISTRIBUTIONS AT STATION I

Fig. 25 COMPARISON OF FLAT-PLATE EXPERIMENTAL RESULTS WITH TWO-LAYER ANALYSIS OF WOOLARD

Testing of external burning ramjets at the Applied Physics Laboratory was initiated in 1958. The first phase of the program consisted of small-scale wedge model tests in a 6-in. by 7-in. high-temperature, Mach 5.0 propulsion tunnel with 100K ft altitude simulation. The principal objective in the first phase of the program was to demonstrate useful thrust on a configuration similar to the type shown in Fig. 2(C). In the second phase, a scaled version of one of the smaller models was tested in a 32-in.-diameter free jet at the Ordnance Aerophysics Laboratory (OAL) at Mach 5.0 with somewhat less than simulated static temperature (260^{o}R vs 390^{o}R) and with pressure altitude simulation from 82K ft to 105K ft. In the last phase of the program, extensive in-stream measurements were made on a flat plate model tested in a 10-in.-diameter Mach 5.0 tunnel with true simulation of flight at 66K ft. Aluminum alkyl fuels,[34] which reacted spontaneously without supplemental ignition sources, were used in the tests. Fuel handling, metering and heating systems were developed[34] to provide a means for fuel flow control and measurement.

The models tested in the small APL facility are shown schematically in inverted position in Fig. 26. Wedge angles and major dimensions are given in the code chart. Side plates, to prevent transverse spillover, were available for all models with width (d) less than the tunnel width of 5.92 inches. Fuel was injected from a number of 0.031-in.-diam fuel ports on 1/2-in. spanwise spacing supplied by one of several available fuel manifolds located at or slightly upstream of the knee. Generally, the models were tested at angles of attack from -4^{o} to $+4^{o}$ and with fuel flow rates from the lean ignition limit to a maximum rate above which the propulsion tunnel would not operate due to excessive heat release.

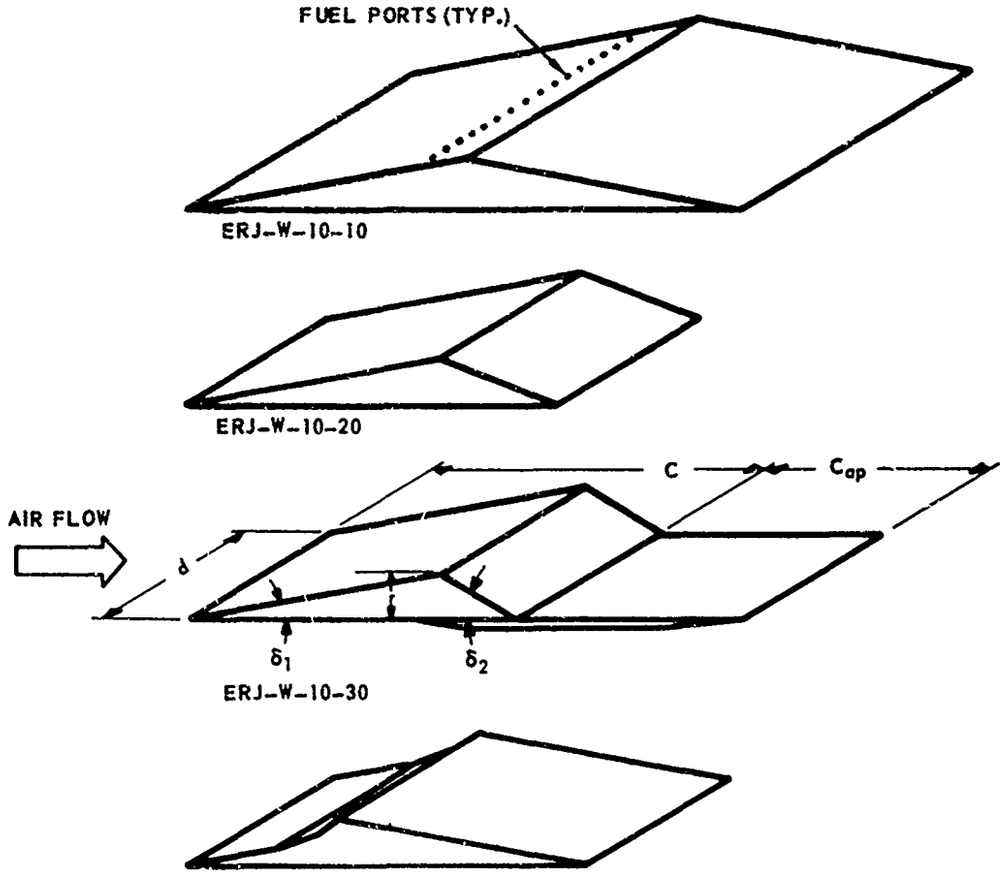

CODE DESIGNATION	δ_1	δ_2	d (in.)	r (in.)	C (in.)	C_{ap} (in.)
ERJ-W-10-10	10°	10°	5.92	1.08	12.10	
ERJ-W-10-20	10°	20°	4.00	1.01	8.51	
ERJ-W-10-30	10°	30°	4.00	1.01	7.44	4.19
ERJ-W-(10-22-38)-10	10°,22°,38°	10°	4.00	1.01	9.03	

Fig. 26 SKETCHES AND DIMENSIONS OF EXTERNAL BURNING MODELS TESTED IN THE 6 IN. BY 7 IN. TUNNEL AT APL

Typical axial and transverse static pressure distributions generated with triethyl aluminum (TEA) fuel on ERJ-W-10-30 at $+4^{o}$ angle-of-attack are shown in Fig. 27. The pressure rise due to combustion on the expansion wedge increased with increasing fuel rates, $\dot{w}_f$, but the pressure rise per lb/sec of fuel $dp/d\dot{w}_f$) decreased. In this test the lean ignition point was near $\dot{w}_f = 0.009$ lb/sec, but in other tests with other models at different angles of attack, lean-limit fuel rates as low as 0.0036 lb/sec were obtained.

Air passing over the model is compressed on the forward surface from a free stream static-pressure/total-pressure ratio of 0.0018 to a ratio of 0.008 by turning through the oblique bow shock. In the absence of heat release, the flow re-expands, at the knee, to a pressure level near that for a simple Prandtl-Meyer turn. When the lean-limit fuel flow is established, the volume source due to thermal expansion in the heat release zone essentially cancels the Prandtl-Meyer expansion in the adjacent (external) air streamtube, so that the pressure on the expansion surface is nearly the same as that on the compression surface. Increasing the fuel rate increases the strength of the oblique shock at the injection station and produces higher forces on the aft wedge. Thus, net thrust can be produced. However, as previously noted, $dp/d\dot{w}_f$ is negative at the higher $\dot{w}_f$ so that specific impulses for thrust and lift decrease as $\dot{w}_f$ is increased. This effect can be seen in a summary plot of the data from ERJ-W-10-30 shown in Fig. 28. The data from Fig. 27 are plotted as curve F, and since the slope for either ΔC_L or ΔC_T versus fuel flow rate is less than that of the corresponding theoretical curve for $\alpha = +4^{o}$, efficiency decreases as fuel rate increases. The only data with a different trend, curves B and C were with fuel heated above the nominal level of 200^{o} F.

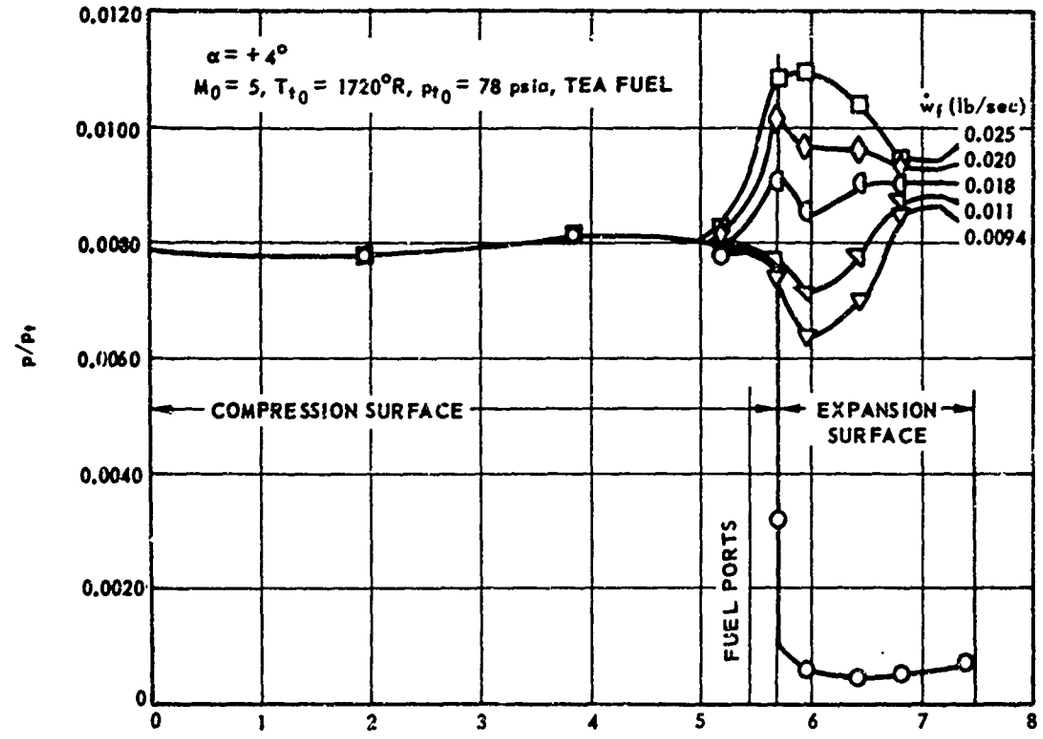

A) AXIAL PRESSURE DISTRIBUTION AT α = +4°

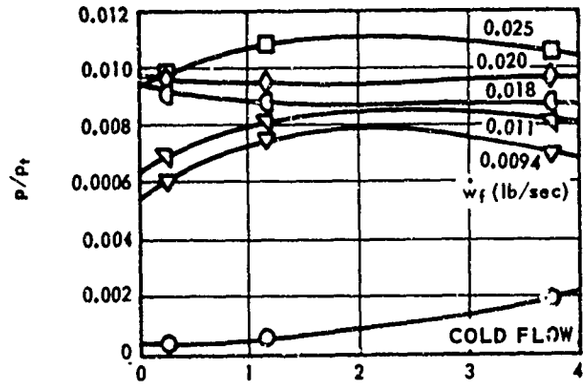

B) TRANSVERSE DISTRIBUTION AT STATION 6.43

Fig. 27 EXPERIMENTAL PRESSURE PROFILES FOR APL MODEL ERJ-W-10-30.

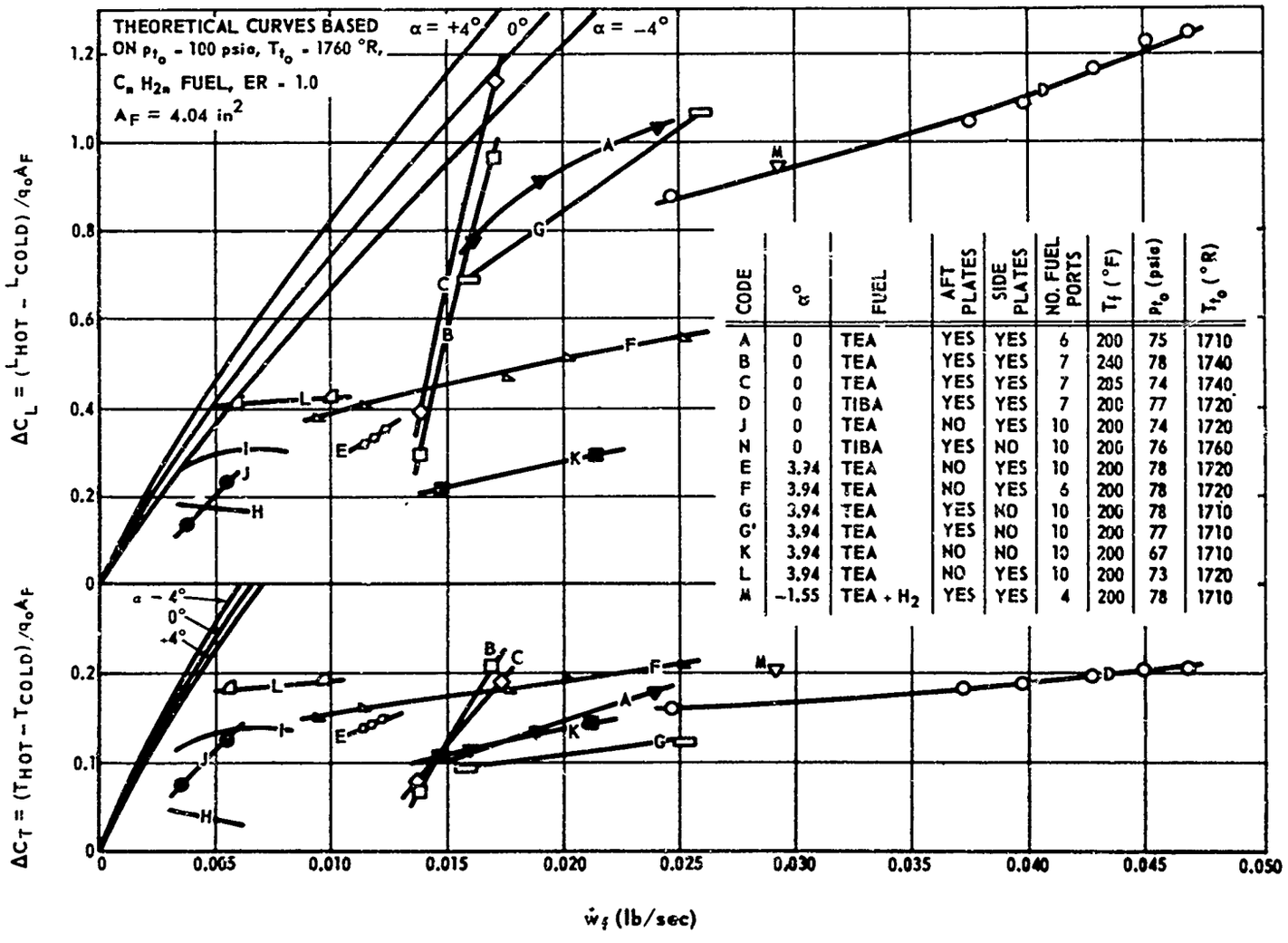

CODE	α°	FUEL	AFT PLATES	SIDE PLATES	NO. FUEL PORTS	T_f (°F)	p_{t_0} (psia)	T_{t_0} (°R)
A	0	TEA	YES	YES	6	200	75	1710
B	0	TEA	YES	YES	7	240	78	1740
C	0	TEA	YES	YES	7	205	74	1740
D	0	TIBA	YES	YES	7	200	77	1720
J	0	TEA	NO	YES	10	200	74	1720
N	0	TIBA	YES	NO	10	200	76	1760
E	3.94	TEA	NO	YES	10	200	78	1720
F	3.94	TEA	NO	YES	6	200	78	1720
G	3.94	TEA	YES	NO	10	200	78	1710
G'	3.94	TEA	YES	NO	10	200	77	1710
K	3.94	TEA	NO	NO	10	200	67	1710
L	3.94	TEA	NO	YES	10	200	73	1720
M	−1.55	TEA + H_2	YES	YES	4	200	78	1710

Fig. 28 LIFT AND THRUST GAINS DUE TO BURNING ON THE APL ERJ-W-10°-30° MODEL TESTS AT MACH 5.

The theoretical curves of Fig. 28 are based on the constant pressure analysis of Section 2.3 (Fig. 15) using C_nH_{2n} fuel at ER = 1.0 rather than for the actual fuels used in the tests. The effect of fuel change would be small because the fuel flow required for a given pressure rise, hence, lift and thrust, is primarily dependent on the heating value of the fuel. TEA has a heating value of 18,360 Btu/lb and TIBA (tri-isobutyl aluminum) has 18,420 Btu/lb as compared to a nominal value of 18,630 Btu/lb for C_nH_{2n} from Ref. 31. Theoretical curves for ER lower than 1.0 would be somewhat better, (see Fig. 16(D)) but since no instream gas sampling or measurement of the capture height Y_1 was attempted, the effective experimental equivalence ratio cannot be determined. Moreover, the theoretical curves do not consider non-equilibrium kinetic effects and/or mixing effects, which for small models probably are very influential in the trends of performance with ER.

In general, the results approach theoretical lift gains more closely than theoretical thrust gains due to the fact that the fuel is injected just ahead of the model knee. The small force component due to injection and combustion on the forward wedge adds to lift but subtracts from thrust, whereas in the theoretical model all pressure rise effects are felt only on the rearward facing surface. The theoretical values are approached only at very low fuel rates or with externally preheated fuel. TEA gives better results than TIBA for a given fuel rate at these conditions (compare A and D).

Pressures on the aft plate extension were generally about the same as on the rearward facing wedge, indicating that heat release was still occurring downstream of the wedge. This pressure increase would increase lift at all angles of attack but would subtract from thrust for positive α

and add at negative α. Residence time based on the air velocity would be about 25 μ sec in the aft wedge zone and an additional 60 μ sec in the extension plate zone. Results from the other models tested were similar, with most efficiencies between 25 and 60 percent and a few very lean operating points having about the theoretical efficiency.

The larger model (Fig. 29) used in the free-jet tests at OAL was geometrically similar to ERJ-W-10-20 tested at APL but was three times larger in linear dimensions. Each fuel manifold fed a row of twenty-one 0.047-in.-diam injection holes on 0.5-in. spacing. The two manifolds used on these tests were located 1.60 in. and 0.25 in. upstream of the knee and were designated F2 and F3, respectively. Figure 29(B) is a photo of the basic model installed in the 32-in.-diam, Mach 5 free-jet nozzle. The removable fuel injection pylons shown in Fig. 29(C) have 30° total-included-angle front wedges and 40°-total-included-angle rear wedges. Six equally spaced, 0.047-in.-diam fuel ports (24 total) were located on each obtuse angle knee of a pylon. Each pylon provides its own bow shocks, which lie transversely within the field of the main body's bow shock. These additional shocks double the static pressure and raise the static temperature by about 50%, i.e., from 400°R to 600°R. Aluminum oxide deposit patterns can be seen on the surface in Fig. 29(C). The presence of oxides upstream of the injector pylons indicates that a boundary layer separation existed during combustion.

The maximum air total temperature that could be provided by the facility was 1500°F, ($\sim 700^{\circ}$R below that required for Mach 5.0 flight simulation), hence the free stream static temperature was $\sim 250^{\circ}$R, or about 140°R low, and some reservation is needed in judging scaling effects

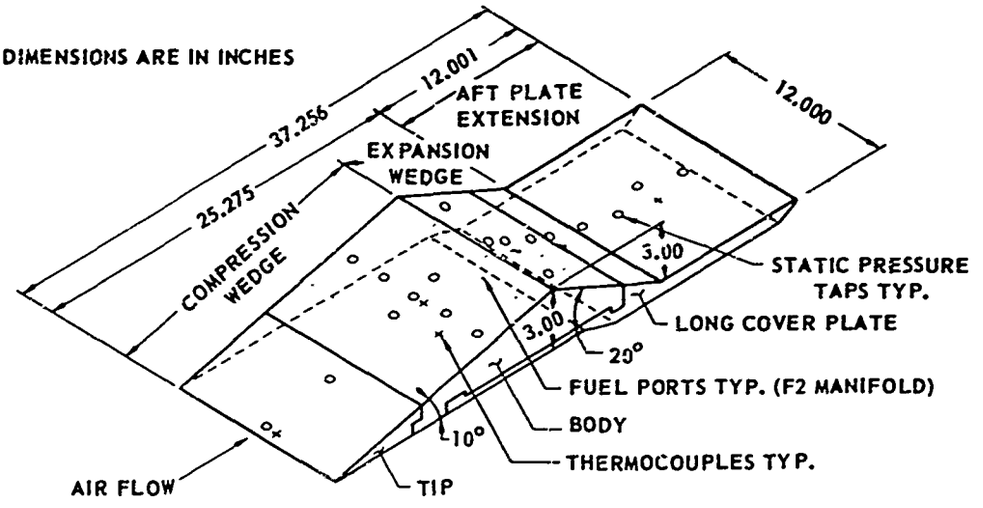

A) SCHEMATIC MODEL WITH AFT EXTENSION PLATE BUT WITHOUT SIDE PLATES

B) BASIC MODEL INSTALLED AT EXIT OF MACH 5 FREE JET NOZZLE. FUEL LINES COME OFF NEAR SIDE, INSTRUMENTATION LINES OFF FAR SIDE.

C) TOP REAR VIEW OF MODEL WITH FUEL INJECTION PYLONS, SIDE PLATES, AND AFT PLATE INSTALLED.

Fig. 29 ERJ MODEL TESTED AT ORDNANCE AEROPHYSICS LABORATORY

between the APL and OAL tests.

Axial pressure distributions for the model with side plates and aft plate extension for 0^{o} and 4^{o} angle-of-attack are given in Fig. 30. For the former, (A) injection is from the forward F2 manifold only, whereas for the latter, (B) injection from F2 and/or F3 is used. In all burning runs the pressure on the expansion wedge is more or less constant. At most fuel rates injection produced a pressure spike which rapidly dissipated at, or just downstream of, the knee. In these tests (as in all others), the pressure spike was located farther aft with injection from the F3 manifold. Some of the effects noted in tests with this and other configurations and test conditions are:

1. For the same ratio of fuel flow to air total pressure, results were better at a total pressure of 100 psia than at 160, 200 or 70 psia. If jet penetration depends primarily on the relative fuel-air momentum, then the penetration of a incompressible liquid into a compressible gas will increase with increasing air pressure for constant fuel port area and ratio of fuel flow to air pressure; e.g., doubling both the fuel rate and the air pressure quadruples the fuel momentum but only doubles the air momentum. Since the penetration (or effective Y_1) increases, the effective equivalence ratio decreases, and it is conjectured that in these tests the optimum ER condition occurred near 100 psia. Optimum ER again involves, not only the optimization of the equilibrium-one-dimensional process per the theoretical analysis but also includes the non-equilibrium effects (reaction rate), atomization of the fuel, mixing and the effects of a hot air boundary layer.

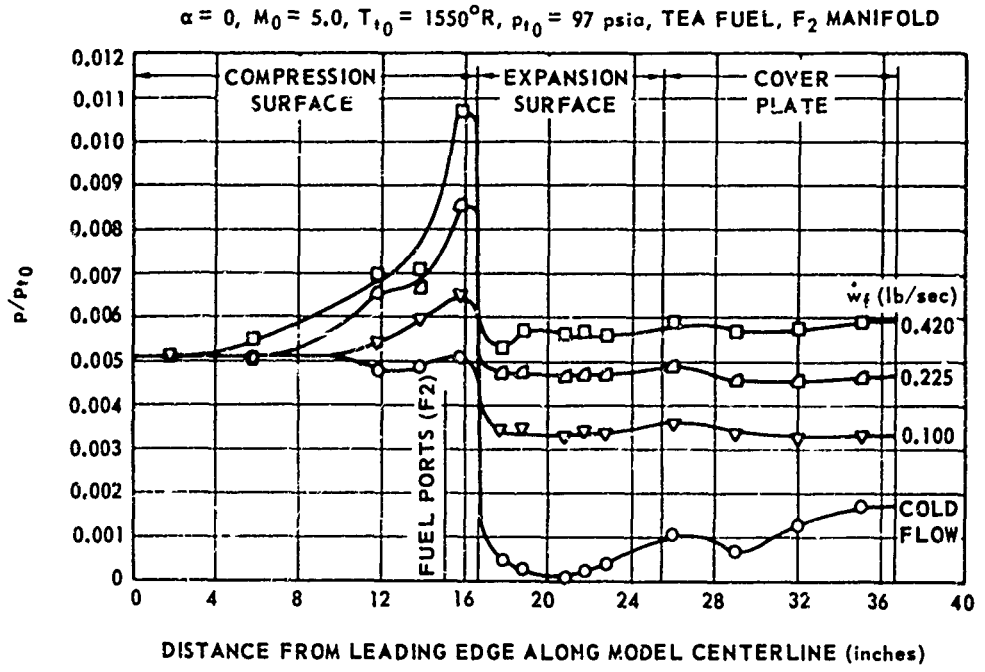

A) AXIAL PRESSURE DISTRIBUTION

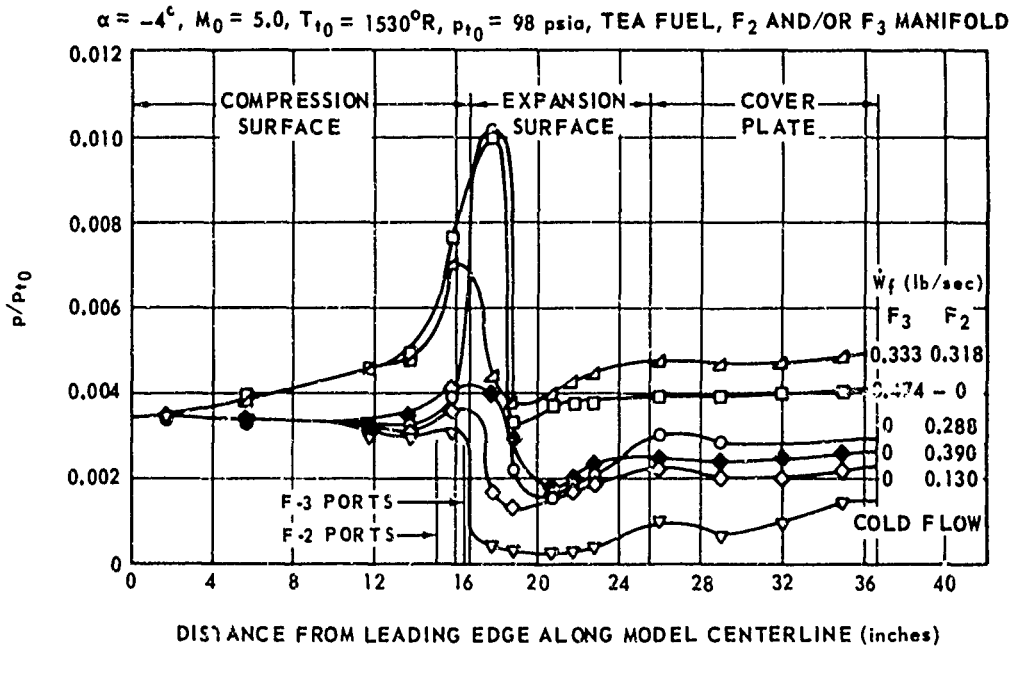

B) AXIAL PRESSURE DISTRIBUTION

Fig. 30 EXPERIMENTAL PRESSURE PROFILES FROM OAL TESTS OF THE 10°–20° WEDGE MODEL WITH SIDE PLATES AND AFT PLATE.

2. Results with the pylons were disappointing in that only slightly higher pressure fields were produced as compared to tests without pylons. Injection from the pylons only was more effective than from combined injection from pylons and body.

3. Combination schlieren-direct luminosity photographs (with a slow shutter on the direct lens) of the basic model show the presence of relatively strong injection shock and weaker combustion induced shocks. Figure 31(A) is a typical photograph showing a luminous main flame zone and a small zone of burning in the boundary layer just upstream of the fuel injection ports. In most cases, the boundary layer flame traveled 3 to 4 inches upstream of the injection point and caused a weak oblique shock in the external flow. Figure 31(B) shows a case with poorer combustion than in Fig. 31(A). There appears to be a region of relatively low heat release (less luminosity) in the first portion of the flame zone and a weaker flame shock. Inspection of the corresponding pressure plots shows that, in this case, the pressure rise due to injection was followed by expansion around the knee before the secondary flame shock was reached, at which point the pressure increased about 25% and remained constant to the trailing edge.

4. In general, the large-scale tests (at OAL) showed lesser thrust and lift gains per pound of injected fuel (50-75%) than the smaller-scale tests (at APL). Besides the aforementioned lower temperature of the OAL tests, it was suggested that dissimilar (cooler and relatively thinner) boundary layer and relative fuel jet penetration may have contributed to the scaling effects.

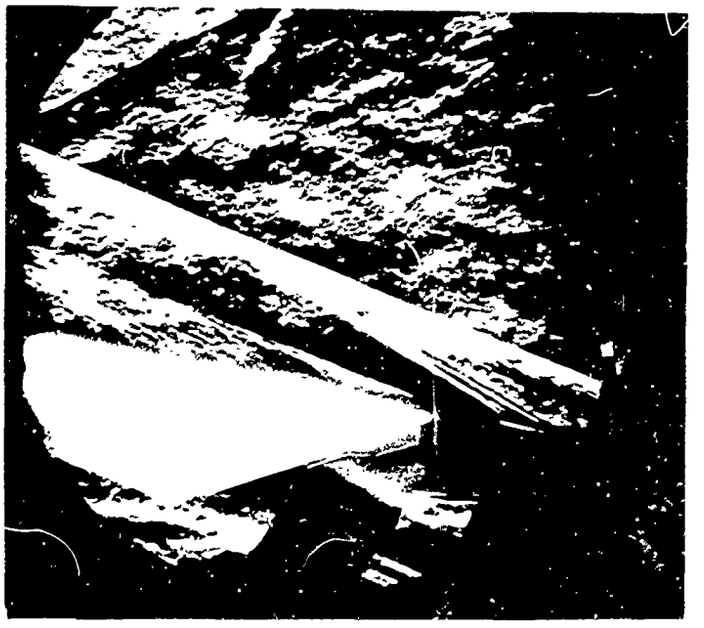

A) INJECTION FROM F2, $\dot{w}_f$ = 0.13 lb/sec, p_{t_0} = 100 psia, $\alpha = +4^\circ$

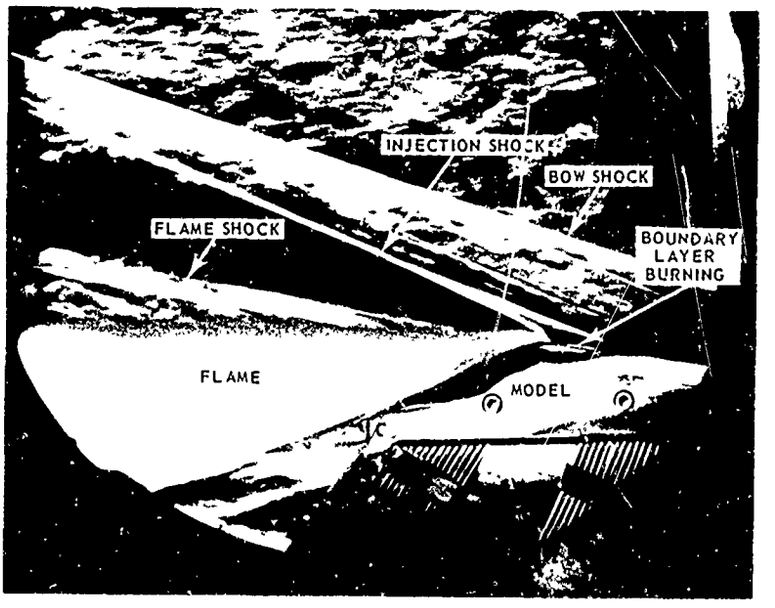

B) INJECTION FROM F3, $\dot{w}_f$ = 0.20 lb sec, p_{t_0} = 195 psia, $\alpha = 0^\circ$

Fig. 31 SCHLIEREN PHOTOGRAPHS FROM OAL TESTS OF BASIC WEDGE MODEL

The flat-plate model tested in the third phase of the program[34] is shown in Fig. 32(A). It is a water-cooled plate 6 inches wide, 15 inches long and 1.25 inches thick. In the tests reported herein, fuel was injected from the most forward fuel manifold which contained twelve 0.031 in. diam. equally spaced fuel ports. The model surface contained numerous static pressure taps, and a traversing pitot tube was used to make surveys of the flow field in the combustion zone. In the tests described, the Mach number in the flow field ahead of the fuel injection shock was 5.04. The static pressure was 0.78 psia and the static temperature was 345-365°R, 25-45°R low for true simulation at 66,000 ft.

Figure 32(B) shows static pressure profiles taken along the model centerline for "cold" flow (no injection) and for toluene and triethyl aluminum (TEA) fuel injection from the forward fuel manifold. The rather abrupt pressure rise 2.5 in. from the leading edge followed by a decay back to about the free-stream level in the toluene curve is as expected for non-reacting liquid injection. Schlieren observations of the flow field confirmed this results.

With TEA injection the pressure first rises, then decays slightly due to the injection shock followed by weak expansion waves, and then rises to a near constant value as the heat release starts to take place. The continuing relatively constant pressure plateau to the trailing wedge indicates that heat release is continuing and has not been completed in the 12 inches.

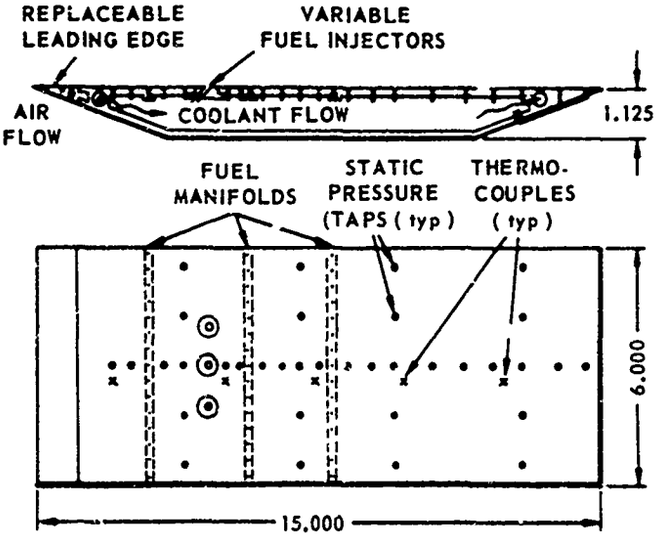

A) SCHEMATIC ILLUSTRATION OF MODEL

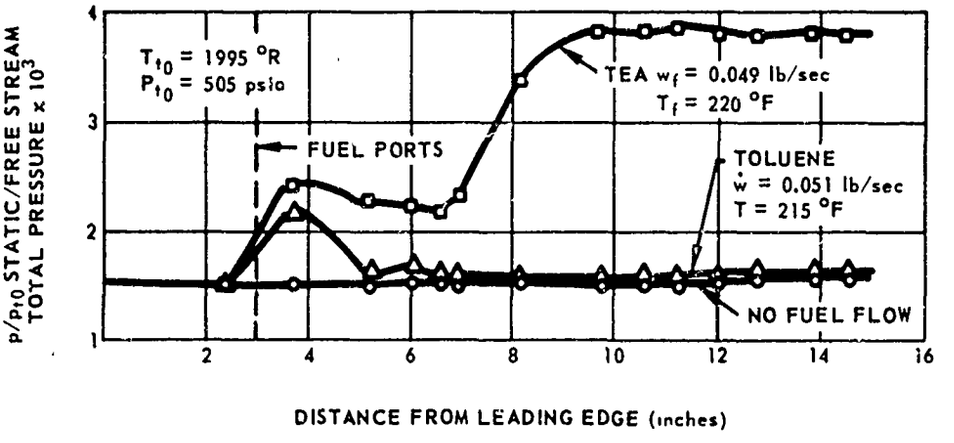

B) LONGITUDINAL PRESSURE PROFILES

Fig. 32 FLAT PLATE COMBUSTOR MODEL TESTED AT MACH 5.04 (Ref. 34)

In order to appraise the latter situation a study of droplet evaporation and diffusion into a second medium was undertaken. The technique proposed by Zwick, Grubman and Hardy,[55] which considers spherical particles with known drag and heat transfer coefficients was used to determine the droplet diameter as a function of time. A necessary input for this calculation is the initial droplet diameter. The empirical relationship of Ingebo and Foster[56]

$$d_0 = 3.9 \left(\sigma_L \mu_L / \rho_g \rho_L u_g^3 \right)^{0.25} d_j^{0.5} \qquad (49)$$

was used to determine the volume mean initial drop diameter. For the TEA flow rate of 0.047 lb/sec at 230°F the calculated d_0 is $.290 \times 10^{-4}$ ft, or about 9 microns. Diffusion coefficients of TEA into air were determined using the rigid sphere model of Hirschfelder, at al[57] based on estimated molecular diameters for TEA.

To calculate the droplet trajectory the analysis by Zwick, et al[55] had to be modified to account for the observed combustion phenomena. In their analysis it was assumed that the droplet is accelerated by an air stream parallel to the plate and therefore the fuel penetration is dependent only on its initial momentum and the ratio of injection and free stream velocities and the physical properties of the fluids. The penetration resulting from this type of calculation would be but a small fraction of an inch at the trailing edge. This is contrary to the observed wedge-shaped luminous region extending from the surface at two inches aft of the injection station to about 1.8 inches from the plate at the trailing edge.

Greater fuel penetration can be postulated in the following way. The fuel penetrates through the separated region with no effective downstream displacement (in fact, some fuel can recirculate upstream and burn in the separated boundary layer, as in the ONI tests), at which point it encounters an airstream moving not parallel to the plate, but away from the surface at an inclination determined by the injection-separation shock strength. The air stream accelerates the droplet both downstream and away from the plate. Subsequent turning of the air stream due to the expansion and recompression by the flame shock similarly affects the droplet. Once the flame shock is crossed, the direction of the main stream is dependent on the distance from the plate according to the postulated constant pressure heat addition model. The stream moves parallel to the plate near the surface but in the direction of the main stream deflection along the hot-cold interface.

Three calculated droplet trajectories are shown in Fig. 33(A). The lowest curve represents a calculation according to the technique by Zwick, et al.[25] The two upper curves were determined according to the above-described modification of that theory. In the trajectory with the greatest penetration the droplet is assumed to be near the hot-cold interface. In the other case, it is assumed to be near the center of the heat addition zone. These curves accordingly diverge 4.5 in. downstream of the injection point where they enter the flame zone. For reference, both the observable luminous zone and the position of the boundary of heat release as deduced from pitot pressure measurements are shown.

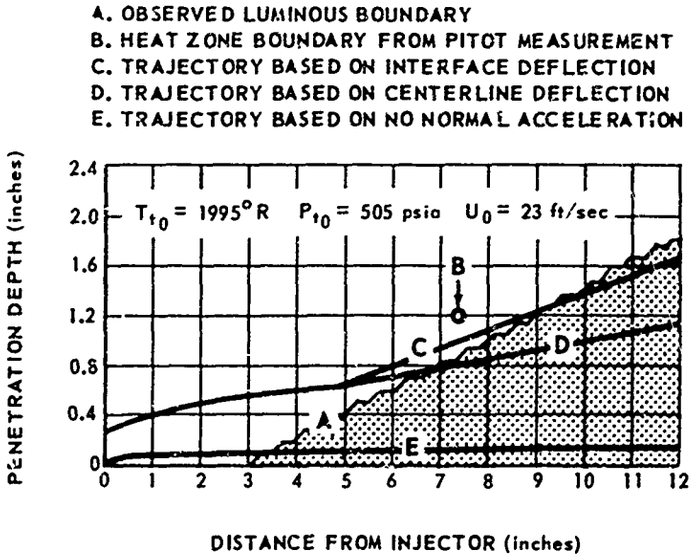

A) DROPLET TRAJECTORIES

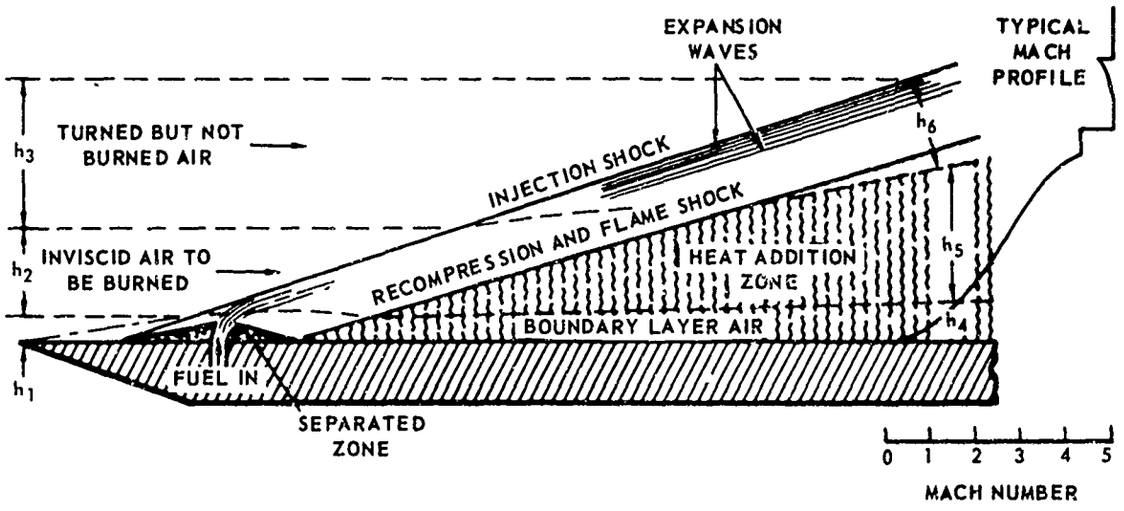

B) SCHEMATIC ILLUSTRATION OF FLOW FIELD

Fig. 33 SCHEMATIC ILLUSTRATION OF FLAT PLATE COMBUSTOR FLOW FIELD AND CALCULATED DROPLET TRAJECTORIES.

In order to analyze the pitot pressure measurements it is necessary to postulate a more applicable flow model than that used in the theoretical study (Fig. 18), since combustion is displaced a slight distance downstream and is only partially completed. A viscous layer is also present. Figure 33(B) shows the concept of the flow picture. The shock wave patterns and flame zone picture are consistent with schlieren and luminosity photographs of the flow field.

In this model the incoming air is divided into three major streamtubes: boundary layer air, inviscid burned air, and air that is turned but not burned. The typical Mach number profile indicates that the properties are not uniform in the major streamtubes as is assumed to be the case in one-dimensional studies. Thus, for detailed analysis the streamtubes must be further subdivided or suitable integrations of properties must be made to reduce the problem to a one-dimensional analysis. The major streamtube boundaries are determined in the following manner: The height of the boundary layer streamtube at the injection shock h_1 is determined by a cold-flow pitot-pressure traverse and checked with a calculated boundary layer thickness. This calculation also provides an estimate for the total mass flow in the streamtube before fuel injection. After fuel injection it is assumed that no further flow into the boundary layer occurs and that the increase in h_4 above h_1 is due to heat release and additional viscous losses. The downstream pitot traverse determines h_6 and the sum of h_5 and h_4. Since the flow in the outside streamtube is inviscid and adiabatic, the upstream height h_3 can be specified by solving wedge-flow relationships consistent with observed shock waves and pressure measurements. The difference between the total

height of the three streamtubes and $h_1 + h_3$ determines h_2. Assuming that the injected fuel is proportionally divided on a mass basis between the two major heat release streamtubes, then all of the necessary conditions are now specified to analyze the combustion except the $\int pdA$ term in the momentum equation for each streamtube.[34] This integral is the product of the local pressure and the incremental projected area in the flow direction summed over the streamtube boundaries.

As a first approximation, the wall static pressure is assumed to be constant in planes normal to the surface. A further refinement can be made by analyzing schlieren pictures of the flow field and actually positioning the shock and expansion waves and calculating the static pressure field. If the Mach profile across h_5 is relatively flat, then the center streamtube can be individually handled as a one-dimensional flow process. In this circumstance the pressure-area integral term is found by assuming the wall static pressure on the plate side of the streamtube and using the wedge flow pressures on the outer side.

For the data point shown, the TEA fuel flow rate was 0.049 lb/sec. The pitot profile measurements showed $h_5 + h_4 = 1.20$ in. The calculated values for h_1, h_2 and h_3 were 0.05, 0.61, and 1.93 in., respectively. At the traversing plane, which was 7.3 in. downstream of the injection port, the calculated average combustion efficiency was 31.5%. The average equivalence ratio in the combustion zone was almost 1.0.

It is possible to relate the experimental result to the more elementary theoretical model of Fig. 18. For the calculated Y_1 and the measured pressure ratio of 0.0038/0.0015 = 2.53 at Mach 5.04, the theoretical length of

the constant pressure region, X_4, is 31.0 in., and the total length is 62.4 in. Combustion would be completed 24 in. from the leading edge and the resulting lift specific impulse would be 5760 sec. An integration of the pressure rise in the test reported with the measured fuel rate gives a normal force specific impulse of 1350 sec.

From the theoretical constant-pressure heat addition model it is also possible to show the variation of total temperature with distance in the heat release zone for a given capture height, Y_1. Thus, for the constant-pressure process the local velocity and Mach number are known as a function of distance. In tests including the above made at nearly the same condition extensive pitot pressure surveys were made and the local Mach number was deduced. The Mach numbers based on measurements made along the centerline streamtube of the heat release zone are shown in Fig. 34 and are compared to the Mach number variation with distance from the theoretical analysis. The distance for the experimental results is the distance along the streamline from the point of first perceptible heat release to the pitot measuring station. The close correlation of data with experiment suggests that the theoretical description of the heat release, viz, a continuous rise in total temperature with distance, is reasonable for these tests.

Hypersonic wind tunnel tests were made at Boeing[58] with the 8° half-angle blunted cone model shown in Fig. 35. Fuel was injected from a single orifice located at the one-quarter body length point. The fuel orifice diameter was varied from 0.003-in. to 0.024-in. and the orientation was either normal to the surface or inclined 45° upstream. Although the model contained pressure instrumentation and was mounted in a two component force balance (normal

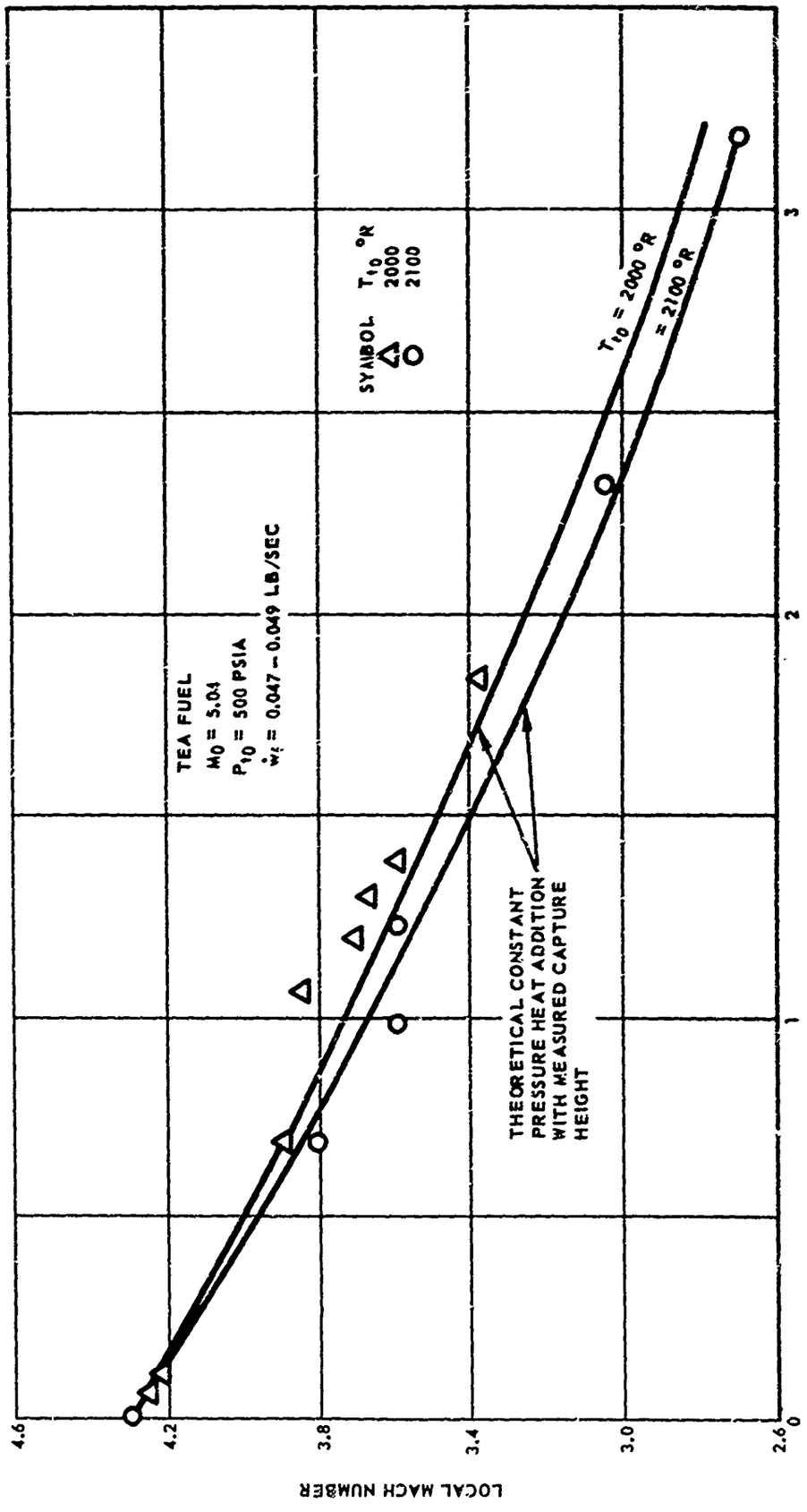

Fig. 24 MACH NUMBER AS FUNCTION OF DISTANCE FROM IGNITION ON FLAT PLATE COMBUSTOR

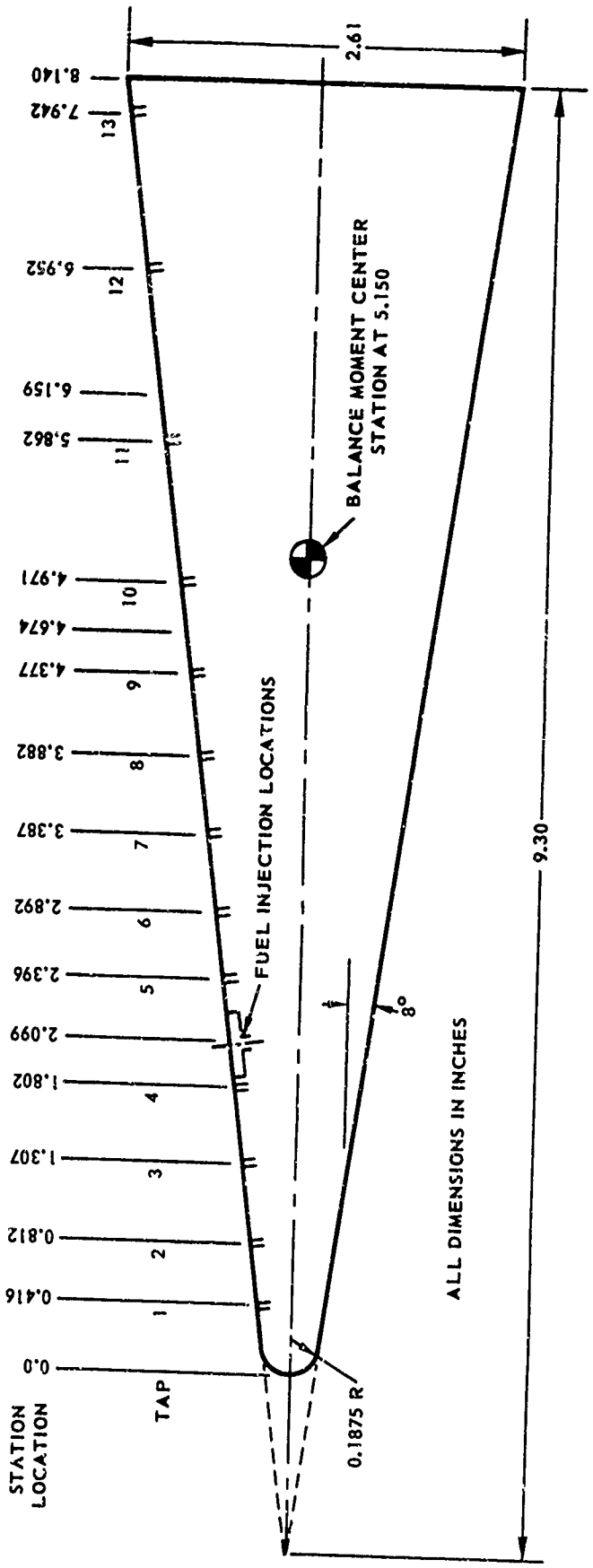

Fig. 35 BLUNTED CONE MODEL USED IN EXTERNAL BURNING TESTS AT BOEING (Ref. 58)

force and pitching moment), both measurements were not made simultaneously. In a typical run the tunnel flow was stabilized, the sting-mounted model was inserted into the air stream, fuel flow was established, and the model was rotated from -30° to $+40^{\circ}$ angle-of-attack. Either pressure or force data were taken, and schlieren and direct luminosity photographs were made.

The tests were made in a 12-in.-diameter open-jet tunnel which was operated at a maximum stagnation pressure of 1000 psia and maximum stagnation temperature of $1460^{\circ}R$. Following some preliminary cold flow and nonreacting injection runs a single test at $M_0 = 6.1$ was made using pentaborane injected from a 0.012-in.-diameter hole oriented normal to the surface. The free stream static conditions for this tests were 0.4 psia and $140^{\circ}R$, or $250^{\circ}R$ low for true simulation. With a fuel flow rate of 0.0048 lb/sec and with the model at zero angle-of-attack, no ignition of the fuel was observed even with a spark ignition source located at the base of the model. Further testing at this Mach number was abondoned and instead a Mach 5.0 nozzle was used in the remainder of the tests. All combustion tests at this Mach number were made with free stream static conditions of 0.75 psia and $250^{\circ}R$, or $140^{\circ}R$ low for simulation. In the first group of successful tests at this condition, pentaborane was injected from 0.009- and 0.012-in.-diameter orifices at 45° upstream and normal to the surface. Direct luminosity photographs revealed that no combustion occured at angles of attack from -30° to 30°. (Again, α is positive for windward side burning.) However, a combustion flame was established on the aft portion of the model at $\alpha = +40^{\circ}$ with all fuel injector configurations. Figure 36 shows the static pressure traces for the different injector conditions tested at

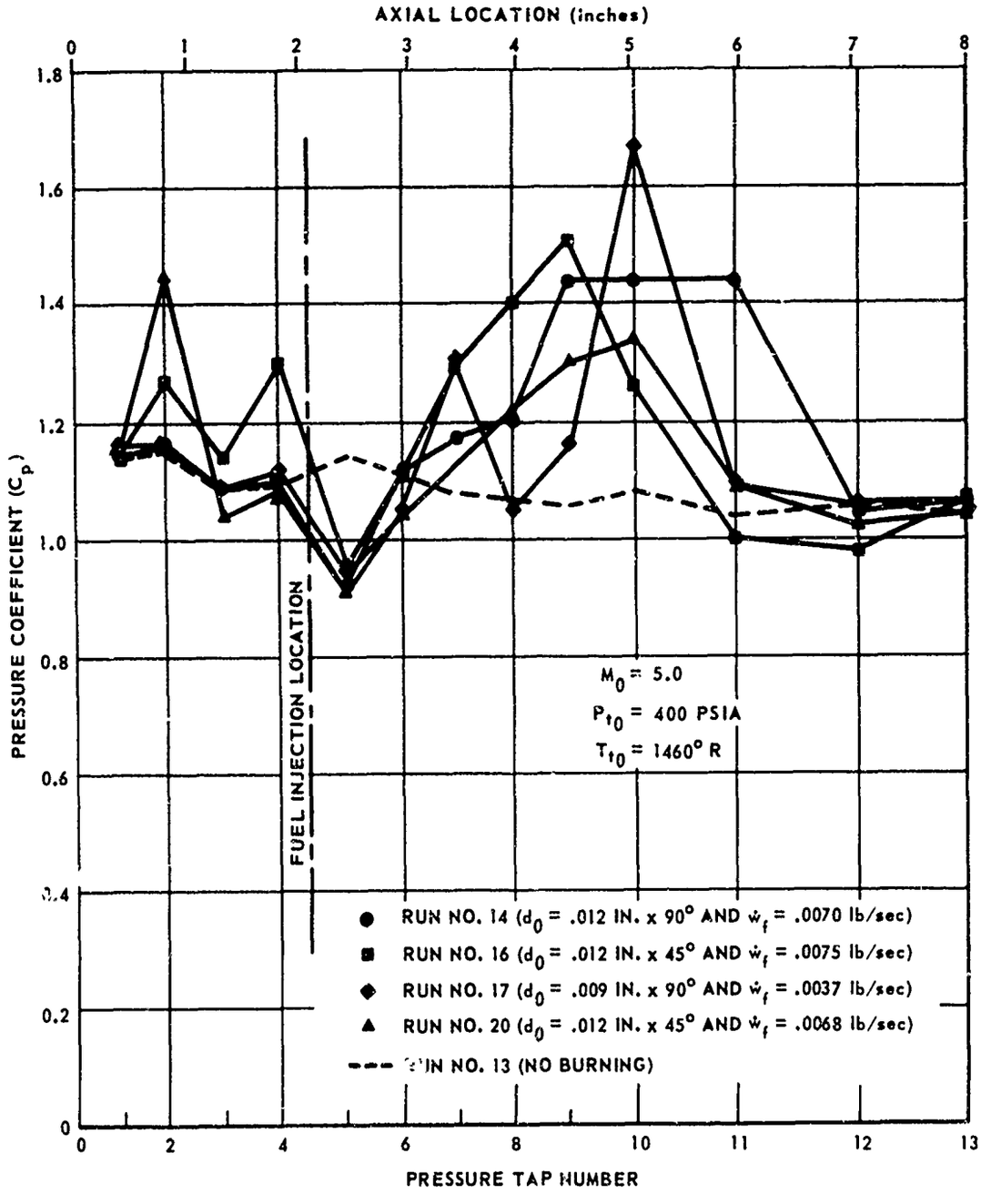

Fig. 36 AXIAL STATIC PRESSURE DISTRIBUTION FOR CONE TEST WITH PENTABORANE AT $\alpha = 40°$

$\alpha = +40^{\circ}$. In all cases a region of negative pressure coefficient occurs downstream of the injection location. Presumably this is the overexpansion region following a pressure spike at the injector, which was not detected in the relatively widely spaced pressure taps. In support of this conjecture are both the schlieren pictures which show the presence of a strong oblique wave at the injector and the higher pressure reading on tap 4 in run 16. No explanation of the high readings on tap 2 in runs 16 and 20 is given. The pressure begins to rise approximately one inch downstream from the injector due to the observable heat release and remains positive for approximately 4 inches farther downstream and then drops due to severe wrap-around at these high angles of attack. Considering the discrepancy between the data from runs 14 and 20 at essentially identical test conditions, no conclusions can be made regarding the effects of fuel orifice diameter and angular orientation on performance. The base ignitor was used in all of these tests and when damage was sustained by it in run 20, a switch to more reactive aluminum borohydride $A\ell(BH_4)_3$ was made. The ignition source was not used in the remainder of the tests.

Using 45° upstream injection from a 0.012-in.-diameter hole, two runs were made with $A\ell(BH_4)_3$, the first a pressure-measuring run with α from -30° to $+40^{\circ}$ and the second a force-balance run with α from -25° and $+25^{\circ}$. The fuel flow rates were 0.0066 lb/sec and an estimated 0.0076 lb/sec respectively. A series of direct luminosity photographs are shown in Fig. 37 for $\alpha = -30^{\circ}$ to $+40^{\circ}$. Combustion initiated at the fuel orifice for all model orientations and contined downstream. With windward

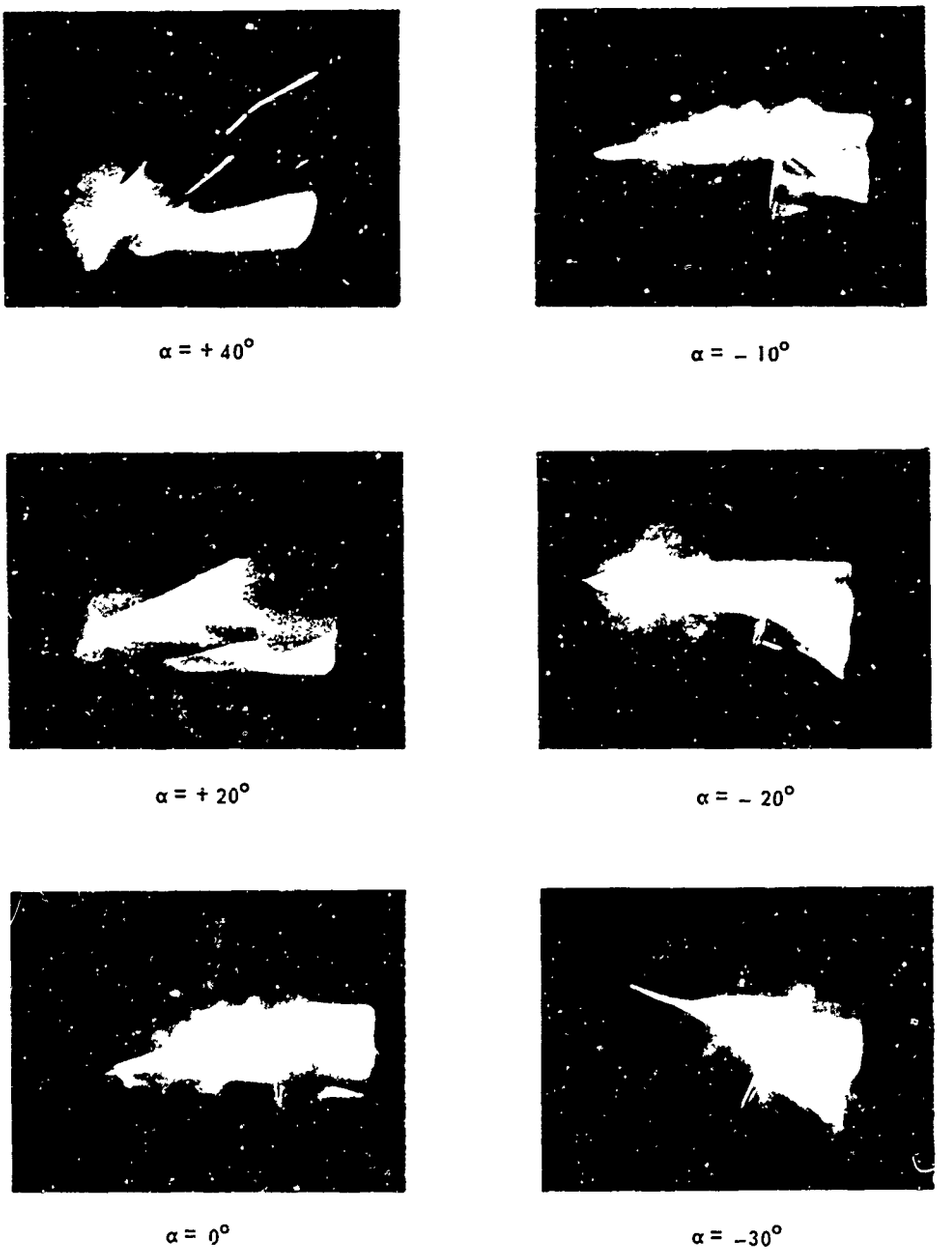

Fig. 37 LUMINOSITY PHOTOGRAPHS OF ALUMINUM BOROHYDRIDE COMBUSTION ON AN 8° CONE (Ref. 58)

burning (positive α) severe wrap-around is observable at $\alpha = 40^{\circ}$ and to a lesser degree at $\alpha = 20^{\circ}$. Pressure traces for $\alpha = 0^{\circ}$, +20 and $+40^{\circ}$ are shown in Fig. 38; plugging of the pressure taps with solid deposits prevented pressure measurements at negative α. Schlieren photographs indicate a significantly stronger disturbance at the injector than is implied by linear interpolation from tap 4 to tap 5. The general trend of the pressure traces is a pressure decay following the initial injection compression and then a pressure rise due to heat release which is significantly different for the three data runs. The writer made an estimate of C_N based on the pressure readings as follows. Assuming that the measured pressures applied to the longitudinal projected area of the model (since the luminous flame appeared to have about the same width as the model at any station), C_N was computed by integrating the pressure profile over this projected area. At $\alpha = +20^{\circ}$ and $+40^{\circ}$ a negative force coefficient was obtained and at $\alpha = 0^{\circ}$ a positive value of $C_N = 0.13$ was computed. The force balance runs made at similar test conditions were interpreted (transient heating of the balance caused significant zero shifts) to give a $C_N = 0.035$ at zero angle-of-attack and $C_N = 0.03$ at $\alpha = -25^{\circ}$. The normal force changed sign at approximately $+3^{\circ}$ angle-of-attack and dropped 0.06 below the non-burning value at $\alpha = +25^{\circ}$. Specific impulses for the two tests at $\alpha = 0$ would be .13 x 68.8/.0066 = 1355 sec based on the integrated pressure run and 0.035 x 68.8/.0076 = 316 sec from the force balance run.

There was virtually no change in pitching moment data at negative and zero α which points out the difficulty in obtaining attitude control with forebody injection when the effects of heat release are being felt both

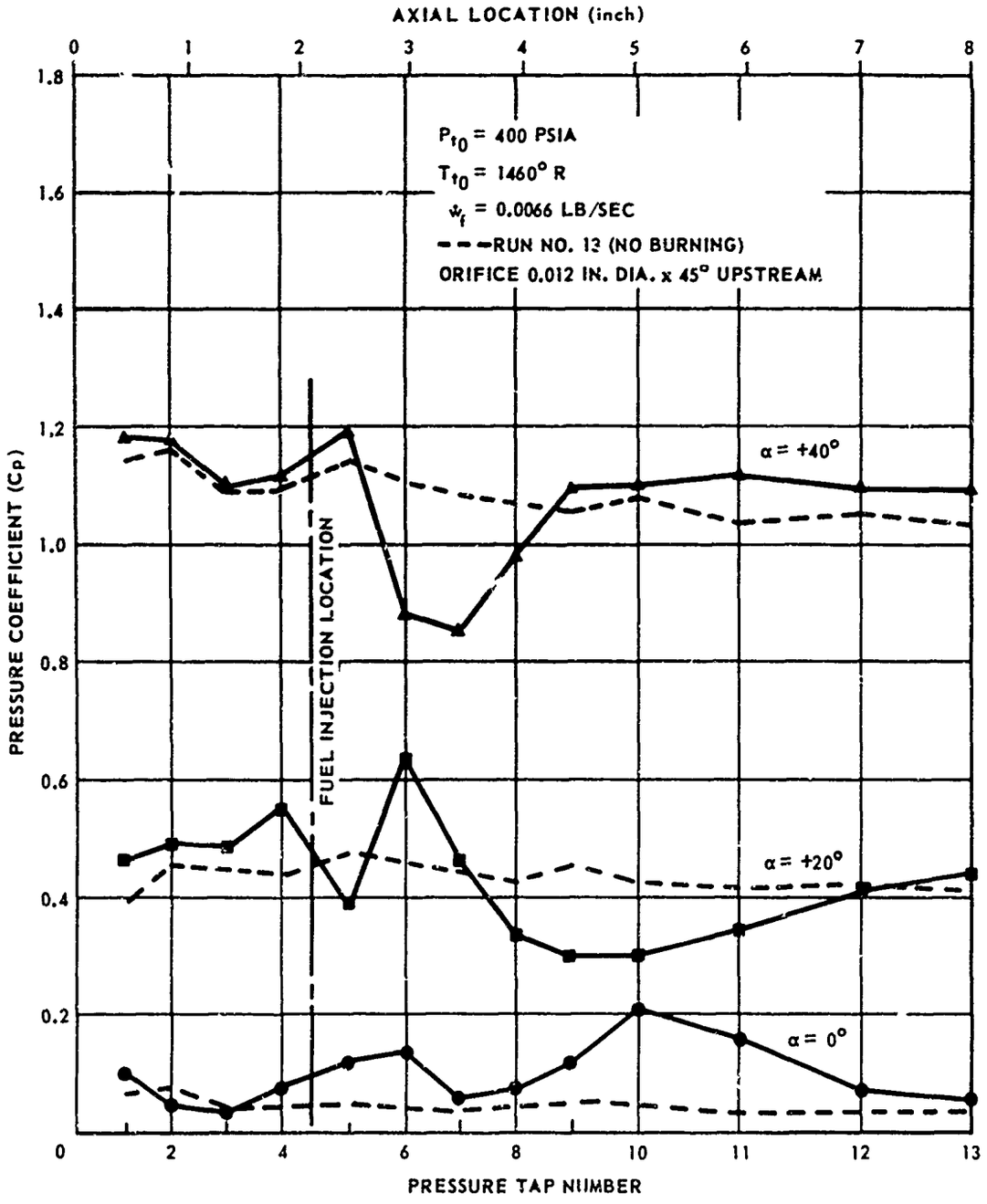

Fig. 38 AXIAL PRESSURE DISTRIBUTION FOR CONE TESTS WITH ALUMINUM BOROHYDRIDE AT MACH 5.0 (Ref. 58)

fore and aft of the model c.g. The change in moment coefficient (C_M) was sizeable at positive α, increasing from about 0 at $\alpha = 0^o$ to ~ 0.025 at $\alpha = 16^o$ and then rapidly decaying to 0 at $\alpha = 25^o$. This strange behavior is due to the large change in the character of the pressure traces at positive α and would lead to control design problems in a flight vehicle because the nature of the pressure variations due to combustion would probably be strongly influenced by flight environment, i.e., at low altitude, higher pressure would accelerate the heat release rates.

A mixture of 25% aluminum borohydride and 75% pentaborane was used in two runs with the same injector used in the 100% $Al(BH_4)_3$ runs. At $\alpha = 0^o$ with both a very low flow rate (not determined) and a flow rate of 0.0052 lb/sec the only combustion observed was in the base region.

Measurements were made from the schlieren photographs to determine the penetration depth of the fuel and comparisons were made with theoretical estimates from a fuel trajectory analysis. Correlation of data with theory for the penetration, defined as the point where the fuel trajectory is inclined 9^o to the airstream direction, was good for both the non-reacting injectants and for the pentaborane which had not ignited at this point on the trajectory. With $Al(BH_4)_3$ the theoretical penetration height was similar to that for pentaborane, but the experimentally determined values were approximately twice as large. Thus, combustion appears to significantly increase the fuel penetration, which is consistent with the measurements and conclusions of Ref. 36.

4. SUMMARY AND CONCLUSIONS

Although conclusions have been drawn from the results of particular theoretical and experimental studies in various sections of this review, it is nonetheless useful to consider the material in its entirety with respect to the state-of-the-art of external burning. Of course, most of the experimental work has been exploratory in nature and more often than not was obtained at testing conditions less favorable for combustion than would be expected in flight. Nevertheless, a careful scrutiny of the available data should provide the systems designer with reasonable estimates of the probable performance realizable from external burning and should serve as a guide to the experimentalist in planning additional tests which can substantiate or negate the conclusions drawn herein.

The experimental data are summarized in Table VII. The testing conditions and fuel flow rates are given along with the principal performance indices; normal and axial specific impulse, I_{fN} and I_f, the maximum pressure coefficient, $C_{p_{max}}$, and the normal force or average pressure coefficient C_N. The normal force specific impulse values are plotted in Fig. 39 as a function of free stream Mach number. Note the break in the Mach number scale at $M_0 = 5.0$ to accommodate the preponderance of Mach 5 data. For comparison two theoretical curves are shown for TEA combustion, one based on linear theory and the other on the constant pressure combustion analysis including expansion.[34] The latter is for the case of a turning angle equal to the turbulent separation value. The linear theory expression can be developed from:

$$I_{fN} = C_p A q_0/\dot{w}_f \qquad (50)$$

Table VII

Summary of Experimental Results from External Burning Tests[a]

Code	Ref.	Model	Length for burning in.	Fuel	Free Stream Conditions M_o	P_o, psia	T_o, °R	$\dot{w}_f$, lb/sec x10^4	C_N x10^3	I_{fN}, sec	$C_{p_{max}}$	I_f, sec
A	Davis	5° wedge-step	2.5	$H_2 + O_2$	1.70	17.2	540	41[b] 156[c]	159	3130 885	.198	379 100
B	52	Circular Arc Airfoil	9.5	$Al(BH_4)_3$	2.47	1.43	253	150	83	3800	.274	-
C	"	" " "	"	"	2.96	0.96	212	150	94	4180	.256	187
D	51	Flat Plate	21.5	"	2.38	0.85	259	160	81	4970	.210	-
E	"	"	46.5	"	2.38	0.85	259	160	46	6170	.210	-
F	APL	10° -10° wedge	6.3	TEA	5.0	0.14	301	138-469	94-163	370-550	.185	62-120
G	"	10° -20° wedge	2.6	"	"	0.14-0.18	260-310	25-200	100-222	240-2160	.242	91-818
H	"	10° -30° wedge	1.7	"	"	0.12-0.14	298	36-252	81-323	220-640	.330	58-285
I	"	10° -30° with ext.	5.9	TEA TIBA	"	0.13-0.14	295-305	138-469	49-212	220-650	.230	43-165
J	"	10° -20° wedge	12.0	TEA	"	0.16-0.36	249-261	110-420	33-152	160-360	.160	10-85
K	"	10° -20° with ext.	24.0	"	"	0.13-0.29	255-267	110-670	34-129	125-630	.230	20-90
L	"	10° -20° ext. & pylons	24.0	TEA TIBA	"	0.13-0.18	256-266	260-700	43-141	75-330	.220	0-30
M	34	Flat plate	12.0	TEA	5.04	0.78	345	490	66	1350	.138	-
N	58	16° cone	5.0	$Al(BH_4)_3$	"	0.75	250	760 660	35[d] 130[e]	316 1355	.155	-

[a] Definitions: $C_N = (L_{hot} - L_{cold})/q_o A_{ref}$, where A_{ref} is projected plan form area under flame; $I_{fN} = (L_{hot} - L_{cold})/\dot{w}_f$; $C_{p_{max}} = (p_{max} - p)/q_o$, maximum pressure coefficient in burning zone; I_f = thrust specific impulse = $(T_{hot} - T_{cold})/\dot{w}_f$

[b] Based on hydrogen flow

[c] Based on hydrogen + oxygen flow

[d] Based on force balance readings

[e] Based on writer's estimates of pressure integration

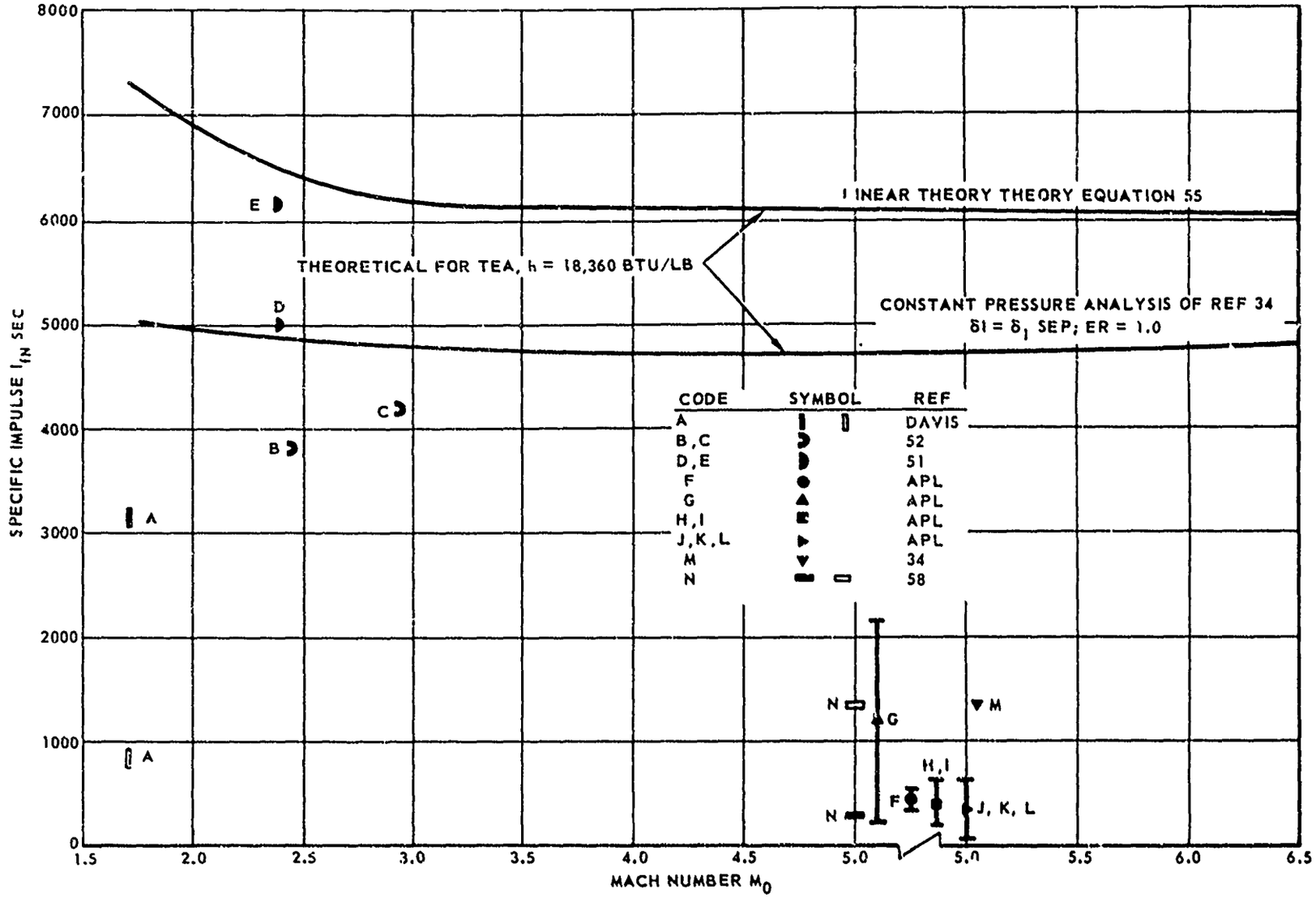

Fig. 39 NORMAL FORCE SPECIFIC IMPULSES AS A FUNCTION OF MACH NUMBER

using Eqs. (7) and (10)

$$\delta = QgJ\ Y/c_p\ T_0\ X_f \quad ; \quad C_p = 2\ \delta/(M_0^2 - 1)^{\frac{1}{2}}$$

$$A = \text{area under flame} = X_f d \tag{51}$$

$$q_0 = \tfrac{1}{2}\ \rho_0 u_0^2 \quad ; \quad Q = h\ \dot{w}_f/\dot{w}_a \quad ; \quad \dot{w}_a = g\ \rho_0 u_0\ Y\ d \tag{52}$$

substituting Eqs. (51) - (52) into (50),

$$I_{fN} = h\ u_0 J/\ c_p\ T_0\ (M_0^2 - 1)^{\frac{1}{2}} \tag{53}$$

with $a_0^2 = \gamma RT_0$, and $R/c_p = (\gamma - 1)/\gamma$, (54)

$$I_{fN} = 778\ h\ (\gamma - 1)\ M_0/a_0\ (M_0 - 1)^{\frac{1}{2}} \tag{55}$$

To obtain theoretical values for the other fuels used, the TEA values can be scaled by the ratio of heating value of the particular fuel to that of TEA, i.e., 29,360/18,360 = 1.6 for B_5H_9, 1.27 for $Al(BH_4)_3$, 2.81 for H_2 and 1.0 for TIBA.

Nearly all of the data fall considerably below the theoretical curves with the notable exception of the early NASA tests[51] using the very reactive fuel, $Al(BH_4)_3$, on relatively long models. Although for many of the tests it may be argued that non-optimum fuel injection systems produced poor fuel-air distributions and performance suffered accordingly, it does not seem reasonable to attribute all of the deficiency to too rich or too lean mixtures, because so many different injection schemes and fuel flow rates have been tried. Rather it is just as likely that the limiting factor is insufficiently rapid kinetic rates; i.e., for the local conditions there was not sufficient time (distance) to complete the heat release. This argument is supported by the NASA results[51], which show a

significant increase in I_{fN} from run D to run E with an increase in length from 21.5 to 46.5-in., and by the instream measurements made at APL (Fig. 34), which showed that the reaction was proceeding in the streamwise direction with a nearly linear temperature rise with length. Similar effects were noted in data from J and K. On the other hand, if these were strictly fuel-air distribution difficulties one would expect a rapid heat release until all of the local oxygen is consumed, followed by a very slow release as additional air mixes with the excess fuel and products. Granting that this may be a reaction-rate-limited situation the question is: How much length will be needed to complete the reaction in flight? Obviously the answer depends on the reactivity of the fuel and on the flight environment. Aluminum borohydride appears to be the fastest reacting fuel tested, followed by pentaborane and the aluminum alkyls TEA and TIBA. Higher pressure generally increases reaction rates, therefore lower altitude should require less length. Compression prior to injection due to the body shape and/or to burning on the windward side at angle-of-attack will help because the local pressure and temperature will be higher and the velocity somewhat lower. Lower flight velocity increases the residence time for a given length but also has associated with it lower maximum temperatures in the boundary layer which may be important. Finally, the wall temperature and the fuel temperature, which could be elevated if the fuel is used as a regenerative coolant, may also be important. All of these factors will affect the answer to the question posed; however; it appears that the length required to complete the reaction will be in the order of feet rather than inches, judging from the results

from runs D and E (which might be extrapolated to about 6 ft) and from the estimate given before of 2 ft for reaction plus another 3 ft for expansion for test M. If lengths of this order are not available, specific impulses are apt to be lower, roughly in proportion to the ratio of the available length to the reaction length. Clearly, there is a need for reaction rate data for these fuels in order to make better estimates. The data possibly could be obtained in much simpler subsonic tests at simulated temperatures and pressures.

For nearly all of the data summarized in Table VII and Fig. 39, the length available for combustion was quite short and/or the static temperature was lower than for simulated flight, therefore, the impulses are correspondingly low. However, there are some case, i.e., B-E and G having roughly half the theoretical I_{fN}, which is much higher than can be obtained with non-reactive thrust vector control systems. The performances of a body of revolution, N , was poorer than for the two-dimensional models, which appears to be due to excessive lateral spillover and again points to the desirability of using longitudinal fences. Thrust specific impulses were calculated for most of the thrust-generating configurations and are listed in Table VII. Nearly all are low compared to either theory or competitive propulsion systems. The highest value of 818 sec for test G was obtained at the lowest fuel flow rate, 0.0025 lb/sec. Conclusions based on the theoretical analysis regarding the performance potentials of external burning systems in the thrust and lift generating modes, Figs. 2B and C, are adequately given in Section 2.3.

The other performance characteristics, especially important in the case of the attitude controller (Fig. 2A) are the normal force and maximum pressure coefficients. For a given normal-force requirement, the control surface area varies inversely with the force coefficient. In most cases, it is desirable to have maximum C_N which, at first glance, would seem to be associated with an external burner which creates a very strong shock, possibly a normal shock. However, this flow situation cannot exist, because at pressure ratios considerably below the normal-shock value, the boundary layer will separate ahead of the heat release zone and the resulting pressure coefficient due to the volume source created by the heat release will be more like that of a separated flow. This point is demonstrated in Fig. 40, in which the maximum pressure and normal force coefficients for the data of Table VII are plotted against free stream Mach number. The maximum pressure coefficients occurring anywhere in the combustion zone are shown as open symbols and the average coefficients in the heat addition region as closed symbols. Most of the data fall near or below the values for turbulent separation based on Ref. [36]. This is not to imply that there is a unique value of $C_{p_{max}}$ for turbulent separation, because there is some Reynolds number dependence, but the theory does represent a reasonable estimate. Moreover, a lot of the data were obtained at low values of Reynolds numbers where the boundary layer should have been laminar, which probably accounts for some of the lower $C_{p_{max}}$ values because laminar separation occurs at lower C_p. [59] Even in the few runs, B-E in which the

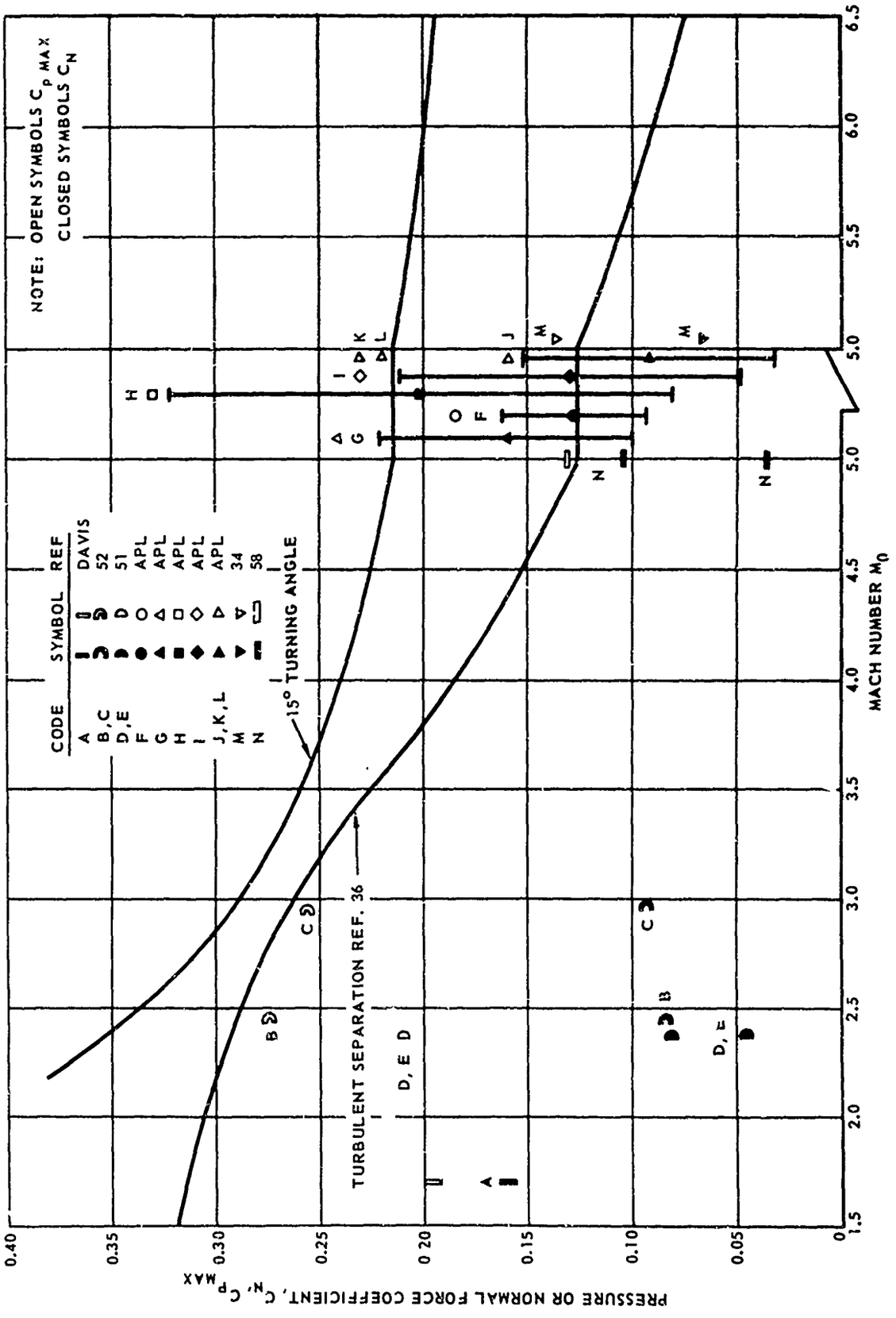

Fig. 40 MAXIMUM PRESSURE AND NORMAL FORCE COEFFICIENTS AS A FUNCTION OF MACH NUMBER

pressure distribution due to injection and heat release was characterized by a pressure spike followed by a rapid decay, the maximum pressure coefficients in the spike region still were of the same order as the turbulent separation value. Also shown for reference is the C_p variation for a turning angle of 15°, which might represent a reasonable upper bound for theoretical system studies. Note that the data in Fig. 40 were plotted at the free stream Mach number condition rather than at the lower local Mach number condition which would exist at the injection point for all but the flat plate tests. Incidentally, the normal shock value for C_p increases from 1.250 at M = 2 to 1.627 at M = 6.5. These values would be obtained if the normal strong detonation (Fig. 6B) could be generated, but this does not seem possible when a boundary layer is present. It appears, then, that the designer of an external-burning system for attitude control will have to contend with relatively low C_p and C_N, probably close to the separation values for the local condition at injection. If higher force coefficients are required, a combination of a compression surface plus external burning will be needed.

Another consideration in the design of external burning systems which are to provide lateral maneuver capability is the control of the moment coefficient. With external burning two choices seem plausible. Either the external burning can be used to provide the moment to turn or trim the body to angle-of-attack to obtain the lateral force, or the external burning can provide the lateral force without turning the body. In the former case for a stable body it appears that the fuel injection should be aft of the body c.g. on the lee side, rather than ahead of the c.g. on the windward side, because

without spillover, the heat release will produce a positive pressure field which will persist in the streamwise direction. Conversely if the external burning is used to trim an aerodynamically unstable body then the injection should be aft of the body c.g. on the windward side. Thus, only for extremely long bodies would the pressure field be sufficiently dissipated with forebody injection to assure a positive moment coefficient. Of course, one might try to exploit the wrap-around characteristics and thus obtain a positive pressure coefficient both on the windward side ahead of the c.g. and on the leeward side aft of the c.g. with forebody injection on a stable body. However, this scheme would seem to have a very unpredictable behavior, because the pressure field would be quite different at each α, as was demonstrated in the Boeing tests.[58]

For the very rapid vehicle maneuvers, the non-turning body may be attractive. In this case the body remains at zero incidence to the stream. Fuel is added on the forebody ahead of the c.g. on the side opposite the desired lateral displacement in order to produce a positive force field that is essentially balanced, in axial distribution, about the c.g., thus producing no turning moment. Fences of course would be required. If the response time were such that the body could be rotated, then the body would be pitched as well, using an auxiliary control to obtain a combined effect. The additional control could possibly be an aft body injector on the opposite side. All of these systems will require a trimming mechanism, which could be a system of small afterbody injectors located at varying circumferential positions.

A final consideration, not previously discussed, is the transient behavior of the external burning system. For a very rapid response system using short bursts of external burning for control, the transient behavior of the pressure field will have to be known. To date neither experimental nor theoretical studies have been made which properly evaluate the transient behavior.

REFERENCES

1. Hicks, Bruce L., "Addition of Heat to a Compressible Fluid in Motion", NACA ACR No. E4A29, 1945.

2. Hicks, B. L., Montgomery, D. J. and Wasserman, R. H., "The One-Dimensional Theory of Steady Compressible Fluid Flow in Ducts with Friction and Heat Addition", NACA TN 1336, July 1947.

3. Hicks, B. L., "Diabatic Flow of a Compressible Fluid", Quarterly of Applied Mathematics, Vol. VI, No. 3, 1948.

4. Hicks, B. L., "On the Characterization of Fields of Diabatic Flow", Quarterly of Applied Mathematics, Vol. VI, No. 4, 1949.

5. Foa, Joseph V. and Rudinger, George, "On the Addition of Heat to a Gas Flowing in a Pipe at Supersonic Speed, Cornell Aeronautical Laboratory, Report No. HF-534-A-2, February 1949.

6. Shapiro, A. H. and Hawthorne, W. R., "The Mechanics and Thermodynamics of Steady One-Dimensional Gas Flow", Journal of Applied Mechanics, Vol. 14, No. 4, December 1947. Also see, Handbook of Supersonic Aerodynamics NAVORD Rept. 1488, Vol I, April 1950 and Shapiro, A. H., "The Dynamics and Thermodynamics of Compressible Fluid Flow, Vol I, The Ronald Press Co., New York, 1953.

7. Tsien, H. S. and Beilock, Milton, "Heat Source in a Uniform Flow", Journal of the Aeronautical Sciences, Vol. 16, No. 12, 1949.

8. Hicks, B. L., Hebrank, W. H. and Kravitz, S., "On the Characterization of Fields of Diabatic Flow", Ballistic Research Laboratory Report No. 720, July 1950.

9. Hicks, B. L., Hebrank, W. H. and Kravitz, "Comment on Heat Source in a Uniform Flow", Journal of the Aeronautical Sciences, Vol. 17, No. 9, September 1950.

10. Pinkel, I. I. and Serafini, J. S., "Graphical Method for Obtaining Flow Field in Two-Dimensional Supersonic Stream to Which Heat is Added", NACA TN 2206, November 1950.

11. Pinkel, I. I. Serafini, J. S. and Gregg, J. L., "Pressure Distribution and Aerodynamic Coefficients Associated with Heat Addition to Supersonic Air Stream Adjacent to Two-Dimensional Supersonic Wing", NACA RM E 51 K26, February 1952.

12. Chu, Boa-Teh, "Pressure Waves Generated by Addition of Heat in a Gaseous Medium", NACA TN 3411, June 1955.

13. Gazley, Carl, Jr., "Linearized Solution for Heat Addition at the Surface of a Supersonic Airfoil", Project Rand Rept. RM-1892, ASTIA AD 133025, Nov. 1956.

14. Mager, A., "Supersonic Airfoil Performance with Small Heat Addition", Journal of the Aero/Space Sciences, Vol. 26, No. 2, February 1959.

15. Tsien, H. S. and Beilock, M., "Heat Source in a Uniform Flow", Journal of the Aeronautical Sciences, Vol. 16, No. 12, December 1949.

16. Shapiro, Ascher H., "The Dynamics and Thermodynamics of Compressible Fluid Flow", The Ronald Press Co., 1953.

17. Willmarth, W. W., "The Production of Aerodynamic Forces by Heat Addition on External Surfaces of Aircraft", Project Rand Rept. RM 2078. ASTIA AD 150681, December 1957.

18. Woolard, H. W., "Tables of Properties of Some Oblique Deflagrations in Supersonic Flow", Johns Hopkins University, Applied Physics Laboratory, TG382, September 1960.

19. Woolard, H. W., "Analytical Approximations for Stationary Conical Detonations and Deflagrations in Supersonic Flow", The Johns Hopkins University, Applied Physics Laboratory, TG 446, May 1963.

20. Chinitz, W., Bohrer, L. C. and Foreman, K. M., "Properties of Oblique Detonation Waves", Fairchild Engine Division, Deer Park, New York, AFOSR TN 59-462 (ASTIA) AD 215-267, April 1959.

21. Luidens, R. W. and Flaherty, R. J., "Analysis and Evaluation of Supersonic Underwing Heat Addition", NASA Memo 3-17-59E, April 1959.

22. Lomax, H., "Two-Dimensional, Linearized Flow with Heat Addition", NASA Memo 1-10-59A, February 1959.

23. Dugger, G. L. and Monchick, L., "External Burning Ramjets, Preliminary Feasibility Study", Applied Physics Laboratory, Johns Hopkins University, CM 948, June 1959.

24. Woolard, H. W., "An Approximate Analysis of the Two-Dimensional Supersonic Flow Past a Plane Wall with Super-Critical Heat Addition in a Normal Plane", The Johns Hopkins University, Applied Physics Laboratory, APL/JHU CM 954, July 1959.

25. Moeckel, W. E., "Approximate Method for Predicting Form and Location of Detached Shock Waves Ahead of Plane or Axially Symmetric Bodies", NACA TN 1921, July 1949.

26. Nicholls, J. A., "Stabilization of Gaseous Detonation Waves with Emphasis on the Ignition Time Delay Zone", University of Michigan, Ann Arbor, Michigan, AFOSR TN 60-442, June 1960.

27. Gross, R. A., "Exploratory Studies of Combustion in Supersonic Flow", Fairchild Engine Co., Deer Park, New York, AFOSR TN 59-587, June 1959.

28. Rhodes, R. P. and Chriss, D. E., "A Preliminary Study of Stationary Shock-Induced Combustion with Hydrogen Air Mixtures", Arnold Engineering Development Center, AEDC TN 61-36, July 1961.

29. Hilsenrath, J., et al, "Tables of Thermal Properties of Gases", NBS Circular 564, November 1965.

30. Feldman, S., "Hypersonic Gas Dynamic Charts for Equilibrium Air", AVCO Research Laboratory, Res. Report 40, January 1957.

31. General Electric Company, "Properties of Combustion Gases/System: C_NH_{2N}-Air Vols. I and II, McGraw-Hill, New York, 1955.

32. Thermodynamics Group, Convair/San Diego, "Combustion Charts, H_2 + Air, ER = 0.8, 1, 2, 4 and 6" private communication from E. Chapman, 1960.

33. Dugger, G. L., "Comparison of Hypersonic Ramjets with Subsonic and Supersonic Combustion", Combustion and Propulsion, Fourth AGARD Colloquim, Pergamon Press, London, 1961.

34. Billig, F. S., "A Study of Combustion in Supersonic Streams", The Johns Hopkins University, Applied Physics Laboratory, BB 321, July 1964.

35. Browne, H. N. and Williams, M. M., "The Theoretical Computation of Equilibrium Compositions, Thermodynamic Properties and Performance Characteristics of Propellant Systems", U. S. Naval Ordnance Test Station, NavWeps Rep. 7043, June 8, 1960.

36. Mager, A., "On the Model of Free, Shock-Separated Turbulent Boundary Layer", J. of Aero. Sci., Vol. 23, No. 2, pps. 181-184, Feb. 1956.

37. Attas, J. E., "Interaction Effects Produced by a Vapourizing Liquid Injected into a High Energy Supersonic Gas Stream", McGill University Report No. 63-2, April 1963.

38. Romeo, D. J. and Sterett, J. R., "Aerodynamic Interaction Effects Ahead of a Sonic Jet Exhausting Perpendicularly from a Flat Plate into a Mach Number 6 Free Stream", NASA Tech. Note D-743, April 1961.

39. Wald, Q., "Reduction of Drag at Supersonic Velocities by Heating the External Air Stream", United Aircraft Corporation Research Dept. M-13362-2, June 1950.

40. Yen, S. M., "One-Dimensional Flow with Heat Addition", Report CV-4, Convair Division of General Dynamics Corporation, San Diego, California, March 7, 1958.

41. McCloy, R. W., "Propulsion by Supersonic Heat Addition", Report CV-1, Convair Division of General Dynamics Corporation, San Diego, California, March 7, 1958.

42. McCloy, R. W., "External Heat Addition for Cases Other than Constant-Pressure Heat Addition", Report CV-5, Convair Division of General Dynamics Corporation, San Diego, California, March 7, 1958.

43. McCloy, R. W., "Specific Fuel Consumption and Over-all Efficiency for External Heating Processes", Report CV-6, Convair Division of General Dynamics Corporation, March 7, 1958.

44. Marino, A., "Theoretical Performance with External Burning on Surface", General Applied Science Laboratory, Rept. No. 506, February 1965.

45. Baker, W. T., Davis, T. and Matthews, S. E., "Reduction of Drag of a Projectile in a Supersonic Stream by the Combustion of Hydrogen in the Turbulent Wake", The Johns Hopkins University, Applied Physics Laboratory, CM-673, June 1951.

46. Scanland, T. S. and Hebrank, W. H., "Drag Reduction through Heat Addition to the Wake of Supersonic Missiles", Ballistic Research Laboratories, Memo Rep. No. 596, June 1952.

47. Snyder, A. D., Robertson, J., Zanders, D. L. and Skinner, G. B., "Shock Tube Studies of Fuel-Air Ignition Characteristics", Monsanto Research Corporation, Tech. Report AFAPL-TR-65-93, August 1965.

48. Fletcher, E. A., Dorsch, R. G. and Gerstein, M., "Combustion of Aluminum Borohydride in a Supersonic Wind Tunnel", NACA RM E55D07a, June 1955.

49. Dorsch, R. G., Serafini, J. S., and Fletcher, E. A., "A Preliminary Investigation of Static-Pressure Changes Associated with Combustion of Aluminum Borohydride in a Supersonic Wind Tunnel", NACA RM E55F07, August 1955.

50. Dorsch, R. G., Serafini, J. S. and Fletcher, E. A., "Exploratory Investigation of Aerodynamic Effects of External Combustion of Aluminum Borohydride in Airstream Adjacent to Flat Plate in Mach 2.46 Tunnel", NACA RM E57E16.

51. Dorsch, R. E., Allen, H., Jr., and Dryer, M., "Investigation of Aerodynamic Effects of External Combustion Below Flat-Plate Model in 10-by 10-foot Wind Tunnel at Mach 2.4", NASA D-282, April 1960.

52. Serafini, J. S., Dorsch, R. G. and Fletcher, E. A., "Exploratory Investigation of Static-and Base-Pressure Increases Resulting from Combustion of Aluminum Borohydride Adjacent to Body of Revolution in Supersonic Wind Tunnel", NACA RM E57E15, October 1957.

53. Dorsch, R. G., Serafini, J. S., Fletcher, E. A., and Pinkel, I. I., "Experimental Investigation of Aerodynamic Effects of External Combustion in Airstream Below Two-Dimensional Supersonic Wing at Mach 2.5 and 3.0", NASA Memo 1-11-59E, March 1959.

54. Woolard, H. W., "Some Analytical Considerations of the Aerothermodynamic Aspects of Supersonic Combustion", Minutes of 44th Meeting of the Bumblebee Aerodynamics Panel, The Johns Hopkins University, Applied Physics Laboratory, TG 14-41, August 1961.

55. Zwick, E. E., Grubman, D. H., and Hardy, L., "Analysis of Droplet Evaporation and Combustion in Hypersonic Streams", Paper presented at AIAA Aerospace Sciences Meeting, January 1964.

56. Ingebo, R. and Foster, H., "Drop Size Distribution for Cross-Current Break-up of Liquid in Airstreams", NASA TN 4087, October 1957.

57. Hirschfelder, J. O., Curtiss, C. F. and Bird, R. B., "Molecular Theory of Gases and Liquids", John Wiley and Sons, Inc., New York, 1954.

58. Kranz, P. G. and Pelky, D. A., "Experimental Investigation of External Burning on an 8° Half-Angle Cone at Mach 5.0 and 6.1", The Boeing Company, No. D2-36037, August 1964.

59. Chapman, D. R., Kuehn, D. M. and Larson, H. K., "Investigation of Separated Flows in Supersonic and Subsonic Streams with Emphasis on the Effect of Transition", NACA Report 1356, 1958.

UNCLASSIFIED
Security Classification

DOCUMENT CONTROL DATA – R&D
(Security classification of title, body of abstract and indexing annotation must be entered when the overall report is classified)

1. ORIGINATING ACTIVITY (Corporate author)
The Johns Hopkins Univ. Applied Physics Lab.
8621 Georgia Ave.
Silver Spring, Md.

2a. REPORT SECURITY CLASSIFICATION
Unclassified

2b. GROUP

3. REPORT TITLE
External Burning in Supersonic Streams

4. DESCRIPTIVE NOTES (Type of report and inclusive dates)
Technical Memorandum

5. AUTHOR(S) (Last name, first name, initial)
Billig, F. S.

6. REPORT DATE	7a. TOTAL NO. OF PAGES	7b. NO. OF REFS
May 1967	115	59

8a. CONTRACT OR GRANT NO.	9a. ORIGINATOR'S REPORT NUMBER(S)
NOw 62-0604-c b. PROJECT NO. Task Assignment A55 c. d.	TG-912 9b. OTHER REPORT NO(S) (Any other numbers that may be assigned this report)

10. AVAILABILITY/LIMITATION NOTICES
Distribution of this document is unlimited.

11. SUPPLEMENTARY NOTES	12. SPONSORING MILITARY ACTIVITY
	Naval Ordnance Systems Command Department of the Navy

13. ABSTRACT

Theoretical and experimental studies of heat addition to external supersonic streams are reviewed, following a brief explanation of the basic fluid mechanical model and possible applications of external burning. Previously developed methods and a new, simplified method for obtaining linearized heat addition solutions are presented. The numerous analyses of combustion via a stationary detonation wave are categorized into four models for planar heat addition, and the equations are developed for the most interesting case of the oblique Chapman-Jouget detonation. The governing equations for a constant-pressure analysis are developed, and performance estimates are given for heat addition adjacent to both double-wedge and flat-plate surfaces. Experimental results of all available external burning tests are discussed, including tests of two-dimensional and axisymmetric bodies. Data are compiled, summarized, and analyzed. The maximum expected pressure coefficient will be near the associated with a separated boundary layer. To obtain the theoretical maximum specific impulse, highly reactive fuels with a combustion length of a few feet will be required.

DD FORM 1 JAN 64 1473

UNCLASSIFIED
Security Classification

14. KEY WORDS
External Burning
Attitude Control
Supersonic Combustion
Maneuvering Re-entry
Ramjets